INVESTIGATION OF HYDROGEN PEROXIDE AND NITRIC OXIDE SIGNALING UTILIZING GENETICALLY ENCODED BIOSENSORS

by

HAMZA YUSUF ALTUN

Submitted to the Graduate School of Engineering and Natural Sciences

in partial fulfillment of the requirements for degree of

Doctor of Philosophy

Sabancı University

July 2024

INVESTIGATION OF HYDROGEN PEROXIDE AND NITRIC OXIDE SIGNALING UTILIZING GENETICALLY ENCODED BIOSENSORS

APPROVED BY:

Prof. Dr Mehmet Selim ÇETİNER .....

(Thesis Supervisor)

Asst. Prof. Dr. Alex LYAKHOVICH .....

Asst. Prof. Dr. Nur MUSTAFAOĞLU VAROL .....

Prof. Dr. Batu ERMAN .....

Asst. Prof. Dr. Ahmet KATI .....

DATE OF APPROVAL: 22/July/2024

ABSTRACT

INVESTIGATION OF HYDROGEN PEROXIDE AND NITRIC OXIDE SIGNALING UTILIZING GENETICALLY ENCODED BIOSENSORS

HAMZA YUSUF ALTUN

Molecular Biology, Genetics and Bioengineering, PhD Thesis, 2024

Thesis Supervisor: Prof. Dr. Mehmet Selim ÇETİNER

Keywords: Hydrogen Peroxide, Nitric Oxide, Genetically Encoded Biosensors, Redox Signaling, Physiological Normoxia

The relationship between hydrogen peroxide (H_2O_2) and nitric oxide (NO) is a critical yet complex aspect of redox biology, with significant implications for cellular signaling and oxidative stress-related diseases. This study aims to demonstrate this relationship using genetically encoded biosensors, HyPer7 for H_2O_2 and O-geNOp for NO, in live-cell imaging. We developed and optimized these tools to achieve high selectivity and spatial resolution, addressing challenges related to simultaneous measurement of reactive oxygen species (ROS) and reactive nitrogen species (RNS). Our experiments demonstrated that cells adapted to physiological normoxia (5 kPa O_2) exhibit enhanced antioxidant capacity and NO bioavailability compared to those adapted to hyperoxia (18 kPa O_2). Using a dual-biosensor endothelial cell line, we investigated the effects of H_2O_2 production on NO dynamics and discovered that physiological normoxia conditions significantly improve cellular redox balance. These findings provide new insights into the interplay between H_2O_2 and NO, highlighting the importance of maintaining physiological O_2 levels for optimal cellular function. The results also underscore the potential of genetically encoded biosensors as powerful tools for studying redox signaling in live cells, paving the way for novel therapeutic strategies targeting oxidative stress-related pathologies.

ÖZET

GENETİK OLARAK KODLANMIŞ BİYOENSÖRLER KULLANILARAK HİDROJEN PEROKSİT VE NİTRİK OKSİT SİNYALİZASYONUNUN İNCELENMESİ

HAMZA YUSUF ALTUN

Moleküler Biyoloji, Genetik ve Biyomühendislik, Doktora Tezi, 2024

Tez Danışmanı: Prof. Dr. Mehmet Selim ÇETİNER

Anahtar Kelimeler: Hidrojen Peroksit, Nitrik Oksit, Genetik Olarak Kodlanmış Biyosensörler, Redoks Sinyalleme, Fizyolojik Normoksi

Hidrojen peroksit (H_2O_2) ve nitrik oksit (NO) arasındaki ilişki, redoks biyolojisinin kritik ancak karmaşık bir yönüdür. Bu ilişkinin hücresel sinyalizasyon ve oksidatif stresle ilişkili hastalıklar için önemli etkileri vardır. Bu çalışma, canlı hücre görüntülemede genetik olarak kodlanmış biyosensörler olan HyPer7, H_2O_2 için, ve O-geNOp, NO için, kullanarak bu ilişkiyi göstermeyi amaçlamaktadır. Reaktif oksijen türlerinin (ROS) ve reaktif nitrojen türlerinin (RNS) eşzamanlı ölçümüyle ilgili zorlukları ele alarak yüksek seçicilik ve uzamsal çözünürlük elde etmek için bu araçları geliştirdik ve optimize ettik. Deneylerimiz, fizyolojik normoksiye (5 kPa O_2) adapte olmuş hücrelerin, hiperoksiye (18 kPa O_2) adapte olmuş hücrelere kıyasla antioksidan kapasite ve NO biyouygunluğu konularında daha gelişmiş seviyede olduğunu gösterdi. Çift biyosensörlü endotel hücre hattı kullanarak H_2O_2 üretiminin NO dinamiği üzerindeki etkilerini araştırdık ve fizyolojik normoksi koşullarının hücresel redoks dengesini önemli ölçüde iyileştirdiğini keşfettik. Bu bulgular, H_2O_2 ve NO arasındaki etkileşime dair yeni bilgiler sağlayarak, optimal hücresel fonksiyon için fizyolojik O_2 seviyelerini korumanın önemini vurgulamaktadır. Sonuçlar ayrıca genetik olarak kodlanmış biyosensörlerin canlı hücrelerde redoks sinyallemesini incelemek için güçlü araçlar olarak potansiyelini vurgulayarak oksidatif stresle ilişkili patolojileri hedef alan yeni terapötik stratejilerin önünü açıyor.

For my family and the people who tragically lost their lives on February 6

ACKNOWLEDMENTS

First and foremost, I would like to express my sincere gratitude to everyone who has supported and guided me throughout my Ph.D. journey.

I am deeply indebted to my mentor, Dr. Emrah Eroğlu, for his unwavering support, insightful guidance, and continuous encouragement throughout my research. His exceptional mentorship and the way he demonstrated the essence of scientific inquiry have left an indelible mark on my academic journey. His expertise and dedication were instrumental in the successful completion of this thesis.

I would like to express my heartfelt gratitude to Prof. Dr. Selim Çetiner, who served as my supervisor in Sabancı. His support and willingness to engage in meaningful conversations throughout the thesis process have been invaluable. His wisdom and guidance have greatly contributed to the development and completion of this Ph.D journey. I am profoundly grateful for his encouragement and the respect he has shown me during this journey.

I would like to extend my sincere thanks to the members of my thesis jury, Dr. Alex Lyakhovich, Dr. Nur Mustafaoğlu Varol, Dr. Ahmet Katı, and Prof. Dr. Batu Erman. Their valuable feedback, constructive criticism, and insightful questions have significantly enriched my research. I deeply appreciate their time, effort, and expertise in evaluating my work and guiding me towards a more comprehensive understanding of my research topic. Their contributions have been crucial in shaping the final outcome of this thesis.

I would like to express my sincere gratitude to Prof. Dr. Giovanni Mann for his wisdom, support, and the meaningful conversations we shared. His insights have greatly enriched my research. I am also deeply thankful to Dr. Fan Yang for her support and friendship during my time in the UK. Her assistance and encouragement were invaluable to me.

I am profoundly grateful to my family for their unwavering love, support, and encouragement throughout my academic journey. A special thanks to my sister, Gül whose constant support and belief in me provided the strength and motivation I needed to overcome challenges. Her understanding, patience, and words of encouragement have been invaluable. To my parents, thank you for introducing in me the values of

perseverance and dedication. Your sacrifices and endless support have made this achievement possible.

Special thanks to my friends Yavuz Eroğlu, Can Dayıoğlu, and Ekrem Gemci for their endless support and companionship throughout this journey. Even when I bothered them with my personal problems, they always stood by me, offering unwavering support and understanding. Their friendship has been a source of strength and comfort, making this journey not only bearable but enjoyable.

I would like to thank the Scientific and Technological Research Council of Turkey (TÜBİTAK) for providing me a scholarship for my Ph.D studies. My studies were supported by TÜBİTAK BİDEB 2211-A program.

TABLE OF CONTENTS

LIST OF FIGURES

LIST OF TABLES

LIST OF SYMBOLS AND ABBREVIATIONS

ATP	Adenosine Triphosphate
CAT	Catalase
DAAO	D-amino Acid Oxidase
EDFR	Endothelium-Derived Relaxation Factor
eNOS	Endothelial Nitric Oxide Synthase
ER	Endoplasmic Reticulum
FAD	Flavin Adenine Dinucleotide
GAF	cGMP phosphodiesterase, adenylate cyclase, FhlA
GFP	Green Fluorescent Protein
JNK	Janus Kinase
κ	Kappa
L-NAME	L-NitroArginine Methyl Ester
NES	Nuclear Export Signal
NLS	Nuclear Localization Signal
NOX	NADPH Oxidase
PTK	Protein Tyrosine Kinase
PTP	Protein Tyrosine Phosphatase
RNS	Reactive Nitrogen Species
ROS	Reactive Oxygen Species
RT	Room Temperature
SD	Spinning Disk Confocal Microscope

sGC	Soluble Guanylate Cyclase
SNR	Signal to Noise Ratio
SOD	Superoxide Dismutase
WF	Widefield Fluorescence Microscope

CHAPTER I: INTRODUCTION

Importance of Hydrogen Peroxide and Nitric Oxide in Cell Signaling

Reactive oxygen species serving as signaling molecules in molecular biology is and old concept which has been investigated for a long time. Due to their reactivity these molecules can easily interact with the other signaling molecules or biomolecules such as lipids, proteins nucleic acids[1]. Interaction with these reactive molecules can lead to covalent, structural or activity changes over biomolecules[2]. The main interactions rely on the redox chemistry of molecules. Reaction between biomolecules and reactive species leads to redox reactions[3]. Redox reaction is an abbreviation of “reduction” and “oxidation” reaction. Reduction denotes gaining electrons of a molecule and oxidation stands for the loss of electrons from a molecule. In molecular biology, redox reactions occurs through transferring radical groups to biomolecules or vice versa where biomolecules are oxidized when radical group interacts biomolecules form bonds[4].

Redox biology studies the interaction of reactive species with biomolecules and effect of cellular signaling[5]. Among the reactive species, reactive oxygen species (ROS) are the most-studied ones. Sources of ROS are varied but they can be defined as molecular oxygen derived oxidizing molecules[6], [7]. There are extracellular sources such as chemical exposure, UV radiation, microbes and intracellular sources [8]. Formation of intracellular ROS molecules serve as signaling molecules for signal transduction[9]. Primary sources of intracellular ROS are mitochondria of the cells due to electron

transport chain where molecular oxygen used as an electron acceptor. Electron transfer to molecular oxygen leads to formation of superoxide which is highly reactive and superoxide rapidly eliminated via superoxide dismutase and converted to less reactive form of ROS, H_2O_2 The second major source of ROS NADPH oxidases[6]. Since many ROS molecules are short-lived and highly reactive, they are converted to more stable ROS species for example superoxide is converted to hydrogen peroxide (H_2O_2)[3]. Although H_2O_2 believed as dangerous molecule previously, H_2O_2 can act as a secondary messenger[10]. The key point of being harmful or being important secondary messenger is concentration of H_2O_2 inside the cell. There's a strict control of H_2O_2 gradient not to disrupt signaling cascade that H_2O_2 involved[11]. Experiments showed that 100-fold gradient is present between extracellular and intracellular H_2O_2. This gradient is controlled via Aquaporins (AQPs)[12]. Similar to Ca^{2+}, H_2O_2 is also maintained strictly intracellularly[6]. There are more than 30 enzymes that are capable to increase intracellular H_2O_2[9]. These enzymes locate in different compartments of the cells which highlights spatial ROS signaling via H_2O_2 (**Table 1.1**). Catalase, peroxiredoxins, glutathione peroxidases are the enzymes mainly remove H_2O_2 or turn H_2O_2 to other oxidants[7], [13], [14]. They have high-rate constants towards H_2O_2 before it reaches higher concentrations.

H_2O_2 is produced mainly dismutation of superoxide but also many oxidases are capable to produce H_2O_2. In mitochondria and locations of NADPH Oxidases(NOXs) H_2O_2 is produced[15], [16]. Understanding production or scavenging of H_2O_2 allows scientist to understand basis of redox status of a cell.

Table 1: Enzymes producing H_2O_2 in cells.

Various enzymes were located inside different cells. Although there are more than 30 enzymes can produce H_2O_2, they can initially produce superoxide than superoxide converted to H_2O_2 rapidly. Moreover, there are enzymes that are capable to produce superoxide as well. ER: endoplasmic reticulum, PM: plasma membrane, M: mitochondria, N: nucleus, C: cytoplasm, G: golgi apparatus, L: lysosome, Px: peroxisome, S: secreted. Table is adapted from ref. [6]

Name	Abbreviation	Location	$O_2^{\bullet}$ Production
NADPH oxidase 4	NOX4	ER,PM, N	No
Dual oxidase 1	DUOX1	PM	No
Dual oxidase 2	DUOX2	PM	No
Superoxide dismutase [Cu-Zn]	SOD1	C, N, M	No
Superoxide dismutase [Mn]	SOD2	M	No
Extracellular superoxide dismutase [Cu-Zn]	SOD3	PM, S	No
Xanthine dehydrogenase/oxidase	XDH	C, PM, S	No
D-Amino acid oxidase	OXDA	Px	No
L-Amino acid oxidase	OXLA	L	No
D-Aspartate oxidase	OXDD	Px	No
Amiloride-sensitive amino oxidase (copper containing)	AOC1	S	No
ERO1-like protein-α	ERO1A	ER	No
ERO1-like protein-β	ERO1B	ER	No
Cytochrome P450 3A4	CP3A4	ER	Yes
Cytochrome P450 2D6	CP2D6	ER	Yes
Cytochrome P450 2E1	CP2E1	ER,M	Yes
Cytochrome P4504A11	CP4AB	ER	Yes
Aldehyde oxidase	AOX1	C	No
Amine oxidase (flavin-containing) A	AOFA	M	No
Amine oxidase (flavin-containing) B	AOFB	M	No
FAD-linked sulfhydryl oxidase ALR	ALR	C, M, S	No
Hydroxyacid oxidase 1	HAOX1	Px	No
Hydroxyacid oxidase 2	HAOX2	Px	No
Membrane primary amine oxidase	AOC3	PM	No
Peroxisomal Ni-acetylspermine/spermidine oxidase	PAOX	Px, C	No
Peroxisomal acyl-CoA oxidase 1	ACOX1	Px	No
Peroxisomal acyl-CoA oxidase 3	ACOX3	Px	No
Peroxisomal sarcosine oxidase	SOX	Px	No
Prenylcysteine oxidase 1	PCYOX	L	No
Prenylcysteine oxidase-like	PCYXL	S	No
Protein-lysine 6-oxidase	LYOX	S	No
Pyridoxine 5 '-phosphate oxidase	PNPO	C	No
Retina-specific copper amine oxidase	AOC2	PM, C	No
Spermine oxidase	SMOX	C, N	No
Sulfhydryl oxidase 1	QSOX1	G	No
Sulfhydryl oxidase 2	QSOX2	N, PM, S	No
Sulfite oxidase, mitochondrial	SUOX	M	No

Maintaining the concentration gradient of H_2O_2 is important due to its pivotal effect (**Figure 1.1**). In here, scientists provided two terms oxidative distress and oxidative eustress. First term is known for a long time where increase in ROS causing detrimental effects on biomolecules and cell signaling. Oxidative eustress is relatively novel term where presence of ROS at a certain level keeps homeostasis of redox signaling. Typically, intracellular concentration of H_2O_2 is around 1-10 nM range after this threshold is passed, cells experience oxidative stress[7], [17].

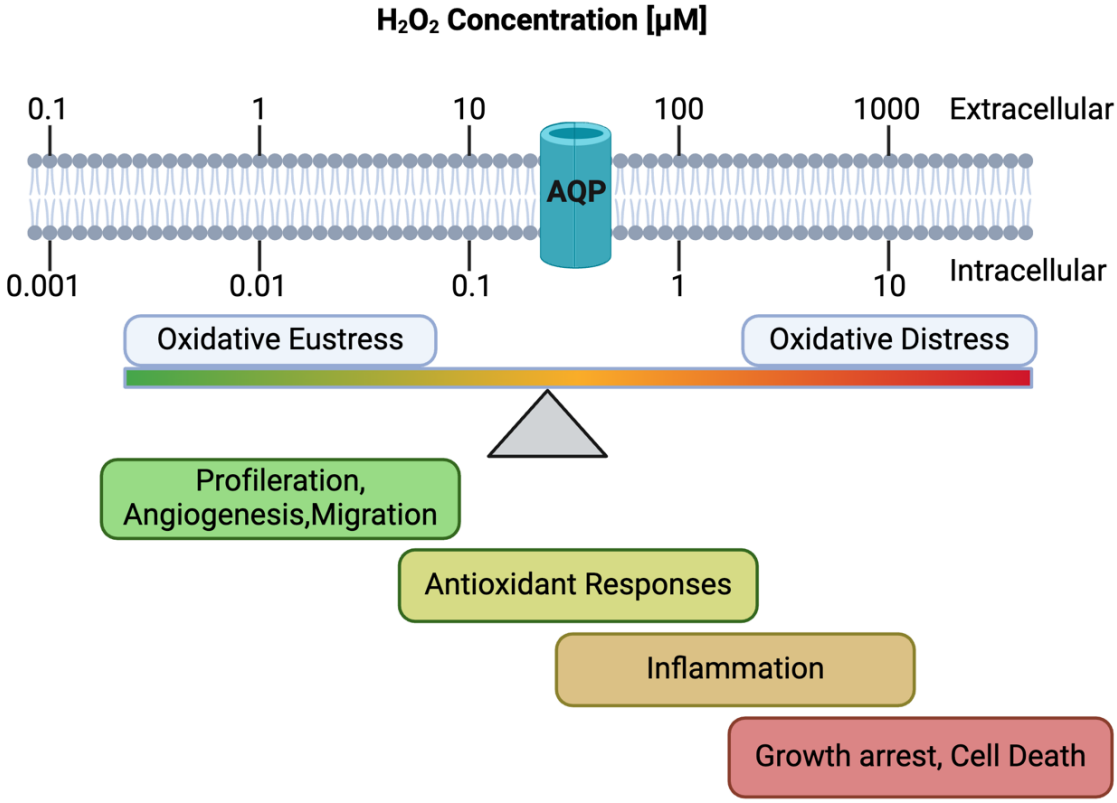

Figure 1.1 Concentration gradient of H_2O_2

Intracellular H_2O_2 concentration is maintained through a gradient between the extracellular and intracellular spaces, facilitated by aquaporins (AQP). At higher concentrations, H_2O_2 disrupts the cellular redox state, leading to oxidative stress over time. At low concentrations, H_2O_2 acts as a signaling molecule, but as concentrations increase, it triggers an antioxidant response. Prolonged exposure to elevated H_2O_2 levels results in oxidative stress and can ultimately lead to apoptosis.Adapted from ref [9].

Increase in H_2O_2 concentration initially affects the cysteine residues in many proteins. Cysteine has low pKa value, so this amino acid affected excessively via redox reactions[18]. Interaction of cysteine with H_2O_2 lead to formation sulfonate on cysteine residues to freely available sulfur group at cysteine[19]. Sulfenylation of cysteine residues causes higher reactivity of cysteine including sites such as sulfonic acid is highly

reactive which can form disulfide bonds with other molecules or neighboring cysteine moieties[20]. High concentration of H_2O_2 often lead to hyperoxidation of cysteine residues lead to formation of sulfinic or sulfonic acid which are irreversible changes on cysteine residue and signs of oxidative stress. An example to effect of cysteine modification on cell signaling is protein tyrosine phosphatases (PTP)[21]. They contain Cys residue in their active site and if oxidation occurs, they are inactivated and cell signaling shifts towards increased activity of protein tyrosine kinases (PTKs). If the PTPs are inactive PTKs takeover the cell signaling. Cysteines are important residues for proteins because they are mainly conserved in the active sites of proteins, and they are not abundant in the composition of proteins. These key residues are susceptible to redox reaction to maintain homeostasis in cell signaling. That's why H_2O_2 is important messenger molecule in cell signaling due to its high activity with cysteine residues. Oxidative distress or eustress comes in with the gradient of H_2O_2 [22]. First reaction of H_2O_2 with the cysteine residues are called reversible oxidation which can modulate the cell signaling. However, increased amount of H_2O_2 or burst of H_2O_2 lead to irreversible oxidations which can disrupt cellular homeostasis. For instance, H_2O_2 can lead either survival signaling or apoptosis depending on the intracellular concentration. Transient activation of JNK via low concentration of H_2O_2 lead to activation of NF-κB signaling for cell survival. However, over activation of JNK via high concentration of H_2O_2 lead to apoptosis[23].

In this study we mainly focused on the cell signaling part of H_2O_2 in endothelial cells. Endothelial cells are responsible for keeping the vessels intact and provide a barrier between blood flow and other organs. These cells are exposed to many stimuli due to their lining in blood flow. Among these stimuli, there are many studies involving ROS molecules affecting endothelial function[24].

Endothelial nitric oxide synthase (eNOS) plays a critical role in maintaining vascular health by producing nitric oxide (NO) in endothelial cells, which is essential for regulating vascular tone[25]. Dysfunction of eNOS is a major cause of several cardiovascular diseases. eNOS catalyzes the conversion of L-arginine to L-citrulline, with NO being a byproduct of this reaction[26]. This enzyme is composed of several domains,

including the N-terminal oxygenase domain, the calmodulin (CaM) binding domain, and the C-terminal reductase domain (**Figure 1.2**)

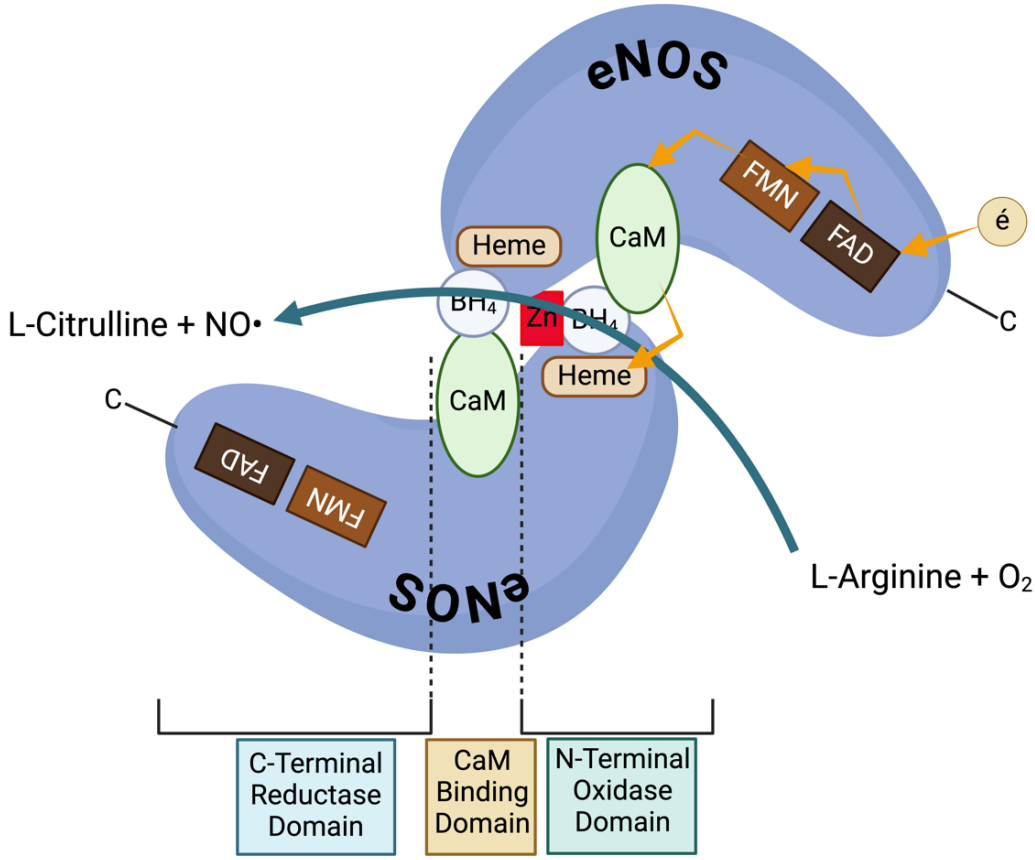

.

Figure 1.2 Domains of eNOS and NO Production.

eNOS has 3 domains: C-terminal reductase domain, CaM binding domain and N-terminal oxidase domain. eNOS monomers dimerize at a point where both monomer's oxidase domain contact. L-arginine and O_2 is converted to L-citrulline and NO. During the conversion electron flow is required. Electron flows through FAD, FMN, CaM and finally it's conveyed to opposing monomer's heme group.

eNOS activation requires dimerization, which is facilitated by calmodulin binding to the CaM binding domain. This binding is dependent on increased cytoplasmic calcium levels. During the conversion of L-arginine to L-citrulline, electrons are transferred through various cofactors to the heme center, enabling NO formation via molecular oxygen and oxidation reactions[27]. Key cofactors, such as nicotinamide adenine dinucleotide phosphate (NADPH), flavin mononucleotide (FMN), and flavin adenine dinucleotide (FAD), are located in the C-terminal reductase domain and interact with the N-terminal oxygenase domain of the opposing monomer. The N-terminal oxygenase

domain also contains a prosthetic heme group and binds (6R)-5,6,7,8-tetrahydrobiopterin (BH4), which interacts closely with cysteine residues near the heme group. Zinc supports the dimerization of eNOS monomers but does not participate in the catalytic function of eNOS[28].

The activity of eNOS is complicatedly linked to the redox state of the cell. The enzyme's catalytic core contains zinc thiolate residues, making it sensitive to redox changes. ROS can disrupt electron flow necessary for eNOS function and also ROS oxidize critical cysteine residues, preventing the dimerization of eNOS monomers[29]. In cases of eNOS uncoupling due to disrupted electron flow, eNOS can produce superoxide anions even oxygenase domain by itself can achieve[30]. This leads to a feedback loop where ROS-induced dysfunction of eNOS further increases ROS production.

NO is a crucial gaseous signaling molecule in various physiological processes, especially within the cardiovascular system. Its discovery and characterization have significantly advanced our understanding of endothelial cell function and vascular health. NO can be produced for different purposes within cells. It plays a role in neurotransmission and can be synthesized in large amounts in response to immune challenges[31]. In endothelial cells, NO is produced to maintain vascular tone and intracellular NO concentration is around 0.1 nM ranges up to 5 nM[32]. NO is a radical with a very short half-life, typically only a few seconds. Before NO was identified, it was referred as endothelium-derived relaxation factor (EDRF). Then, it has been realized that EDFR is NO in mammalian cells[33]. NO diffuses into the inner lining of blood vessels, where it activates soluble guanylate cyclase (sGC) to produce cGMP using GTP, leading to the relaxation of smooth muscle cells and vasodilation of the vessel[34].

The diffusion of NO can be influenced by several factors, with its bioavailability being the most critical. To enhance diffusion, eNOS is primarily located in the plasma membrane of endothelial cells. eNOS is also found in the Golgi apparatus, where its main function is to nitrosylate proteins that are trafficked to the Golgi for post-translational

modification[35]. Numerous studies have demonstrated that NO production is regulated by the phosphorylation of eNOS at multiple sites[36], with serine 1177 (S1177) being the most studied residue. The PI3K/Akt signaling pathway is one well-understood mechanism leading to eNOS phosphorylation and subsequent NO production[37]. However, some studies suggest that phosphorylation of eNOS does not always result in NO production, indicating that additional regulatory mechanisms are involved[38].

NO's role extends beyond normal physiological processes to include significant implications in pathophysiological conditions. Dysregulation of NO production and signaling is implicated in various cardiovascular diseases. Endothelial dysfunction, characterized by reduced NO bioavailability, is a hallmark of conditions such as hypertension, atherosclerosis, and diabetes[39]. In these diseases, oxidative stress and inflammation lead to a decrease in NO levels and impaired vasodilation, contributing to the progression of vascular damage. Superoxide formation decreases available NO due to reaction with NO to form peroxynitrite ($ONOO^-$)[40]. Superoxide reaction rate with NO is faster than its scavenging enzyme called superoxide dismutase (SOD). There are studies indicating that eNOS can be protective enzyme upon oxidative stress by producing NO to scavenge superoxide for less damaging radical peroxynitrite. However, peroxynitrite interacts and oxidizes one of the cofactors of eNOS, BH4, leading to eNOS uncoupling[29]. Then uncoupled eNOS produces superoxide then transforms into oxidative stress generating enzyme.

In hypertension, for example, impaired NO signaling results in increased vascular resistance and elevated blood pressure[41]. In atherosclerosis, reduced NO levels promote the development of atherosclerotic plaques by enhancing leukocyte adhesion and smooth muscle cell proliferation[42]. In diabetes, hyperglycemia-induced oxidative stress diminishes NO production, exacerbating endothelial dysfunction and increasing the risk of cardiovascular complications[43].

Although H_2O_2 has traditionally been studied as a toxic molecule, research has shown that it also functions as a signaling molecule. As a member of the reactive oxygen species

(ROS) family, H_2O_2 has a slower reaction rate compared to superoxide. Nitric oxide (NO) is produced via the activation of endothelial nitric oxide synthase (eNOS), but both eNOS activity and NO bioavailability can be negatively affected by ROS, including H_2O_2. However, numerous studies have demonstrated that H_2O_2 can activate eNOS through the activation of kinases such as protein kinase G (PKG), which can, in turn, activate other kinases like Akt to phosphorylate eNOS[44].

There are studies supporting both the inhibitory and activating effects of H_2O_2 on NO production. The intricate relationship between these two molecules remains elusive, largely due to the complexities of studying redox biology. Many redox-active molecules have short lifetimes and interact with numerous factors, making it challenging to elucidate their precise roles and interactions.

Challenges in Redox Biology

The field of redox biology is wide, encompassing the study of reactive molecules and their interactions with signaling pathways, proteins, and other cellular components. The primary challenge in redox biology is not the involvement of these molecules in various signaling pathways but the nature of the molecules themselves. Many redox molecules are free radicals, characterized by their short lifetimes and high reactivity, especially ROS and reactive nitrogen species (RNS). Additionally, these molecules can be harmful to cellular processes, necessitating the presence of an antioxidant defense system that rapidly eliminates free radicals or oxidized biomolecules. These swift reactions complex the detailed investigation of the sequential events in redox processes.

Current methodologies strive to address these challenges, aiming to understand the biological implications of redox reactions more thoroughly. However, despite advancements in technology, some key reactions and signaling pathways remain elusive due to challenges which can be physiological and technical challenges.

Physiologically, ROS molecules are highly reactive and have short half-lives, making their capture and identification challenging. The most studied ROS molecule, superoxide, has a half-life measured in milliseconds[45]. While technological advancements allow us to resolve reactions within this timeframe, superoxide is often not freely available even within milliseconds due to the cellular antioxidant systems that rapidly scavenge it with high-rate constants[7]. This makes resolving the interactions of superoxide particularly difficult. Moreover, ROS molecules can produce other ROS downstream; for example, superoxide is rapidly converted to the less reactive H_2O_2 by superoxide dismutase (SOD). However, H_2O_2 can subsequently lead to the production of superoxide through downstream signaling events, such as the uncoupling of eNOS[46], complicating the dissection of ROS effects on cellular signaling.

Researchers have also investigated the effects of ROS molecules, such as H_2O_2, on cells using supraphysiological concentrations[6]. While this approach is valid in certain contexts, such as immune reactions or inflammation[47], H_2O_2 functions as a signaling molecule at physiological concentrations, like other secondary messengers. Studies using high concentrations of H_2O_2 can yield controversial results due to the difficulty in mimicking physiological conditions accurately. Physiological conditions are challenging to determine because of the ultra-local redox hotspots within cells. For example, many studies administer high concentrations of H_2O_2 to cells to study oxidative stress signaling, yet intracellular H_2O_2 concentrations vary across different compartments even within the single organelle like mitochondria[7]. Consequently, local production in specific redox hotspots cannot be adequately investigated by supplying exogenous H_2O_2 both in vivo and in vitro.

Signaling often occurs in specific cellular compartments and is relayed through kinase activation or transmission via less toxic species such as lipid peroxides[48]. During these processes, the signal is amplified, broadening the effect and making it harder to understand the initial activation. Additionally, many redox-related enzymes can produce both superoxide and H_2O_2. Given that superoxide is converted to H_2O_2 almost

instantaneously, investigating the local effects of ROS is challenging due to the molecular dynamics involved.

As we transition to the technical challenges, it's important to recognize that addressing these physiological complexities is fundamental for advancing our understanding of redox biology. Technological advancements are essential to overcome these hurdles, enabling more precise and accurate studies of redox processes.

ROS and RNS are highly reactive, making them difficult to capture and measure accurately. Various techniques have been developed to measure these molecules with precision. In our study, we focus on two specific molecules: H_2O_2 and NO. The primary technical challenges lie in the selectivity of the measurement methods. Due to the high reactivity of ROS and RNS, a single method can often detect multiple species simultaneously. For example, H_2O_2 can be measured using Amplex Red, a Horseradish peroxidase (HRP)-oxidizing substrate. However, the presence of superoxide can inactivate Amplex Red, complicating the measurement process[49]. These two molecules can coexist in a single signaling event, further challenging their selective detection. Another example related to NO measurement involves Diaminofluorescein (DAF), a fluorescent dye used for detecting NO. Intracellular ascorbic acid, homocysteine, or reduced glutathione (GSH) can interfere with DAF, decreasing the dye's sensitivity to the millimolar range, which is not a physiological concentration for NO.[50].

To understand the relationship between these two molecules, a method that can be applied intracellularly under physiological conditions is needed. Phenylboronate probes can measure intracellular H_2O_2, but they lack sufficient sensitivity and react slowly with H_2O_2. Additionally, boronate probes react more quickly with other oxidants, such as peroxynitrite, necessitating the use of inhibitors to prevent the formation of peroxynitrite for accurate detection of H_2O_2, which is not suitable method to use for understanding H_2O_2 and NO relationship due to inhibitors prevent formation of NO.

Moreover, there are methods like chemiluminescence, electron parametric resonance (EPR) for NO detection. However, these methods are not suitable for intracellular

detection of NO due to toxicity and low spatial resolution[51], [52]. These methods are relatively old. Biochemical methods, such as the Griess assay, are also used to measure NO, but they cannot directly detect cellular NO levels. There are fluorescent probes that can measure NO directly, such as DAF, diaminorhodamines, and metal-based NO sensors. However, these sensors have disadvantages, including accumulation within cells, lower sensitivity, and potential toxicity [50].

Besides biochemical methods or chemical dyes, genetically encoded biosensors offer high selectivity and high spatial resolution due to their genetic encoding. Genetically encoded biosensors consist of two basic domains. The first domain is a reporter domain that includes a fluorescent protein. The second domain is a sensing domain that is sensitive to the analyte of interest. Genetically encoded biosensors for H_2O_2 detection rely on a dithiol switch[53], where two cysteine moieties form a disulfide bridge in the presence of H_2O_2. This switch leads to a change in the fluorescence intensity of the reporter domain. There are many H_2O_2 specific genetically encoded biosensors but HyPer and roGFP families were the most used ones in redox biology especially recent version of HyPer, HyPer7 [54] and peroxiredoxin based roGFP2[55].

For NO measurements, there are a few genetically encoded biosensors, with only one that can directly measure NO. Biosensors such as NOA-1, sNOOPy, and pnGFP indirectly measure NO levels by detecting cGMP, nitrite/nitrate, or peroxynitrite, respectively[56]. The geNOPs biosensor can directly measure NO due to its NO-specific sensing domain derived from bacteria[57].

Genetically encoded biosensors allow high spatial resolution for short-lived molecules, and they are non-invasive methods concerning the side-effects of biochemical methods. For that purpose, we utilized these powerful tools to identify relationship between H_2O_2 and NO

Objectives and Scope of the Research

The primary objective of this study is to elucidate the relationship between H_2O_2 and NO using genetically encoded biosensors. This relationship has been a longstanding enigma in the field of redox biology due to various technical and methodological challenges. Our initial aim was to develop a robust live-cell imaging method to investigate this relationship in real-time.

Firstly, we focused on developing and optimizing imaging tools. This involved optimizing HyPer imaging for visualizing local H_2O_2 dynamics and enhancing the functionality of the chemogenetic tool mDAAO for mimicking localized H_2O_2 production. Additionally, we aimed to refine the use of the geNOp biosensor, developed in our laboratory, for accurate NO detection. Next, we sought to investigate the effects of localized H_2O_2 production on NO dynamics. By utilizing mDAAO and geNOp, we aimed to understand the direct interaction between chronically produced localized H_2O_2 and NO in endothelial cells. After that we sought for the development of a dual-biosensor endothelial cell line that simultaneously expresses both HyPer and geNOp, enabling the concurrent measurement of H_2O_2 and NO for direct relationship of these molecules. We also recognized the need for optimizing multiparametric imaging to ensure accurate and reliable measurement of both analytes. This involved addressing challenges related to selectivity, sensitivity, and signal resolution in live-cell imaging.

In order to measure these molecules under physiological conditions we showed the influence of ambient O_2 levels. We compared the physiological O_2 conditions with regular room air conditions while measuring H_2O_2 and NO using double stable cells expressing HyPer and geNOps.

CHAPTER II: OPTIMIZATIONS OF MEASURING AND PRODUCTION IN HYDROGEN PEROXIDE USING GENETICALLY ENCODED BIOSENSORS AND CHEMOGENETIC TOOLS

Measuring H_2O_2 using HyPer biosensor

In 2006, first generation of HyPer biosensor was introduced. On the basis of designing genetically encoded biosensors, initial design of HyPer is based on using circularly permuted yellow fluorescent protein (cpYFP) as a reporter domain and *Escherichia Coli* derived OxyR domain inserted in cpYFP as a sensing domain[58]. OxyR serve as H_2O_2 sensitive regulatory protein. It contains two domains: H_2O_2 sensing domain (Regulatory Domain, RD) and DNA binding domain. Through genetic engineering only H_2O_2 domain is used and inserted to cpYFP. In the presence of H_2O_2, sensing domain causes conformational change due to cysteines in this domain. Then, OxyR is capable to bind DNA. H_2O_2 sensing domain of OxyR contains two specific cysteine residues in a hydrophobic pocket, C199 and C208[59]. Upon oxidation of C199, disulfide bridge forms with C208 and then conformational change occurs. Amplitude of conformational change is high in the flexible region of OxyR-RD residues 205-222. This region is important because conformational change can lead an increase in fluorescence intensity of cpYFP. These residues are potential insertion site for cpYFP. Highest responsive clone of OxyR-RD-cpYFP-OxyR-RD chimera is selected and expressed in cells. This chimera is

observed as ratiometric containing two excitation peaks at 420 nm and 500 nm, one emission peak at 530 nm wavelengths. **Figure 2.1** shows the design of HyPer.

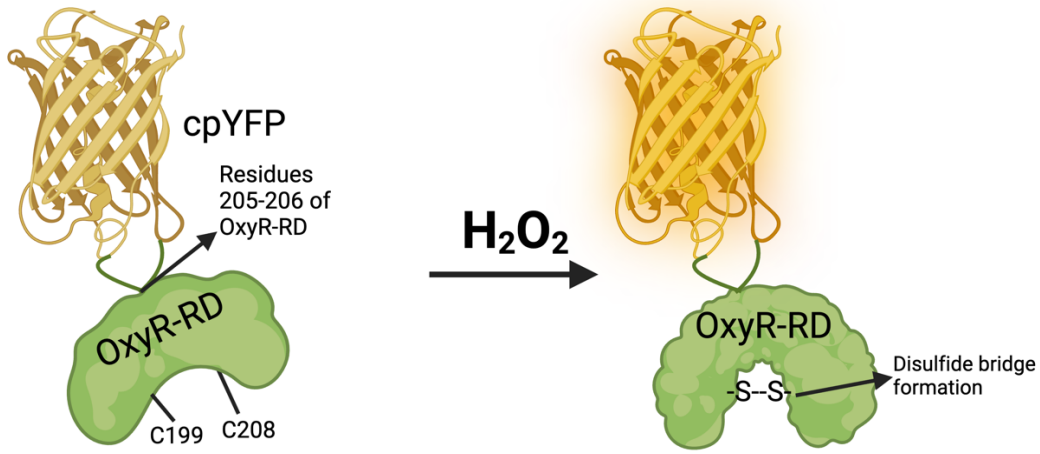

Figure 2.1:First generation of HyPer oxidized in the presence of H_2O_2.

HyPer biosensor contains two elements. One is reporter domain consisting of cpYFP, second one is sensory domain consisting of H_2O_2 sensitive and *E.Coli* derived OxyR-RD. cpYFP is inserted to OxyR's 205 and 206 residues with a short amino acid linkers. OxyR-RD contains two specific cysteine molecules in a hydrophobic pocket. Upon oxidation with H_2O_2 these two cysteines form disulfide bridge.

Other versions of HyPer were introduced until today. After first generation of HyPer, a new version was developed, HyPer3. Mutations were introduced in OxyR-RD led to increase in dynamic range of a biosensor. By means of dynamic range, amplitude of the signal in response to H_2O_2 and also returning of a signal upon retrieval of H_2O_2 are significantly advanced[60]. This improvement allows HyPer to detect signals with a higher resolution. Mutation points were provided in the research article and mainly mutations were introduced considering dimerization interface of OxyR which affects conformational change of OxyR.

Next, HyPer Red is introduced due to spectral properties of earlier versions. Many of the genetically encoded biosensors, including HyPer, and roGFP for redox measurements, have similar spectral properties and many of them contains single fluorophore mostly GFP. Spectrally distinct biosensors are required to monitor different analytes simultaneously[61]. Thus, HyPer Red is developed by changing cpYFP with red fluorescent protein, mApple, previously developed in Ca^{2+} biosensor R-GECO1[62]. Although dynamic range is less improved compared to HyPer3 but the performance of HyPer Red is comparable with previous versions.

In 2020, latest version of HyPer was developed and called HyPer7[54]. The reason behind the development is older versions of HyPer are sensitive to pH changes and also, they are sensitive to high concentrations of H_2O_2. pH changes can be controlled via HyPer's mutant version where C199S mutation is introduced. However, due to physiological strong stimuli such as cytokines or apoptosis, high concentration of H_2O_2 can be present in the cell. On top of that, if cellular redox state is high, biosensor is already saturated, and no visible response is obtained. Thus, there is a requirement for higher dynamic range compared to older versions of HyPer. For the new version of HyPer, first sensing domain is selected from 11 bacterial species and among them OxyR-RD from *Neisseria meningitidis* was most responsive when cpYFP is inserted in position 126-127. In the experiments, new version of HyPer was responsive to 2 μM H_2O_2 in living cells. To overcome pH sensitivity various mutations were introduced in cpYFP and these mutations enhanced the brightness of HyPer around ~15-17-fold. Mutations led cpYFP to have identical chromophore with wild type GFP. New version HyPer is called HyPer7. Similar to HyPer1, Hyper7 has two excitation peaks at 400 nm and 499 nm and one emission peak at 516 nm enabling ratiometric imaging. In the study of HyPer7, it allowed scientist to determine H_2O_2 locally.

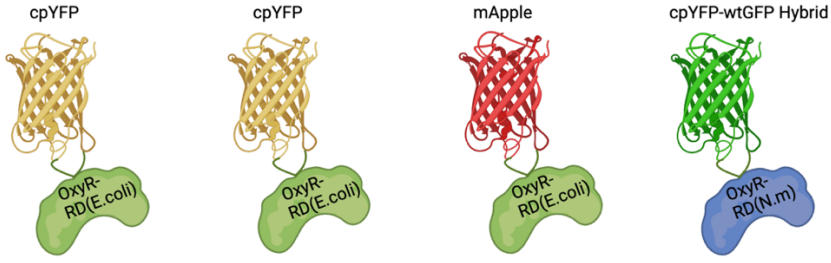

	HyPer 1	HyPer 3	HyPer Red	HyPer 7
Readout	Ratiometric (F400/500)	Ratiometric (F400/500)	Single Channel (F575)	Ratiometric (F400/500)
pH Dependency	Yes	Yes	Weak	Weak
Fold Change	3 ± 0.4 Fold	6 ± 0.4 Fold	2 ± 0.2 Fold	15-17 Fold

Figure 2.2 Comparing the versions of HyPer Probes.

From HyPer1 to HyPer7 various versions of HyPer probes were introduced. Until HyPer7, H_2O_2 sensing domain OxyR-RD derived from E.coli and subjected mutations. Hyper7 contains OxyR-RD of N.meningitidis. Readout, pH dependency and fold change (dynamic range) are compared. Latest version of HyPer is far improved than the initial version of HyPer within 2 decades.

The development and utilization of the genetically encoded biosensor HyPer have significantly advanced our understanding of redox signaling, offering several advantages such as the ability to target the biosensor to different cellular compartments, providing a reversible signal, diverse spectral properties, and ratiometric readouts that facilitate accurate concentration measurements. A notable study using HyPer7 revealed the existence of an H_2O_2 gradient between the cytosol and mitochondria, underscoring the crucial role of peroxiredoxins in maintaining this gradient between cellular compartments[63]. Additionally, an innovative study employed HyPer7 to tag the proteome, enabling the detection of ultra-local H_2O_2 changes and offering a deeper understanding of localized redox dynamics[64]. The genetic encoding of HyPer has thus paved the way for precise measurements of local redox shifts. Advancements in the design and application of HyPer have enhanced our ability to measure these shifts with increased speed and minimal disruption, thereby facilitating more detailed and accurate investigations into redox biology.

Development of co-culture-based imaging method using HyPer7 in endothelial cells

One of the key advantages of using genetically encoded biosensors is their ability to be precisely targeted within cells. Redox reactions, particularly those involved in signaling, occur in specific cellular compartments, each with a unique redox tone[7]. To measure local redox molecules via redox probes has some disadvantage due to factors such as molecular crowding and local pH variations can influence the sensitivity of probes, but many studies were performed to understand signaling pathways[65][66]. Technical limitations in visualization methods complicate the understanding of differential signals. For example, due to visible spectrum range, up to 3 different biosensors can be visualized in a simple fluorescence microscope. There are techniques to overcome this issue like MOSAIC[67], capable of utilizing up to 20 different biosensors in a single field of view, have been developed to address these issues. Acquiring multiple parameters in a single field of view increase and facilitates our

understanding in cellular signaling. Differential and simultaneous measurement of H_2O_2 necessitates the use of more than one biosensor, with each needing to be spectrally distinct to avoid interference. While HyPer Red and HyPer7 are spectrally distinct, their differing kinetics and dynamics present additional challenges[54], [61]. The broad application of multiparametric imaging in redox biology still requires more user-friendly methodologies.

In this study, we aimed to investigate H_2O_2 signaling in endothelial cells using genetically encoded biosensors. We selected the EA.hy926 cell line as our endothelial cell model, derived from the hybridization of HUVEC and A549 cell lines, resulting in a well-characterized and immortalized endothelial cell line. However, transient transfection methods proved inefficient for expressing biosensors in these cells. To address this, we generated a cell line stably expressing the biosensors. Genetic encoding allowed us to target biosensors to specific cellular compartments. Thanks to Vsevolod Belousov, the inventor of HyPer7, we had access to differentially targeted HyPer7 biosensors. In this study, we utilized cytosol-targeted HyPer7 (H.7-NES), nuclear-targeted HyPer7 (H.7-NLS), and mitochondria-targeted HyPer7 (Mito-H.7) to investigate compartment-specific H_2O_2 signaling in endothelial cells. Using certain localization signals added to N or C termini of the biosensors will locate them in a specific compartment. For cytosolic measurement HyPer7 is tagged with C-terminal nuclear export signal (NES), H.7-NLS measures H_2O_2 in nucleus via tagging with nuclear localization signal (NLS) and for mitochondrial measurement COX8 tandem is added to N-terminus of HyPer7. Expression and localization of the HyPer7 constructs were validated. Images and plasmid designs of differentially located HyPer7 is shown in **Figure 2.3**.

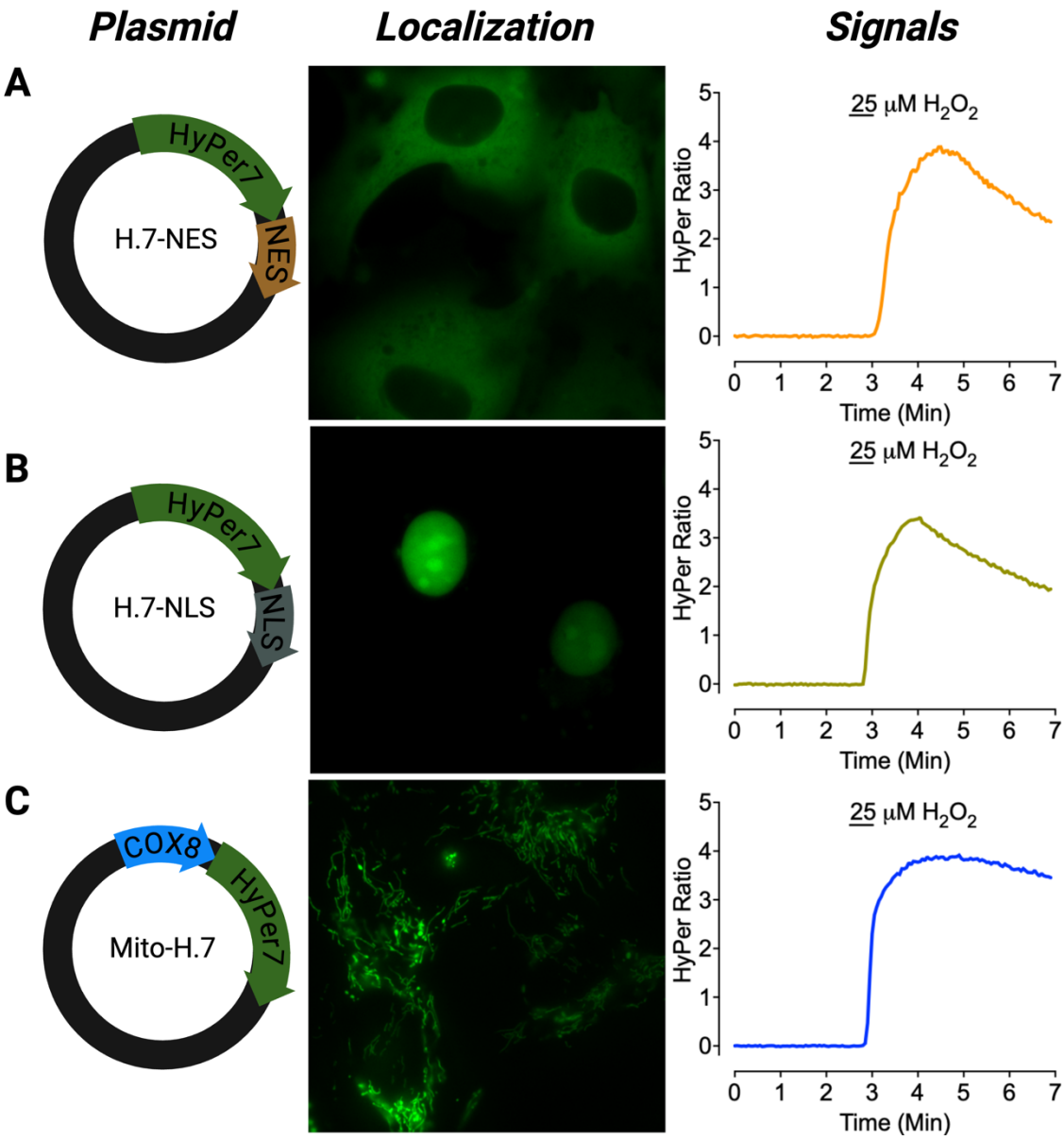

Figure 2.3: Functionality of differentially located HyPer7.

Panels demonstrate design of plasmid, fluorescence image of EA.hy926 cell expressing HyPer7 for localization and real-time signals from cells expressing HyPer7 in response to 25 µM H_2O_2. First panel shows H.7 plasmids contains Hyper7 and NES**(A)** or NLS**(B)**, signal sequence is added to C-terminal of HyPer7 to provide cytosolic or nuclear location respectively. For Mito-H.7 COX8 tandem is placed into N-terminal to provide mitochondrial location **(C)** Middle panel shows the representative images of EA.hy926 cells expressing H.7-NES **(A),** H.7-NLS **(B),** Mito-H.7 **(C)** respectively. Images obtained using 475 nm excitation light and emission is collected at 525 nm (HyPer High Setup). Last panel shows the real time traces of cells expressing H.7 NES (Orange line) **(A)**, H.7-NLS (Green line) **(B)** or Mito-H.7 (Blue line) **(C)** while 25 µM H_2O_2 is provided then withdrawn as indicated respectively. All experiments performed in triplicate and 30 cells were selected for analysis in each experiment.

Following the functionality tests, our objective was to develop a cell line stably expressing different H.7 probes due to the technical challenges associated with transient transfection methods[68]. For this purpose, the open reading frames (ORFs) of H.7-NES, H.7-NLS, and Mito-H.7 were used for molecular cloning to transfer these ORFs into lentiviral expression vectors. Specifically, we selected the pLenti-MP2 vector and replaced its ORF with the H.7 sequences. After verifying the molecular cloning, the resulting plasmids were designated as pLenti-H.7-NES, pLenti-H.7-NLS, and pLenti-Mito-H.7, respectively. To produce lentivirus carrying the H.7 ORFs, we employed a second-generation lentivirus production system. This system utilizes three plasmids for the transfection of HEK293 cells. The first plasmid, known as the packaging plasmid, contains the ORFs of gag and pol. The second plasmid, termed the envelope-encoding plasmid, contains the ORFs of the HIV envelope protein VSV-G. The third plasmid, the transfer plasmid, contains the ORFs of the H.7 probes. This setup ensures efficient production of lentivirus capable of stable integration and expression of the H.7 probes in target cells (**Figure 2.4**).

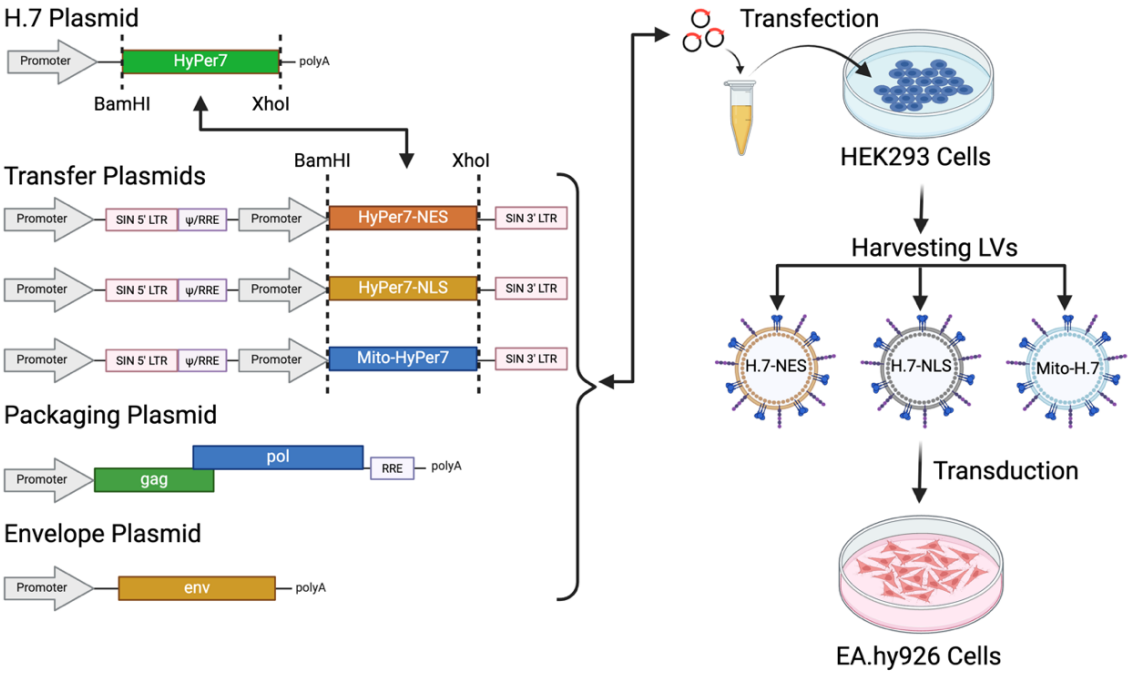

Figure 2.4:Production lentivirus encoding HyPer Constructs.

Each Hyper ORFs cloned into transfer plasmids. Along with packaging and envelope plasmids HEK293 cells are transfected individually. After 48-72h lentiviral particles for each HyPer construct are harvested and transduced to EA.hy926 cells.

After obtaining the lentiviral particles, EA.hy926 cells were transduced, and the expression of each HyPer probe was routinely monitored using a fluorescence microscope. Positive cells were observed 24-72 hours post-transduction. To select the positive cells, fluorescence-activated cell sorting (FACS) was employed. We selected the top 30% of expressing cells rather than isolating a single clone to achieve a variable population.

We successfully obtained EA.hy926 cells individually expressing HyPer constructs in the cytosol, nucleus, and mitochondria. To investigate the H_2O_2 dynamics in each compartment individually, our lab developed a strategy to co-culture all cell types equally within a single field of view. Conducting individual experiments for each compartment would be time-consuming and result in non-identical conditions for the cells. Therefore, to visualize all three compartments under identical conditions, EA.hy926 cells expressing H.7-NES, H.7-NLS, and Mito-H.7 were mixed equally before seeding the plate for experiments. Under the fluorescence microscope, the cells were visualized, and an equal mixture of cells was observed. The number of cells expressing differentially localized H.7 was not significantly different (**Figure 2.5A** and **B**, respectively).

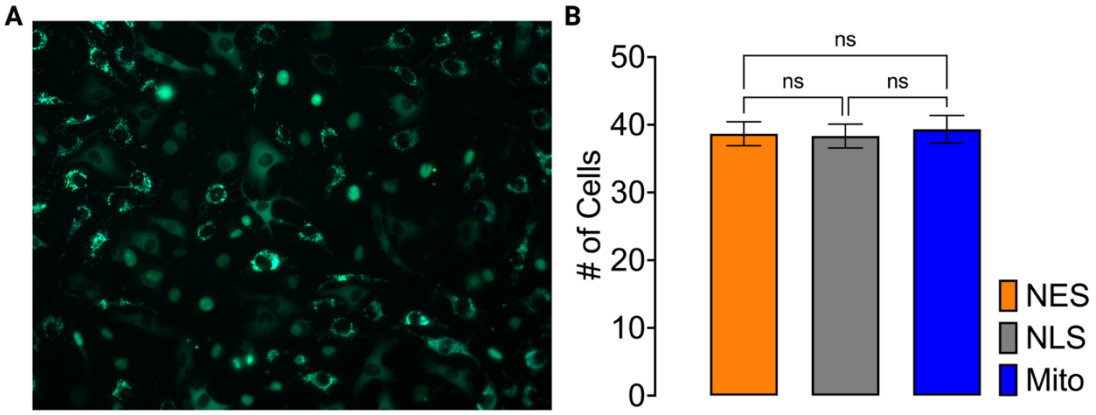

Figure 2.5: Visualizing differentially located HyPer7 in a single field of view.

(A) EA.hy926 cells stably expressing H.7-NES, H.7-NLS and Mito-H.7 were equally mixed for experiments. Representative image of co-cultured cells under fluorescence microscope visualized using 20x objective **(B)** Bar plot demonstrates average number of cells expressing H.7-NES (Orange bar), H.7-NLS (Grey bar) and Mito-H.7(Blue bar) in different fields of view (n=3). Data presented as mean ± SEM. For statistical significance one-way ANOVA and Tukey's multiple comparison posttest applied to compare each column.

Co-culturing EA.hy926 cells expressing differentially localized HyPer7 resulted in an equally mixed population, with no artifacts observed in the fluorescence images. During the experiments, our initial aim was to measure basal H_2O_2 levels by comparing the basal ratios of HyPer7. The basal ratio is calculated by taking the ratio of HyPer7 signals under resting conditions without the addition of any chemicals. Cells under identical conditions showed similar basal ratios, except for the mitochondrial basal ratio, which was lower compared to other compartments (**Figure 2.6A**). Furthermore, variations in the basal ratio were observed in all compartments, with the mitochondria exhibiting the highest variations, as indicated by the standard deviation error bars (**Figure 2.6A**). Mitochondria are one of the most active compartments in terms of redox reactions, which may result in high variations between different cells. This underscores the potential redox variations that can occur between different cellular compartments.

Subsequently, we investigated H_2O_2 dynamics by providing H_2O_2 extracellularly. Extracellular provision of H_2O_2 demonstrates the kinetics of H_2O_2 entry into the cell. Initially, a low concentration of H_2O_2 was provided to the cells and then withdrawn. After a certain period, a second provision of 500 μM H_2O_2 was administered to observe the signals in different compartments in response to low or high concentrations of H_2O_2 (**Figure 2.6B**). Providing a low concentration of H_2O_2 elicited a robust response in each compartment. However, the fold change in the HyPer7 response was higher in the mitochondria compared to other compartments indicating that H_2O_2 is trafficked more towards mitochondria (**Figure 2.6C**). When the cells were challenged with a high concentration of H_2O_2, the nuclear and cytosolic responses were similar, but the mitochondrial response was higher (**Figure 2.6D**). This could be due to mitochondrial H_2O_2 levels not returning to their basal levels before providing H_2O_2.

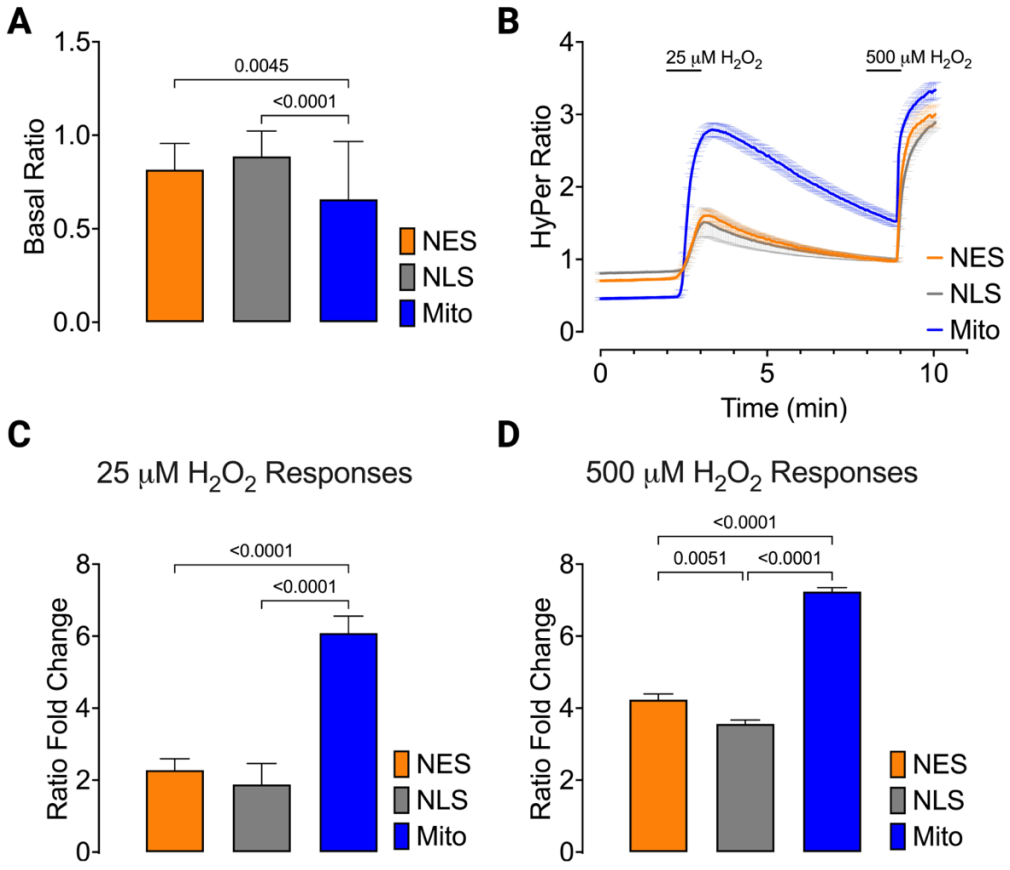

Figure 2.6: Extracellular application of H_2O_2 demonstrated localization specific redox responses.

(A) Bar plot represents basal ratio of EA.hy926 cells expressing H.7-NES (orange bar), H.7-NLS (grey bar) and Mito-H.7 (blue bar) under resting conditions. Data presented as mean ± SD, one-way ANOVA and Tukey's multiple comparison test applied to compare all columns. p-values are indicated on top of the bars if p-value < 0.05. **(B)** Traces indicate Hyper7 signals of cells expressing H.7-NES (orange line), H.7-NLS (grey line) and Mito-H.7 (blue line). Cells were provided with 25 µM and 500 µM H_2O_2 as indicated after each provision H_2O_2 was removed by changing the imaging medium (n=3). **(C)** Bar plot represents HyPer7 ratio fold change of cells expressing H.7-NES (orange bar), H.7-NLS (grey bar) and Mito-H.7 (blue bar) upon provision of 25 µM H_2O_2 or **(D)** 500 µM H_2O_2 . Data presented as mean ± SEM, one-way ANOVA and Tukey's multiple comparison test applied to compare all columns. p-values are indicated on top of the bars if p-value < 0.05 (n=3)

After understanding the redox variations in different cellular compartments, including the amplitude of the signals and the initial redox state of the cells, the next step in our experimental system was to compare the redox kinetics of each compartment. Analyzing the live-cell imaging data provided insights into the rate at which H_2O_2 entered each

compartment and how quickly H_2O_2 was scavenged. The scavenging rate of H_2O_2 is a crucial indicator of the redox tone of a cellular compartment.

Using our experimental setup, we obtained fluorescence images every three seconds. This time resolution allowed us to pinpoint the entry of H_2O_2 into each compartment accurately. Surprisingly, upon provision of 25 µM H_2O_2, mitochondria were the first compartment to encounter H_2O_2, as evidenced by the initial fluorescence signals. This rapid response in mitochondria may be attributed to their high metabolic activity and dynamic redox environment. In contrast, when 500 µM H_2O_2 was provided, all compartments responded similarly, indicating a more uniform distribution of H_2O_2 at higher concentrations (**Figure 2.7A** and **B**).

Investigating the kinetics of each HyPer probe provided valuable information about the entry and scavenging rates of H_2O_2. For the initial entry, we compared the rate of HyPer7 ratio changes in each compartment. The results demonstrated that mitochondrially located HyPer7 captured H_2O_2 more quickly compared to other compartments (**Figure 2.7C**). Nuclear entry was slower compared to cytosolic entry, but the difference was not statistically significant. This can be hypothesized based on the close-up signals (**Figure 2.7A**), where the initial signals were observed in Mito-H.7. Following the withdrawal of H_2O_2, compartment-specific H_2O_2 scavenging proteins would act to eliminate H_2O_2. To understand the reversal kinetics, we analyzed the rate of decrease in H.7 signals for each compartment. The removal of H_2O_2 from mitochondria was significantly faster compared to other compartments. Nuclear removal was slower compared to cytosolic removal, though not significantly different (**Figure 2.7D**). Additionally, the removal of H_2O_2 was much slower compared to its entry, indicating a distinct difference in the dynamics of H_2O_2 handling within cellular compartments.

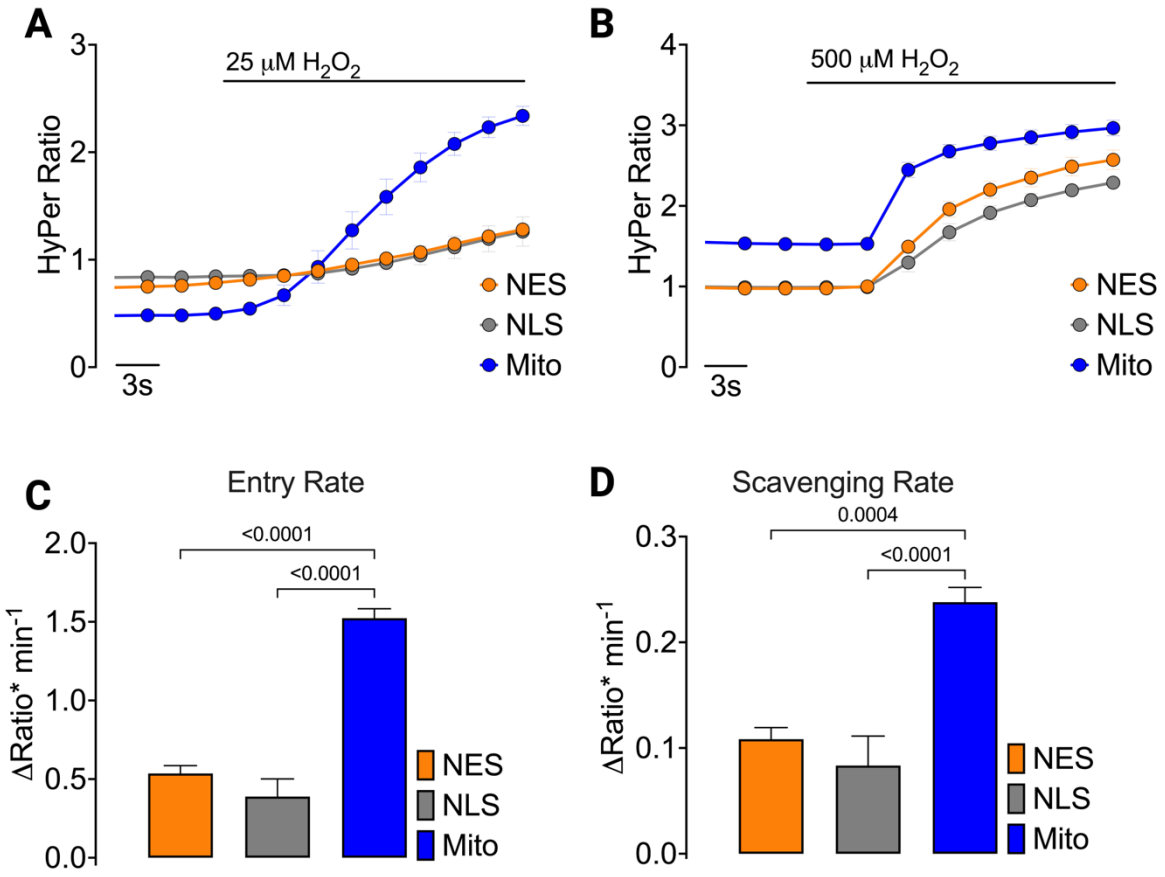

Figure 2.7: Kinetics of HyPer7 signals in different compartments.

(A) Close-up curves in Figure 2.6B in the presence of 25 μM H_2O_2. Time points represent H.7-NES (orange line with dots), H.7-NLS (grey line with dots), Mito-H.7 (blue line with dots) responses. Time scale represents 3s. **(B)** Close-up curves in Figure 2.6B in the presence of 500 μM H_2O_2. Time points represent H.7-NES (orange line with dots), H.7-NLS (grey line with dots), Mito-H.7 (blue line with dots) responses. Time scale represents 3s. **(C)** Bar plot represents rate of change in HyPer ratio when cells challenged with 25 μM H2O2. Bars represent average increase rate of HyPer signals in cells expressing H.7-NES (orange bar), H.7-NLS (grey bar) and Mito-H.7(blue bar). **(D)** Bar plot represents rate of change in HyPer ratio after withdrawal of 25 μM H_2O_2. Bars represent average decrease rate of HyPer signals in cells expressing H.7-NES (orange bar), H.7-NLS (grey bar) and Mito-H.7(blue bar). Data presented as mean ± SEM, one-way ANOVA and Tukey's multiple comparison test applied to compare all columns. p-values are indicated on top of the bars if the p-value < 0.05 (n=3)

In two decades, HyPer is developed and final HyPer probe is called HyPer7. This probe is highly selective and sensitive for H_2O_2 to monitor intracellular H_2O_2 dynamics[54]. The application of genetically encoded HyPer7 biosensors has significantly advanced our understanding of compartment-specific H_2O_2 dynamics in endothelial cells. By co-culturing EA.hy926 cells expressing differentially localized HyPer7, we prepared an equally mixed population, allowing for accurate comparisons across cellular compartments without the introduction of artifacts (**Figure 2.5**). Initially, measurements of basal H_2O_2 levels revealed that while the cytosolic and nuclear compartments displayed similar basal ratios, the mitochondrial basal ratio was notably lower and exhibited greater variability (**Figure 2.6**). This is expected while considering the mitochondria's role as a primary site for redox reactions, which essentially results in higher fluctuations in redox state compared to other compartments. Moreover, we provided extracellular H_2O_2 at low and high concentrations yielded highest amplitude of response in mitochondria as well in live-cell imaging experiments.

Our investigation into the redox kinetics of each compartment using live-cell imaging provided further insights into the dynamics of H_2O_2 entry and scavenging. The temporal resolution of our imaging setup, capturing fluorescence signals every three seconds, allowed us to precisely monitor the rate of H_2O_2 entry. Upon provision of 25 µM H_2O_2, mitochondria were the first to show a response, indicating a rapid influx of H_2O_2 (**Figure 2.7**). This rapid response could be attributed to contact points of mitochondria with plasma membrane[69]. In contrast, when a higher concentration of 500 µM H_2O_2 was administered, the responses across all compartments were similar but mitochondria response was faster. This suggests a more uniform distribution of H_2O_2 in cellular compartments at elevated levels. Thus, we cannot distinguish redox differences using high concentrations of H_2O_2 in further redox studies.

Analyzing the kinetics of HyPer7 probes provided crucial information about the rates of H_2O_2 entry and scavenging in different compartments. The mitochondrially localized HyPer7 captured H_2O_2 more quickly than the nuclear and cytosolic HyPer7. This observation was supported by the initial signals recorded in close-up graphics, which showed a faster response in Mito-H.7. As we mentioned earlier this can be due to contact

points of mitochondria with plasma membrane which facilitates communication and signaling between these parts of the cells [69]. There are studies that demonstrate mitochondria has contacts with endoplasmic reticulum (ER) via mitochondria-ER cortex anchor protein (MECA) also mitochondria have contacts with caveolae which is invagination of plasma membrane where many signaling events occur [70]. Additionally, the rate of H_2O_2 scavenging differed significantly among compartments. Mitochondria exhibited the fastest H_2O_2 removal, followed by the cytosol and then the nucleus. The removal of H_2O_2 was generally slower than its entry, highlighting the distinct kinetics of H_2O_2 handling within cellular compartments.

These findings underscore the importance of compartment-specific redox dynamics in cellular signaling and stress responses. The rapid uptake and removal of H_2O_2 in mitochondria reflect their crucial role in redox homeostasis and oxidative stress management. The observed differences in kinetics also suggest that mitochondria have a more robust system for managing H_2O_2 levels, which may be essential for their function as cellular powerhouses and sites of intense metabolic activity. Production of H_2O_2 in mitochondria is higher due to superoxide formation during electron transport in ETC. However, there is specific enzyme located in mitochondria to scavenge H_2O_2 like peroxiredoxin 3 (Prx3) and peroxiredoxin 5(Prx5) to maintain H_2O_2 balance[71]. Unlike entering of H_2O_2, mitochondria are also responsible for trafficking H_2O_2 outside of the mitochondria such as cytosol, nucleus or plasma membrane[72]. High redox activity in mitochondria necessitates fine-sequestering of H_2O_2 between compartments to prevent disruption of redox signaling.

The experimental approach of co-culturing cells expressing differentially targeted HyPer7 biosensors allowed us to observe redox events under identical conditions, providing a more accurate representation of intracellular H_2O_2 dynamics. This method overcomes the limitations of individual compartment experiments, which can introduce variability due to differing experimental conditions.

Overall, the use of genetically encoded HyPer7 biosensors has provided new insights into the compartmentalized nature of redox signaling within endothelial cells due to spatiotemporal resolution capability. Understanding these dynamics is critical for elucidating the roles of H_2O_2 in cellular function and pathology, and for developing targeted therapeutic strategies to modulate redox states in specific cellular compartments.

Local production of H_2O_2 utilizing chemogenetic tool called mDAAO

Redox signaling occurs in various locations within the cell, with redox molecules such as H_2O_2 acting as signaling agents to relay redox changes. However, the concentration of these molecules is tightly regulated to prevent unnecessary signaling events, as elevated levels can be detrimental to cells[22]. H_2O_2, a relatively stable ROS and signaling molecule, has traditionally been studied by providing it extracellularly. However, there is an approximately 100-fold gradient between intracellular and extracellular H_2O_2 concentrations[6]. To observe the effects of H_2O_2, scientists often use supraphysiological concentrations, which may not accurately reflect physiological conditions. Enzymes that produce ROS, including H_2O_2, are localized in specific cellular compartments and generally do not exert widespread effects[6]. Local production of H_2O_2 initiates redox signaling by modifying critical cysteine residues on proteins, leading to their activation or inhibition in signaling cascades, thereby relaying the redox signal[73].

Providing extracellular H_2O_2 has some relevance in studying ROS signaling, particularly in contexts such as inflammation[47]. However, to study redox homeostasis within specific organelles, such as mitochondria, spatial production of H_2O_2 is required. Extracellular provision of H_2O_2 can have systemic effects, influencing cytosolic and membrane-related redox mechanisms and potentially causing contradictory results between studies[74][75]. Therefore, dissecting the local production of H_2O_2 necessitates technical or pharmacological tools. While pharmacological tools can be effective, they

often rely on inhibiting or activating specific pathways, which lacks the precision of controllable ROS production[76].

To generate H_2O_2 various techniques presented and categorized as chemogenetic or optogenetic. Term genetic in these categories represents genetic encoding of these tool. Utilizing genetic encoding, these tools can be targeted various compartments of the cell using localization signals. Chemo- term represents chemical production of H_2O_2 and Opto- term represents production of H_2O_2 using light energy. In chemogenetic tools, mainly enzyme's specific substrate is provided to produce H_2O_2 but in optogenetic tools this is different. Activation of optogenetic protein is aided by light energy. Also, optogenetic tools are mainly produces superoxide due to electron transfer from protein to molecular oxygen but SOD tethering to these proteins results in production of H_2O_2. Glucose oxidase (GOX), D-amino acid oxidase (DAAO) enzymes can be used to produce H_2O_2 chemogenetically [77]. KillerRed is an optogenetic tool produces superoxide upon light exposure. When KillerRed coupled with SOD1, upon light exposure this chimera produces H_2O_2 due to high reactivitiy of SOD towards superoxide [78]. Among these tools, glucose oxidase (GOX) catalyzes the oxidation of D-glucose to form D-glucono-δ-lactone (GDL) [79]. During this process, FAD acts as an electron carrier, ultimately transferring electrons to O_2, which is then reduced to H_2O_2. Similarly, D-amino acid oxidase (DAAO) catalyzes the conversion of D-amino acids to pyruvate[80]. This reaction also involves electron transfer, resulting in the formation of H_2O_2 as a byproduct. In the case of KillerRed-SOD1, light induction triggers the capture of electrons by O_2, producing superoxide. SOD1, which has high reactivity towards superoxide, then catalyzes its conversion into H_2O_2.

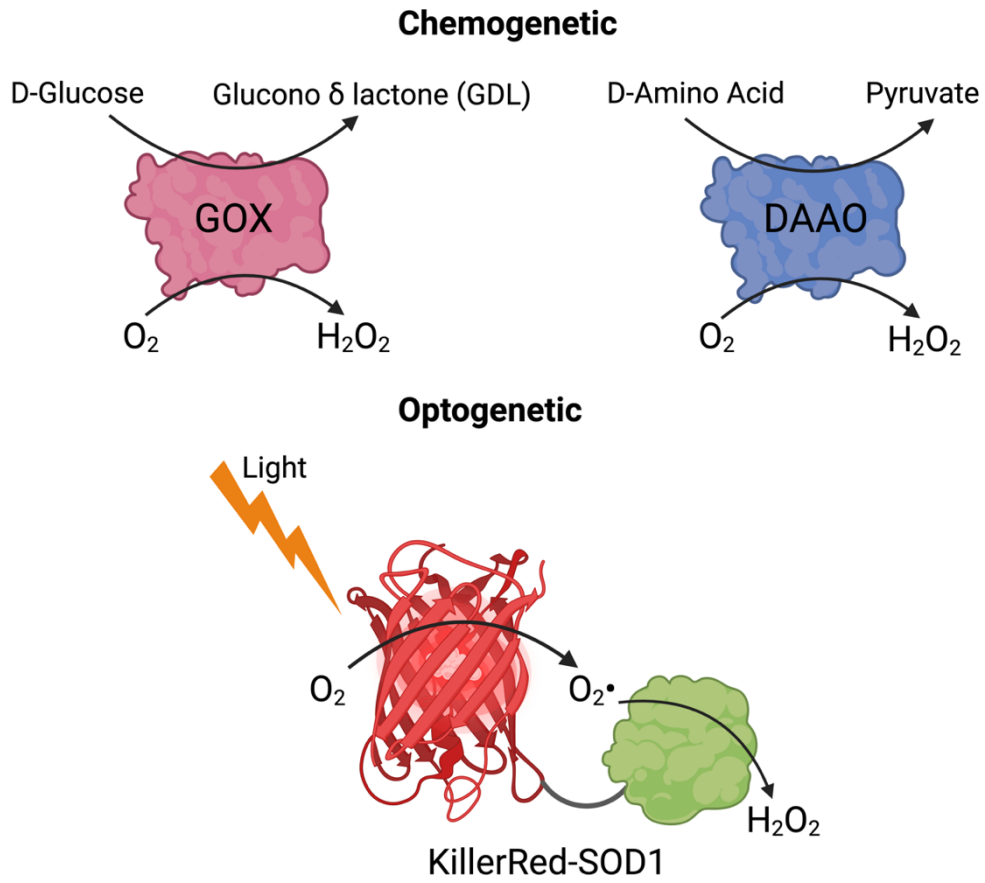

Figure 2.8: Tools can generate H_2O_2 intracellularly

Chemogenetic tools require substrate to catalyze their reactions. During these reactions H_2O_2 forms as a byproduct. For optogenetic production light induces formation of superoxide. Then enzymatic activity of SOD convert superoxide to H_2O_2

Both chemogenetic and optogenetic methods for generating H_2O_2 enable localized ROS signaling. Chemogenetic tools offer controlled H_2O_2 production through the addition or withdrawal of specific substrates. Furthermore, the reactions catalyzed by chemogenetic enzymes should not interfere with normal cellular processes. Optogenetic tools, on the other hand, use light to provide precise control of H_2O_2 production, typically through laser application. However, light penetration is limited in thicker samples, which restricts the use of optogenetics in certain contexts. Therefore, chemogenetic tools can have broader applications due to their versatility and ease of use in a variety of sample types.

In our study we decided to use DAAO enzyme as chemogenetic tool. Moreover, recent years this enzyme is used to produce local H_2O_2 to understand different signaling pathways. Although using the DAAO is advantageous, there are parameters to be consider. For that reason, we have started to fine-tune enzyme parameters. Initially, we needed to develop a system where DAAO produces H_2O_2 and measured with HyPer7 (**Figure 2.9**)

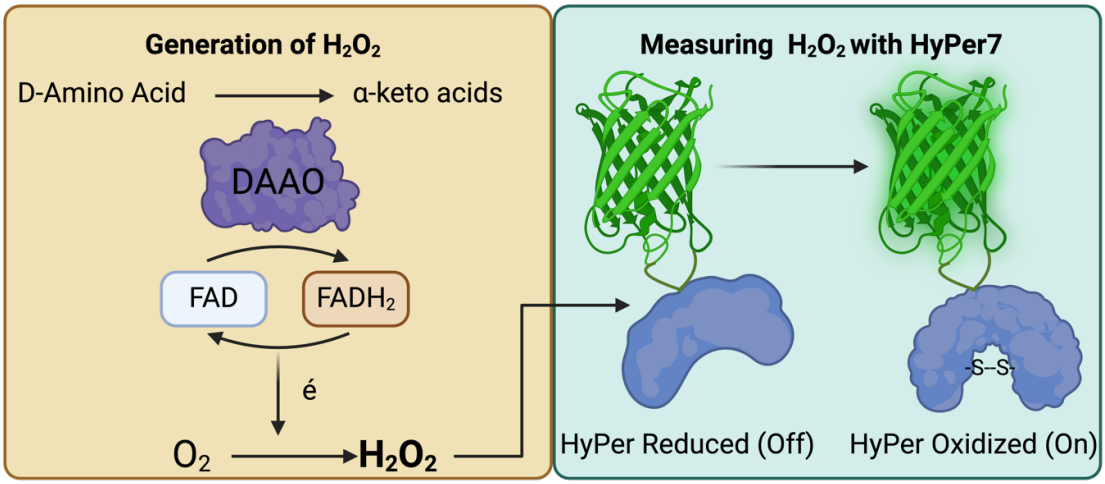

Figure 2.9: Generation and detection of H_2O_2 via DAAO and HyPer7.

DAAO generates H_2O_2 as a by-product of D-amino acid catalysis. H_2O_2 produced via DAAO can be visualized using HyPer7 probe in which H_2O_2 oxidize HyPer7 and turn on fluorescence.

After establishing our system, we wanted to investigate certain parameters for DAAO enzyme. Initially, experiments performed by our lab demonstrated that DAAO is stereospecific. Only D-Alanine (D-Ala) did produce robust HyPer7 response but not L-Alanine (L-Ala) [81]. From that point we decided to use mutant version of DAAO called mDAAO. mDAAO contains several mutations to improve catalysis of DAAO enzyme. To dissect localized enzyme kinetics, we initially co-transfect differentially localized mDAAO and HyPer7 to establish our generate and detect system. For that purpose, using molecular cloning techniques we fused mDAAO with mCherry to ensure correct localization. Then we developed constructs that have localization signals for mitochondria (Mito-mCherry-mDAAO), cytosol (mCherry-mDAAO-NES) and nucleus (mCherry-mDAAO-NLS). These constructs were co-transfected with corresponding HyPer7 construct. Such as mCherry-mDAAO-NLS co-transfected with H.7-NLS to measure H_2O_2 at production site. HEK293 cells co-transfected with these constructs and visualized under high-resolution microscope to ensure correct localization (**Figure 2.10**)

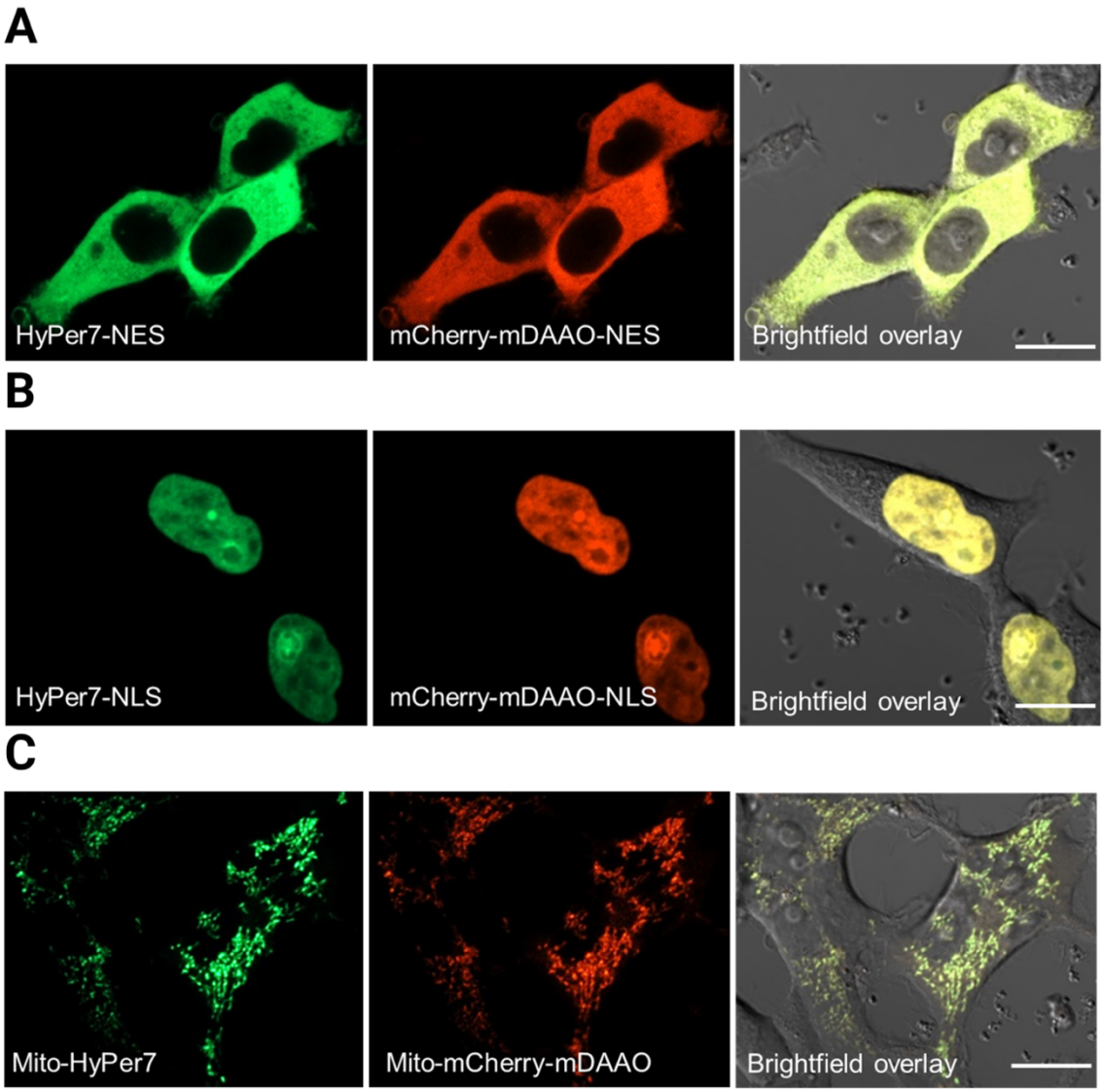

Figure 2.10: Fluorescence images of differentially localized HyPer7 (H.7) and mDAAO in HEK293 cells

(A) Cells expressing H.7-NES (left), mCherry-mDAAO-NES (middle), and an overlay with the bright field (right). **(B)** Cells expressing H.7-NLS (left), mCherry-mDAAO-NLS (middle), and an overlay with the bright field (right). **(C)** Cells expressing Mito-H.7 (left), Mito-mCherry-mDAAO (middle), and an overlay with the bright field (right). Scale bar: 20 µm.

Ensuring the correct localization of both mDAAO and HyPer7 was crucial for understanding their behavior within the cell. By targeting mDAAO and HyPer7 to specific cellular compartments, we could accurately study compartment-specific redox dynamics. Upon providing D-Ala to cells expressing differentially localized mDAAO, we observed a robust response in each compartment. Moreover, we studied different kinetics of the enzyme for each compartment such as EC50 value using different

concentrations of D-Ala [81].This confirmed that the enzymatic activity of mDAAO and the subsequent production of H_2O_2 were effectively compartmentalized, allowing us to investigate the localized redox signaling with high precision.

To investigate the versatile response of mDAAO to various amino acids, we provided chemically distinct D-amino acids, such as polar (D-serine), hydrophobic (D-alanine, D-phenylalanine, D-valine, and D-tryptophane), charged (D-arginine), and sulfur-containing (D-cysteine and D-methionine) amino acids. Each amino acid was administered at a concentration of 1 mM. To assess the differences in amino acid catalysis, we co-transfected HEK293 cells with mCherry-mDAAO and HyPer7. The results indicated that D-methionine was catalyzed the fastest, while D-valine was catalyzed the slowest by mDAAO [81]. Additionally, we investigated the competition between D-alanine (D-Ala) and L-alanine (L-Ala) during cellular entry. When cells were exposed to an equal concentration mixture of D-Ala and L-Ala, the response was slower compared to the response with the same concentration of D-Ala alone. This result indicates that there is competition between D- and L-amino acids at the level of cellular entry [81].

Additionally, we investigated the performance of mDAAO in different cell lines. Cell lines were co-transfected with mDAAO and HyPer7, and their responses were examined upon the addition of 1 mM D-Ala or D-Met. The results indicated that HEK293 cells were the most responsive to D-amino acid addition, while U87-MG and EA.hy926 cells were the least responsive. Therefore, optimization is necessary before using mDAAO in any cell line to ensure effective performance [81].

Another important aspect of local redox manipulation is the requirement of O_2, as ROS formation depends on the presence of oxygen. Previous studies have demonstrated that mDAAO performs better under low O_2 and low D-amino acid conditions[82]. To investigate this, we designed an experimental setup to study mDAAO performance under low O_2 conditions. Our setup included a hypoxia chamber equipped with an O_2 sensor and an airtight lid to monitor and ensure the maintenance of low O_2 levels (**Figure 2.11A**). To achieve low O_2 conditions, we purged the hypoxia chamber with N_2 gas for an

extended period until the desired conditions were met. Due to the low volume of the hypoxia chamber, O_2 levels dropped significantly within a short time. Prior to conducting experiments, we purged the chamber with N_2 gas for 2 hours. Additionally, the experimental media was bubbled with N_2 gas for at least 2 hours to remove dissolved O_2. During incubation and experimentation, we continuously supplied N_2 gas and monitored O_2 levels to maintain the hypoxic environment (**Figure 2.11B**)

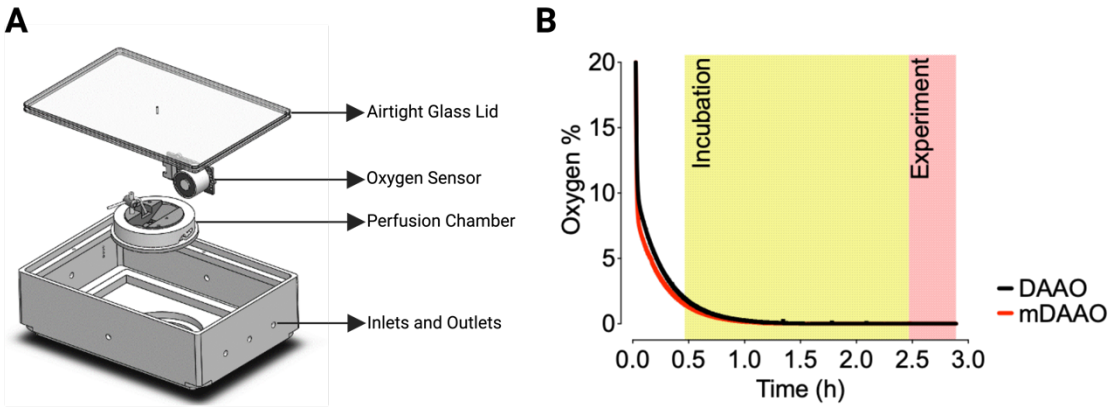

Figure 2.11: Hypoxia Chamber Design and Oxygen Levels Monitoring.

(A) The 3D-printed hypoxia chamber includes inlets and outlets for medium and gas flow, a perfusion chamber for cells, an O_2 sensor to monitor oxygen levels during incubation and experimentation, and an airtight glass lid to maintain an isolated environment. **(B)** The graph represents O_2 levels obtained via the O_2 sensor inside the hypoxia chamber. After purging the chamber with N_2 gas, it was maintained under N_2 flow for 2 hours of incubation. During the experiment, the N_2 gas flow continued to keep the hypoxia chamber under low O_2 conditions. The black line shows O_2 levels during experiments with cells expressing DAAO, and the red line indicates O_2 levels during experiments with cells expressing mDAAO

After setting up the hypoxia chamber, we investigated the performance of DAAO and mDAAO under both room air conditions and low O_2 conditions. First, we examined the effect of O_2 on cells expressing mDAAO. Under room air conditions, mDAAO-expressing HEK293 cells catalyzed D-Ala faster compared to low O_2 conditions. Although the enzyme performed robustly in both conditions, the presence of O_2 significantly affected the kinetics of mDAAO (**Figure 2.12A**).

Next, we compared the performance of DAAO and mDAAO under low O_2 conditions. Provision of 10 mM D-Ala elicited a robust response in both DAAO- and mDAAO-expressing cells. As a positive control, we provided 100 µM H_2O_2 extracellularly (**Figure 2.12B**). The responses of HyPer in the presence of extracellular H_2O_2 were similar, but the responses to D-Ala differed in terms of kinetics (**Figure 2.12C**) and the amplitude of HyPer signals (**Figure 2.12D**). Under low O_2 conditions, mDAAO catalyzed D-Ala faster than DAAO, as indicated by the rate of change in HyPer signals. Additionally, mDAAO produced more H_2O_2 compared to DAAO under low O_2 conditions, by comparing the amplitude of HyPer signals.

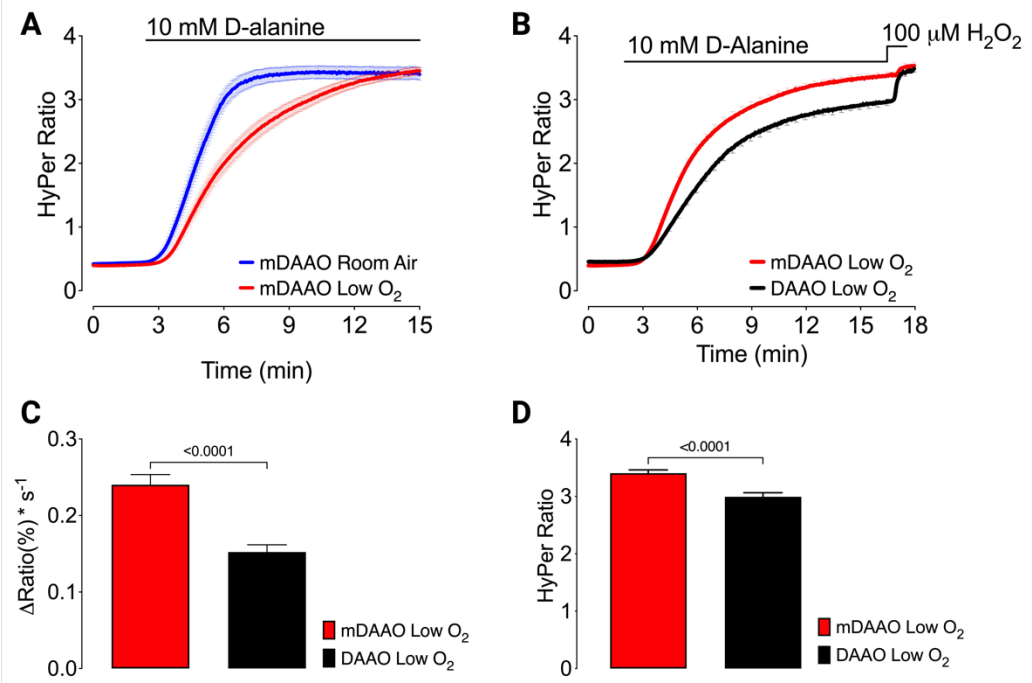

Figure 2.12: Comparison of performances of mDAAO and DAAO under different oxygen conditions.

(A) Traces represent average HyPer ratios of HEK293 cells expressing mDAAO under room air conditions (blue line) or low O_2 conditions (red line) in response to 1 mM D-Alanine provision. **(B)** Graphic demonstrates average HyPer signals of HEK293 cells under low O_2 conditions expressing mDAAO (red line) or DAAO (black line) in response to 1 mM D-Alanine and 100 µM of H_2O_2 **(C)** Bar graph represents rate of change in HyPer ratios of cells expressing mDAAO (red bar) or DAAO (black bar) in response to 10 mM D-Ala under low O_2 conditions. **(D)** Bar graph represents maximum responses of cells expressing mDAAO (red bar) or DAAO (black bar) in response to 10 mM D-Ala under low O_2 conditions. Data presented as mean ± SEM, Student's t-test applied to understand significant differences. p-values are indicated on top of the bars if the p-value < 0.05 (n=3)

In this study, we investigated and demonstrated how parameters can be fine-tuned to use chemogenetic tool, mDAAO, efficiently. First, we established generate and detect system using genetically encoded biosensor HyPer (**Figure 2.9**). Next, mDAAO is expressed in different compartments of the cell then the performance and kinetics of differentially located mDAAO is investigated (**Figure 2.10**). Moreover, we provide insights about different D-amino acid substrates, and we demonstrated performance of mDAAO in various cell lines. Additionally, we compared the usage of O_2 by mDAAO and DAAO (**Figure2.12**). Previously it has been shown that mDAAO performs better under low substrate and low O_2 conditions. We took this further by designing hypoxia chamber to study low O_2 conditions (Figure 2.11). We demonstrated that O_2 has effect on performance of mDAAO and also mDAAO outperforms DAAO in terms of production kinetics and production amplitude of H_2O_2 under low O_2 conditions (**Figure 2.12**).

Concluding Reflections on Measuring and Production of Local H_2O_2

In this chapter, our aim was to understand and optimize local redox signaling through the precise measurement and production of H_2O_2 using genetically encoded biosensors and chemogenetic tools. Using genetic encoding we are able to target biosensors or enzyme to compartments of the cells. Here we provide an initial targeting by simply using the most used targeting signal peptides for HyPer and mDAAO such as nuclear export signal (NES), nuclear localization signal (NLS) and mitochondrial localization signal (COX8). For HyPer we developed an imaging method to understand local redox dynamics and for mDAAO we fine-tuned certain parameters before mDAAO is applied to study mimicking local redox signaling.

The advancements in the HyPer biosensor have significantly enhanced our ability to monitor compartment-specific H_2O_2 dynamics with high sensitivity and accuracy. Besides, there are other H_2O_2 biosensors for local detection, but we decided use HyPer7 biosensor due to prior establishment of our experimental setup on HyPer biosensor. The

development of HyPer7, which overcomes limitations of earlier versions such as pH sensitivity and amplitude of response towards H_2O_2, has allowed us to study localized H_2O_2 changes more effectively due to its sensitivity which is in nanomolar range intracellularly. When we target HyPer7 to different cellular compartments (cytosol, nucleus, and mitochondria) in EA.hy926 cells, we could measure basal H_2O_2 levels and observe compartment-specific responses to extracellular H_2O_2. This imaging method allowed us to monitor all three compartments within same field of view which provides identical experimental conditions for the cells expressing either H.7-NES, H.7-NLS and Mito-H.7. Besides establishing an imaging method, our findings demonstrated the dynamic nature of mitochondrial redox signaling, with mitochondria exhibiting rapid H_2O_2 uptake and removal, indicating their crucial role in redox homeostasis and oxidative stress management. It was unexpected for us to see mitochondria is the first compartment that responds extracellular H_2O_2 unlike cytosol but there are studies showing that mitochondria have contact points with plasma membrane especially at caveolae or ER[69], [70]. Also, previous studies highlighted AQPs which facilitates transport of H_2O_2 to different compartments from extracellular sources[12]. In addition, compartmentalization of ROS is a well-known phenomenon. These results highlight the importance of mitochondria in local redox signaling and further experiments are required to prove extracellular to mitochondria trafficking of H_2O_2.

In addition to using HyPer7 for H_2O_2 measurement, we employed the chemogenetic tool mDAAO to produce localized H_2O_2 within cells. Local production of H_2O_2 is crucial as many ROS-producing enzymes are compartmentalized, even within specific locations in particular compartments. Utilizing mDAAO in redox studies allows for a better understanding of how local H_2O_2 production affects redox signaling. By targeting mDAAO to various compartments, we could investigate its enzymatic activity and kinetics, demonstrating its stereospecificity and superior performance compared to DAAO. Co-transfecting cells with mDAAO and HyPer7 enabled us to establish a robust generate-and-detect system, facilitating precise compartment-specific redox measurements. This system allows us to mimic local H_2O_2 production and measure it accurately, providing deeper insights into compartmentalized redox dynamics.

We also explored the versatility of mDAAO by testing its response to various D-amino acids and assessing its performance across different cell lines. Which are important parameters for those who are going to use mDAAO for their experiments. Our results indicated that mDAAO is highly efficient under low O_2 conditions, outperforming DAAO in both the kinetics and amplitude of H_2O_2 production. The design and utilization of a hypoxia chamber further facilitated our study of mDAAO under controlled low O_2 conditions, revealing the significant impact of oxygen availability on enzyme performance. Important issue with O_2 is certain experimental conditions necessitates low O_2 levels during the experiments such as hypoxia reperfusion injury, tumor spheroids[82]. Redox studies in these experiments favor the use of mDAAO due to its performance under low O_2 conditions

These comprehensive investigations underscore the importance of local H_2O_2 production and measurement in understanding redox signaling. The ability to generate and detect H_2O_2 in specific cellular compartments with high precision provides valuable insights into the spatial and temporal dynamics of redox processes. Our study highlights the potential of using advanced biosensors like HyPer7 and chemogenetic tools like mDAAO to dissect the intricate mechanisms of redox regulation, paving the way for future research and therapeutic strategies targeting oxidative stress and redox imbalances in various disease contexts.

Overall, our work contributes to a deeper understanding of compartment-specific redox dynamics and offers a framework for optimizing the tools and methods used to study local redox signaling. This knowledge is critical for advancing our comprehension of cellular redox biology and developing interventions that modulate redox states to maintain cellular health and prevent disease.

Materials and Methods

Chemicals

Dulbecco's modified Eagle's Medium (DMEM), 100 U/ml penicillin and 100 µg/ml streptomycin, Fetal Bovine Serum (FBS) and trypsin were purchased from Pan Biotech (Aidenbach, Germany). 100 µg/mL normocin was purchased from InvivoGen (San Diego, CA,USA). 2% HAT solution (Sodium Hypoxanthine (5 mM), Aminopterin (20 µM), and Thymidine (0.8 mM)) was purchased from ATCC (Manassas, VA, USA). Polyjet transfection reagent was purchased from SignaGen Laboratories (Maryland, USA). 10 µg/mL Polybrene infection reagent was purchased from Sigma-Aldrich (St.Louis, MO, USA). $CaCl_2$, KCl, NaCl, $MgCl_2$, KH_2PO_4, $NaHCO_3$, NaH_2PO_4, D-Glucose were purchased from NeoFroxx (Darmstadt, Germany). 1 mM HEPES, 0.1% MEM Vitamins, 0.2% essential amino acids were purchased from Pan Biotech (Aidenbach, Germany). D-alanine, D- phenylalanine, D-arginine, D-methionine, and D-tryptophan were purchased from Alfa Aesar (Landau, Germany). D-serine, D-valine, were purchased from Sigma Aldrich (St.Louis, MO, USA). D-cysteine was purchased from ChemCruz (Heidelberg, Germany). L-alanine was purchased from NeoFroxx (Darmstadt, Germany).

Buffers and Solutions

Live-cell imaging performed under HEPES-based buffer solution. Final concentrations of chemicals in this buffer are: 138 mM NaCl, 5 mM KCl, 2 mM $CaCl_2$, 1 mM $MgCl_2$, 10 mM D-glucose, 10 mM HEPES. Prior to experiments cell were stored in storage buffer solution for 1 hour. Final concentrations of each chemical in cell storage buffer are 138 mM NaCl, 5 mM KCl, 2 mM $CaCl_2$, 1 mM $MgCl_2$, 10 mM D-glucose, 10 mM HEPES, 2.6 mM $NaHCO_3$, 0.44 mM KH_2PO_4, 0.34 mM Na_2HPO_4, 10 mM D-glucose, 0.1% vitamins, 0.2% essential amino acids, and 1% penicillin/streptomycin.

Chemicals are used in live-cell imaging experiments were dissolved in live-cell imaging buffer solution. After preparation of solutions pH is adjusted to 7.42. For experiments performed under low O_2 conditions N_2 purged live-cell imaging buffer solution's pH is adjusted after N_2 purge.

Molecular Cloning and Plasmids

Differentially targeted HyPer7 constructs were kindly provided by Vsevolod Belousov. mDAAO constructs that contains NES and NLS signaling sequences in C-terminus were synthesized and ordered. Then these constructs subcloned into pAAV2-MCS vector via restriction digestion using KpnI and HindII enzymes. To visualize mDAAO red fluorescent protein mCherry2 added N-termini of mDAAO-NES and mDAAO-NLS using restriction sites of EcoRI and KpnI enzymes. For mito-mCherry-mDAAO tandem of COX8 sequence is added using restriction sites for EcoRI and AgeI.

For lentivirus production second generation lentiviral system is used. For that purpose, psPAX2 as a packaging plasmid is used (Addgene #12260). For envelope plasmid we used p.MD2.G (Addgene #12259). For transfer plasmid, we used empty backbone of lentiviral transfer vector called pLenti.MP2 (Addgene #36097) to subclone differentially HyPer7 constructs. Sequence of HyPer7 is subcloned into lentiviral transfer vector via BamHI and XhoI restriction sites.

Cell Culture and Lentivirus Generation

Human Embryonic Kidney cells (HEK293) were cultured using DMEM supplemented with 10%FBS, 100 µg/ml streptomycin and 100 U/ml penicillin. EA.hy926 cells were cultured using DMEM supplemented with 10% FBS, 100 µg/ml streptomycin and 100 U/ml penicillin, 100 µg/mL Normocin and 2% HAT solution. Cells were maintained under humidified CO_2 chamber at 37 C°. Confluency of the cells were controlled daily under light microscope and every 2 days respective medium of the cells were replaced. Upon confluency cells were trypsinized, detached and 1:5 subculturing

performed. For experiments, cells were seeded on 6-well plate containing 30 mm glass coverslips (Glaswarenfabrik Karl Knecht Sondheim, Germany)

HEK293 cells were cultured in antibiotic-free medium to perform transfection for lentiviral production. When the cells reached 80–90% confluency, they were co-transfected with 3 µg of psPAX2 (Addgene #12260), 3 µg of pMD2.G (Addgene #12259), and 6 µg of the respective HyPer7 lentivirus shuttle vectors. The transfection was performed using PolyJet transfection reagent following the manufacturer's instructions. Twenty-four hours after transfection, the medium was replaced with fresh DMEM. Following additional 24-hour and 48-hour incubation periods, the cell culture medium containing virus particles was collected and filtered using a 0.45 µm low protein binding medium filter (T.P.P., Switzerland). The filtrate was then concentrated by ultrafiltration using a 100 kDa Amicon® Ultra-15 Centrifugal Filter Unit (3000× g, 30 min, 4 °C). The filtered virus particles were aliquoted and either used immediately or snap-frozen in liquid nitrogen and stored at −80 °C.

EA.hy926 cells were seeded onto a 6-well plate and allowed to attach before being exposed to an antibiotic-free transduction medium. This medium contained 10% FBS, 10 µg/mL Polybrene infection reagent and respective lentivirus particles encoding for differentially targeted HyPer7. To optimize lentiviral transduction, serial dilutions of the viral-particle-containing filtrates were used. The cells were maintained in the virus-containing medium for 48–72 hours. After successful transduction, cells were cultured for an additional week in fresh complete DMEM before undergoing fluorescence-assisted cell sorting (FACS). The top 30% of HyPer7-positive cells were selected based on green fluorescence emission, detected using a 488 nm laser excitation wavelength (Filter type: BP 530/40 nm) on a B.D. Influx Cell Sorter.

For transient transfection method, we used PolyJet as a transfection reagent. Cells were seeded on 6-well plate and after they reach 70-80% confluency 1 µg of respective plasmids were mixed with Polyjet according to manufacturer’s instruction. Medium of respective cells were replaced after 4 hours and cells were used for live-cell imaging next day.

Live-cell Imaging

Live-cell imaging experiments performed using Zeiss Axio Observer Z7.1 (Carl Zeiss AG, Oberkochen, Germany). 20x and 40x-oil plan-apochromat objectives were used with an NA of 0.8 and 1.4 respectively. Axio Observer equipped with Colibri 7 LED light source. For mDAAO visualization, 555/30 nm excitation LED light was used. Emitted light pass through FT570BP and collected through 605/70 BP emission filter. For HyPer imaging, alternating excitations were used via 423/44nm (HyPer Low) and 469/38nm (HyPer High) using LED modules of Colibri 7. Emissions were collected using beam splitter combinations FT455 (HyPer Low) , FT495 (HyPer High) and emission filter 525/50 BP was used.

High-resolution confocal images were captured using a Zeiss LSM 800 laser scanning confocal microscope equipped with a Plan-Apochromat 40x/1.3 oil immersion objective. Differentially targeted HyPer7 were excited with 488 nm and 405 nm lasers, and emissions were collected using a 509 nm filter system. Fluorescence detection was performed with an A GaAsP-PMT detector and a 400–565 nm filter, utilizing a Multialkali-PMT detector. mCherry-mDAAO constructs were excited with a 561 nm laser, and emissions were captured between 616 and 700 nm. The digital detector gain for all channels was set to 1, with detector gain applied between 500 and 1000 V.

Live-cell imaging experiments were performed using home-made perfusion system allowing to addition or withdrawal of chemicals. Cells were visualized using perfusion chamber (NGFI, Austria). Prior to experiments cells were incubated in cell storage buffer.

To acquire data and visualization Zen Blue 3.1 Pro software (Carl Zeiss AG, Oberkochen, Germany) was used.

Design and usage of hypoxia chamber

The oxygen-controlled on-stage chamber was designed using computer-aided design (CAD) to fit the microscope stage of an Axio Observer.Z1/7. The chamber was 3D printed using stereolithography methods with a Formlabs Form 3 printer (Cat No: PKG-F3-WSVC-BASIC, USA) and white resin (Formlabs White Resin, Cat No: RS-F2-GPWH-04, USA). Post-printing, the chamber was washed with isopropanol and cured by exposing it to 405 nm light at 65°C for 1 hour (Form Cure, Cat No: FH-CU-01, USA). For live-cell imaging under oxygen-controlled conditions, cells were placed in a perfusion chamber (NGFI, Austria) inside an airtight hypoxia chamber sealed with Plexiglas. The chamber air was replaced with 99.9% N_2 gas using silicon tubing holes. Oxygen levels were monitored with an Arduino IDE-based oxygen sensor integrated into the chamber (Grove Oxygen Sensor, Winsen, Cat No: 101020002, China). Buffers were also gassed with 99.9% N_2 using a magnetic stirrer. Once oxygen levels in the chamber dropped below 5%, cells were incubated under low oxygen conditions (5%–1% O_2) for 2 hours before the experiment. After pre-incubation, real-time imaging experiments were conducted using N_2-gassed buffers.

Statistical Analysis

All experiments performed as triplicate fashion. Data analysed using GraphPad Prism Software version 10 (GraphPad Software, San Diego, USA). All statistical data are presented as ±SEM in addition to the representative real-time traces shown as curves (if not indicated otherwise). For the statistical comparisons of multiple groups, one-way ANOVA analyses of variances with post-test Tukey's test to compare all columns were performed. For two groups' analysis Student's test were used. Statistical significances were considered significant, and p-values were indicated as stated.

CHAPTER III: OPTIMIZATIONS TO UNDERSTAND HYDROGEN PEROXIDE AND NITRIC OXIDE RELATIONSHIP

History of genetically encoded nitric oxide probe (GeNOp)

Nitric oxide (NO) is a gaseous molecule responsible for diverse biological reactions, including vasodilation, inflammation, and neurotransmission [83]. In endothelial cells, NO plays a critical role in maintaining vascular homeostasis. It is produced by endothelial nitric oxide synthase (eNOS) and contributes to the regulation of blood flow by inducing vasodilation[25]. NO diffuses into the smooth muscle cells of blood vessels, where it activates soluble guanylate cyclase (sGC), leading to the relaxation of smooth muscle fibers[84]. This mechanism is crucial for controlling blood pressure and provides tissue perfusion.

NO is a free radical and has a very short lifetime, on the order of seconds, and interacts with metal-containing proteins, especially Fe^{2+} and Zn^{2+} containing proteins, to serve as a signaling molecule by forming metal-nitrosyl complex with transition metals[85]. This complex lead to inactivation/activation of these proteins such as sGC [86]. This interaction is significant in the modulation of various signaling pathways and cellular functions. NO's ability to interact with proteins makes it vital in processes such as the inhibition of platelet aggregation and leukocyte adhesion, both of which are essential for preventing thrombus formation and inflammation within the vasculature.

Despite its critical functions, the radical nature of NO makes it challenging to trace and study. The short lifespan and high reactivity of NO necessitate advanced methods to detect and measure it accurately within biological systems[56]. Although the role of NO in various biological reactions is well established, further studies are essential to understand the dynamics of NO in these processes. This includes elucidating how NO production and signaling are regulated in physiological and pathological conditions, particularly within the vascular system, where NO is pivotal for endothelial function and overall cardiovascular system.

Different NO detection methods have been developed over the years, including electrochemical methods, enzymatic assays, spectroscopic assays, and fluorescent probes[57]. However, these methods are primarily end-point assays or do not directly measure NO itself, limits their utilization in investigating intracellular NO dynamics. In 2016, Eroglu et al. introduced genetically encoded biosensors for NO detection, called geNOps. These biosensors utilize a fluorescent reporter protein (FP) and a GAF (cGMP phosphodiesterase, adenylate cyclase, FhlA) domain from NorR (NO reduction and detoxification Regulator) derived from *E. coli* as the sensing domain[57]. NorR, a transcription factor under anaerobic conditions, binds DNA in response to NO to activate the expression of NO-reducing flavorubredoxin [87]. The GAF domain, a small protein containing a non-heme iron center where NO binds and activates NorR, serves as the sensing component. This domain's Fe^{2+} is coordinated by five amino acids: Arg81, Asp96, Asp99, Asp131, and Cys113. Mutations in this coordination center eliminate iron and NO binding, confirming that iron is necessary for NO capture in the GAF protein [88].

To create the NO sensor, a chimera of the fluorescent protein and the GAF domain was constructed, resulting in various color variants of geNOps such as Cyan-geNOp (C-geNOp), green-geNOp (G-geNOp), mint green-geNOp (M-geNOp), yellow-geNOp (Y-geNOp), and orange-geNOp (O-geNOp). Among these, C-geNOp (containing enhanced cyan fluorescent protein, ECFP), g-geNOp (containing enhanced GFP, EGFP), and o-geNOp (containing mKusabira Orange kappa, mKOκ) are the most widely used (**Figure 3.1**).

Before experiments, Fe^{2+} is supplemented using an iron booster solution, including a Fe^{2+} source and Vitamin C to maintain iron in its reduced state under room air conditions. Recent optimizations of the Fe^{2+}/Vitamin C content of the iron booster solution have minimized the toxic effects of iron supplementation on the cells.

The development of geNOps permits the direct measurement of NO, addressing a significant limitation of traditional NO detection methods, which often lack reversible signals. In geNOps, the signal returns to its initial state after NO removal. While Fe^{2+} and NO can form covalent, often irreversible, bonds in different metalloproteins, the interaction in geNOps is reversible due to the non-heme iron center. Unlike many biosensors, NO binding to geNOps does not increase fluorescence but instead quenches it, likely due to increased absorbance of the GAF protein in the Fe^{2+}-NO bound state between 500 nm and 600 nm [88].

geNOps have been used in various studies to understand NO dynamics. For instance, the direct measurement of NO with geNOps has differentiated the relationship between eNOS phosphorylation and NO production. This important study used geNOps and highlighted that even though eNOS is phosphorylated at S1177, it did not produce NO, underscoring the importance of direct intracellular NO measurement[38]. This capability provides critical insights into the complex regulation of NO signaling and its physiological and pathological roles, demonstrating the significant advancements geNOps bring to redox biology research.

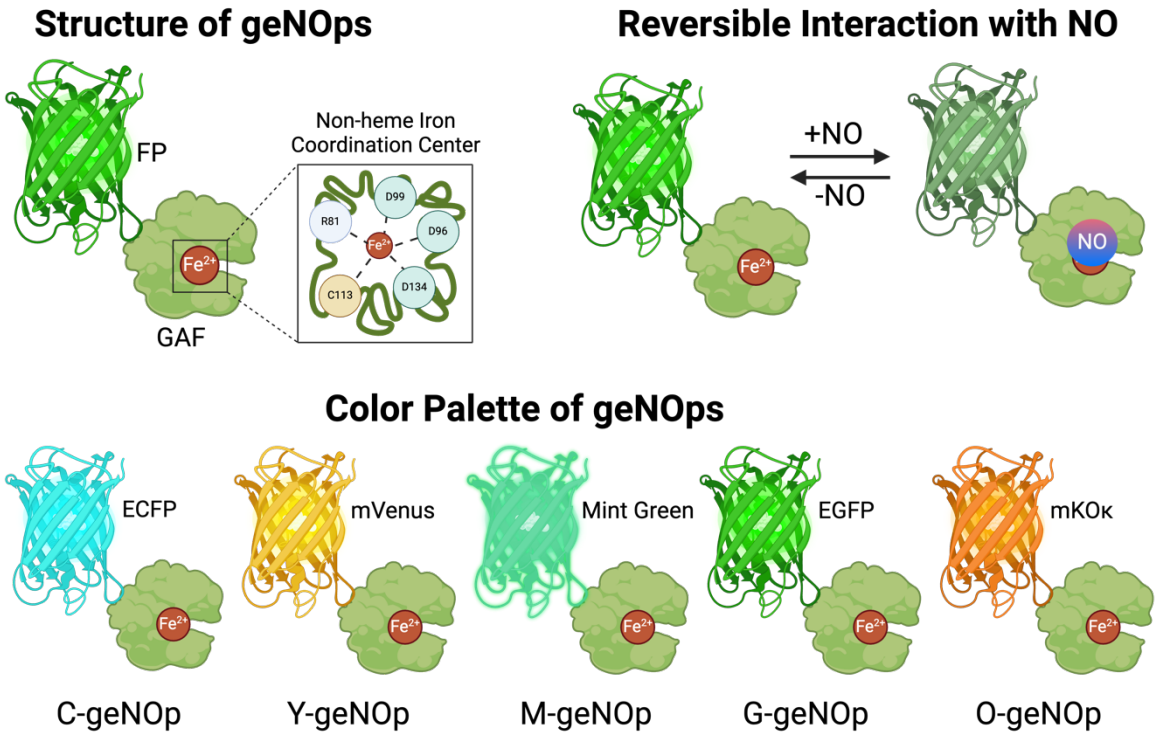

Figure 3.1: Structure and function of genetically encoded NO probe (geNOps).

geNOps contain GAF domain which includes non-heme iron center coordinated by 5 different amino acids. In the presence of NO fluorescent protein of geNOp quenches and without NO fluorescence increases again. Using different FPs, various geNOp variants are invented adapted from ref [57].

In our lab, we routinely use geNOp biosensors and HyPer7. These two biosensors offer significant advantages for understanding NO and H_2O_2 dynamics, such as high sensitivity and specificity. Their spectrally distinct properties allow us to perform multiparametric live-cell imaging. In the previous chapter, we utilized HyPer7 to monitor H_2O_2 changes, and by using geNOps, we can detect NO changes. Expressing both biosensors in a single endothelial cell enables us to investigate the primary aim of this study: the relationship between H_2O_2 and NO. Additionally, we employed the chemogenetic tool mDAAO to produce intracellular H_2O_2. These three tools together facilitate a comprehensive understanding of the interplay between these two molecules, allowing us to directly observe and monitor their dynamics via genetically encoded biosensors.

Development of double stable cell line and characterization of the cell line

To understand the relationship between H_2O_2 and NO in endothelial cells, we decided to generate a stable endothelial cell line expressing both HyPer7 and geNOps. Multiparametric imaging allows us to directly observe the relationship within the same cell. The spectrally distinct properties of these biosensors enable effective pairing, with HyPer7 being paired with the orange variant of geNOps (O-geNOp). Previously, the interaction between these two molecules has not been effectively investigated due to technical challenges and misunderstandings regarding the physiological context of H_2O_2 signaling, leading to contradictory results in the literature [74]. Our goal was to develop a cell line that could provide clear insights into the direct relationship between H_2O_2 and NO, overcoming these previous technical challenges.

The EA.hy926 cell line, routinely used in our lab, was chosen for this purpose. We previously generated stable cell lines expressing differentially localized HyPer7 biosensors using a lentiviral system[89]. In this study, we used two different lentiviruses to simultaneously infect cells, one carrying the differentially localized HyPer7 biosensors and the other carrying O-geNOp. For the O-geNOp construct, we used O-geNOp-NES, which localizes to the cytosol. Reciprocal localization with HyPer7 biosensors was unnecessary due to the gaseous nature of NO, which can rapidly diffuse throughout the cell and even to neighboring cells within seconds. The lentiviruses carrying the respective biosensors were transduced into EA.hy926 cells. Using FACS, we selected cells positive for both HyPer7 and O-geNOp. As a result, we generated three different cell lines expressing H.7-NES and O-geNOp-NES, H.7-NLS and O-geNOp-NES, and Mito-H.7 and O-geNOp-NES (**Figure 3.2**).

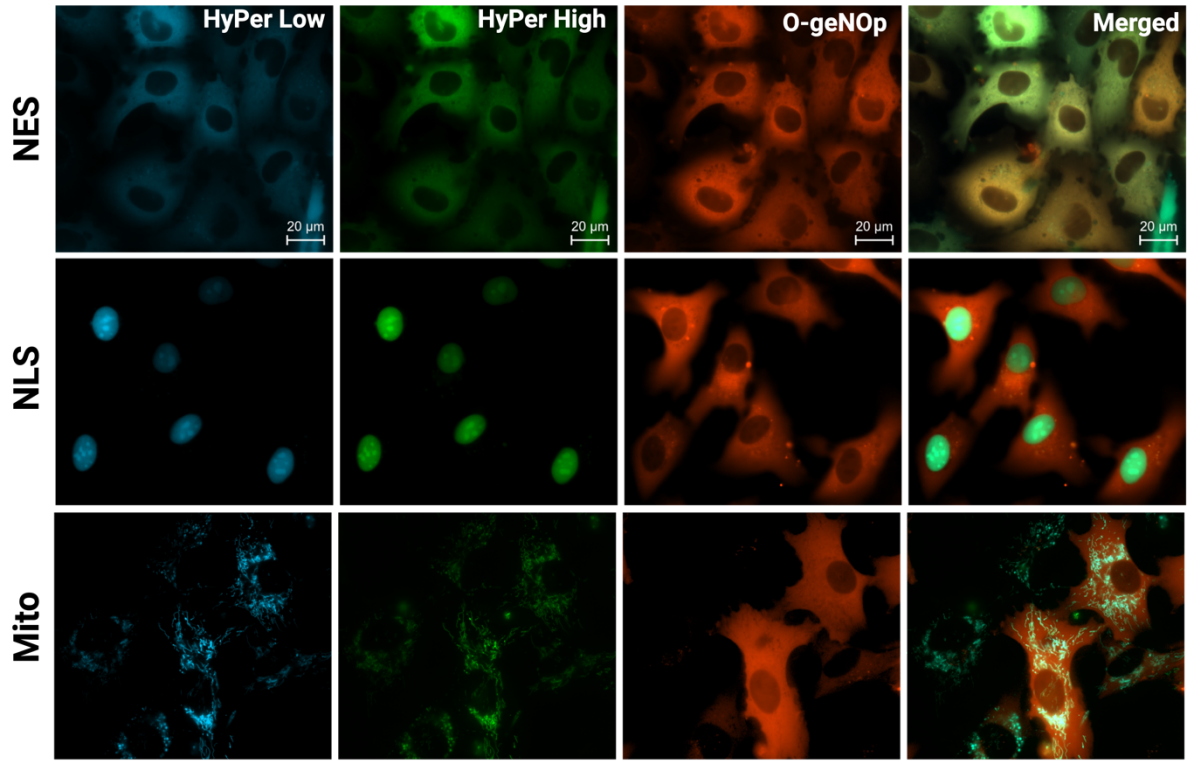

Figure 3.2: Visualization of Stable EaHy.926 Cells

Representative images of EaHy.926 cells expressing O-geNOp-NES and Hyper7.2-NES (First row), O-geNOp-NES and Hyper7.2-NLS (Second row), O-geNOp-NES and Mito-Hyper7.2 (Third row) are shown. Images are obtained using 3 different channels (Hyper Low: 430nm/520nm, HyperHigh: 475nm/520nm, O-geNOp: 555 nm/610nm). Scale bars represent 20 µm.

After generating the stable cell lines, we tested the functionality of each probe by providing their respective analytes extracellularly. For HyPer7 constructs, we added extracellular H_2O_2 during live-cell imaging experiments, and for geNOps, we provided the NO donor, NOC-7. Each cell line showed a robust increase in signals in response to H_2O_2 or NOC-7 (**Figure 3.3A**: H.7-NES and O-geNOp, **Figure 3.3B**: H.7-NLS and O-geNOp, **Figure 3.3C**: Mito-H.7 and O-geNOp).

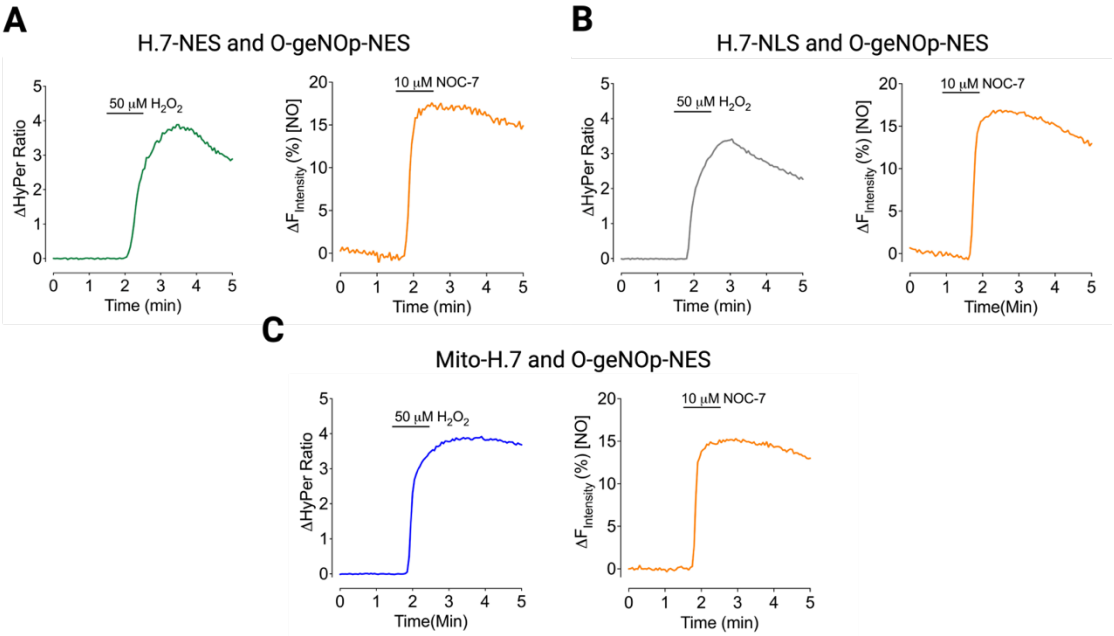

Figure 3.3:Functionality tests of double stable cells.

(A) EA.hy926 cells expressing H.7-NES and O-geNOp NES were imaged under fluorescence microscope to test each biosensor. For Hyper7, average signals were traced in response to provision of extracellular 50 µM H_2O_2 as indicated (left panel). For O-geNOp-NES, average signals recorded in response to 10 µM NOC-7 as indicated. Same experimental conditions were applied to H.7-NLS and O-geNOp-NES expressing cells **(B)** and Mito-H.7 and O-geNOp-NES expressing cells **(C)**. All experiments performed at least three times.

After confirming the functionality of both biosensors, we proceeded to test the Ca2+ dynamics in the double-stable cell lines. It is essential to confirm that these cells have functional Ca^{2+} dynamics because NO production requires Ca^{2+} changes to activate eNOS, which produces NO from L-arginine. For this purpose, we used the Ca^{2+}-specific dye FURA2-AM, which is ratiometric, with two excitation peaks at 340 nm and 380 nm and a single emission at 510 nm.

To compare Ca^{2+} dynamics, each double-stable cell line was tested alongside native EA.hy926 cells. During live-cell imaging, cells were treated with histamine, which potentiates Inositol-3-Phosphate dependent Ca^{2+} release and thus activates eNOS. The FURA signals were traced, and each cell line was individually compared with native EA.hy926 cells. The Ca^{2+} signals were similar in each cell line (**Figure 3.4A**). Comparing the amplitude of Ca^{2+} responses between native cells and double-stable cells, the increase

in Ca^{2+} in response to histamine was consistent across all cell lines. Therefore, in terms of Ca^{2+} dynamics, the double-stable cell lines did not differ from the native cells.

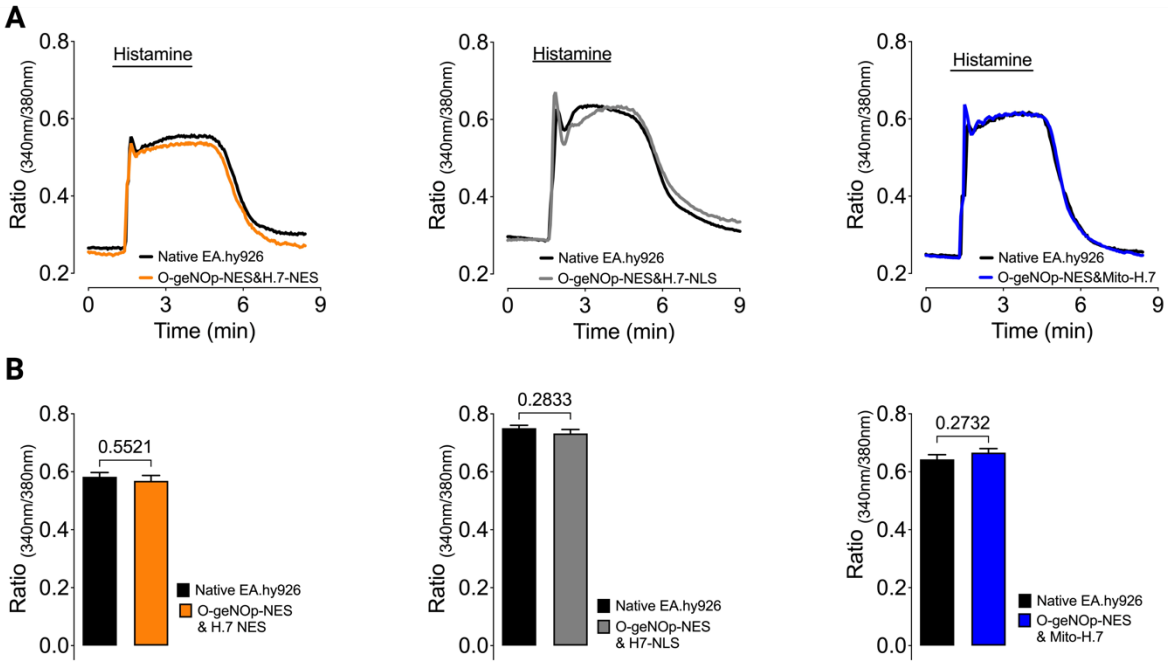

Figure 3.4: Ca^{2+} dynamics of double stable cell line using FURA2-AM.

(A) EA.hy926 cells expressing O-geNOp-NES and H.7-NES (left panel, orang curve), O-geNOp-NES and H.7-NLS (middle panel, grey curve) O-geNOp-NES and mito-H.7 (right panel, blue curve) along with native EA.hy926 cells were treated with 100 µM Histamine and average FURA signals were traced in each panel comparing with native EA.hy926 cells (black curves).(n=3) **(B)** Bar graphs indicate statistical analysis of Histamine derived Ca^{2+} responses of each cell type. Left panel compares maximum responses of cells expressing O-geNOp-NES and H.7-NES (orange bar) with native cells(black bar), middle panel compares maximum responses of cells expressing O-geNOp-NES and H.7-NLS (grey bar) with native cells(black bar), right panel compares maximum responses of cells expressing O-geNOp-NES and mito-H.7 (blue bar) with native cells (black bar). Data presented as mean±SEM and Student's t-test performed. p-values were indicated in bar graphs (n=3).

In conclusion, we successfully developed a double stable endothelial cell line expressing both HyPer7 and geNOps (**Figure 3.2**), which allows for the simultaneous monitoring of H_2O_2 and NO dynamics within the same cell. By utilizing spectrally distinct biosensors, we can perform multiparametric live-cell imaging to directly observe the interplay between these two crucial signaling molecules. The robust responses to

extracellular H_2O_2 and the NO donor NOC-7 confirmed the functionality of the biosensors in each of the generated cell lines (**Figure 3.3)**.

Additionally, we verified the functional Ca^{2+} dynamics in the double stable cell lines using the Ca^{2+}-specific dye FURA2-AM. The Ca^{2+} responses to histamine treatment in double stable cell lines were comparable to those in native EA.hy926 cells, indicating that the Ca2+ dynamics necessary for NO production via eNOS activation were intact (**Figure 3.4**).

This advancement might address previous technical challenges and provides a powerful tool to explore the relationship between H_2O_2 and NO with high precision and accuracy. These cell lines will facilitate a deeper understanding of redox signaling and the complex interactions between these reactive species in endothelial cells.

Acute and chronic effect of extracellular H_2O_2 in NO signaling

After establishing an intact double stable cell line capable of measuring both H_2O_2 and NO, we began investigating the effect of H_2O_2 on NO signaling under various conditions. Many studies on this relationship initiate with the exogenous application of H_2O_2 [90], [91], [92], [93]. Acute and chronic applications of H_2O_2 can elicit different signaling responses; for instance, inflammation causes a rapid increase in extracellular H_2O_2, while endothelial cells experience elevated extracellular H_2O_2 levels in pathological conditions such as atherosclerosis[42]. To explore these dynamics, we utilized a double stable cell line expressing both H.7-NES and O-geNOp-NES to monitor changes in NO levels alongside H_2O_2 levels. **Figure 3.5** illustrates the simultaneous imaging of both analytes. Initially, we provided an NO donor to the cells to confirm the functionality of O-geNOp. Once the O-geNOp signals returned to baseline, we applied a

short pulse of H_2O_2 to observe changes in NO signals. However, we did not observe any changes in NO levels in response to the short application of H_2O_2.

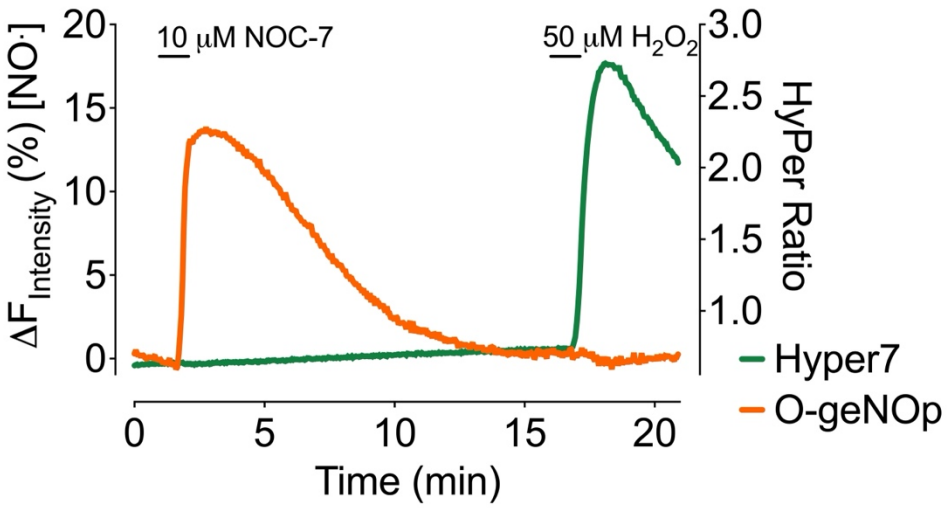

Figure 3.5: Acute application of extracellular H_2O_2 in double stable cells.

Cells that are expressing both H.7-NES and O-geNOp-NES exogenously treated with 10 µM NOC-7 and 50 µM H_2O_2 as indicated. Orange curves indicate signals NO signals and green curves indicate H_2O_2 signals that are obtained using O-geNOp-NES and H.7-NES consecutively (n=3)

Next, we investigated NO dynamics during chronic exposure to H_2O_2 in EA.hy926 cells expressing both biosensors. Endothelial cells were maintained under different H_2O_2 levels for five days to adapt to chronic oxidative conditions. Specifically, we used 100 µM and 300 µM H_2O_2 in the culturing medium, replacing it every two days with fresh medium containing either no H_2O_2, 100 µM H_2O_2, or 300 µM H_2O_2. Cell viability was monitored using light microscopy during this adaptation period. After adaptation, we conducted live-cell imaging experiments to assess NO levels (**Figure 3.6**). During the experiments, we provided ATP to produce NO responses in each condition. ATP yielded robust NO responses, and we subsequently added L-NAME (L-NitroArginine Methyl Ester), an eNOS inhibitor, to diminish eNOS-derived NO responses, allowing for the calculation of initial NO state (**Figure 3.6A**).

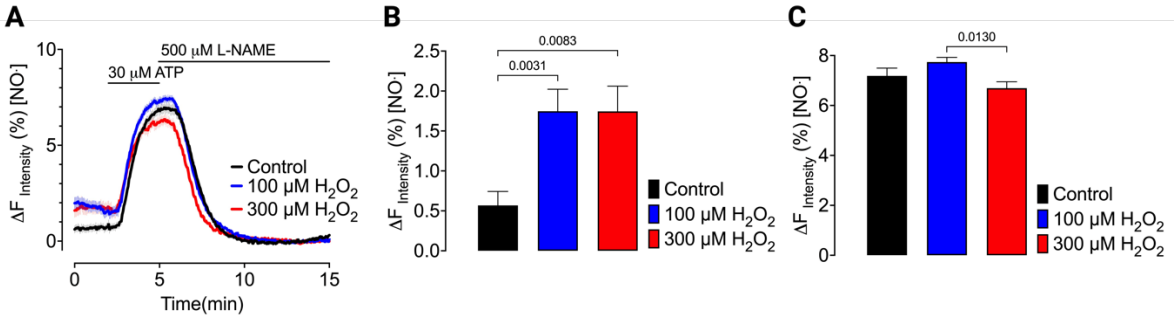

Figure 3.6: Effect of chronic exposure of extracellular H_2O_2 on NO signaling.

EA.hy926 cells expressing O-geNOp-NES and H.7-NES were cultured under different conditions for 5 days with no H_2O_2 (Control), with 100 µM H_2O_2 and 300 µM H_2O_2. After chronic exposure to H_2O_2 cells were imaged using fluorescence microscope (A) Curves represent O-geNOp signals of cells adapted to control (black curve), 100 µM H_2O_2 (blue curve) and 300 µM H_2O_2 (red curve) conditions in response to 30 µM ATP and 500 µM L-NAME consecutively. (B) Bar graphic represents average signals of O-geNOp-NES cells adapted to control (black bar), 100 µM H_2O_2 (blue bar) and 300 µM H_2O_2 (red bar) conditions under resting state (basal) before ATP challenge. (C) Bar graphic represents average signals of O-geNOp-NES cells adapted to control (black bar), 100 µM H_2O_2 (blue bar) and 300 µM H_2O_2 (red bar) conditions in response to 30 µM ATP. Data presented as mean±SEM. One-way ANOVA and Tukey's multiple comparison test are performed. p-values were indicated in bar graphs (n=3)

Comparing the initial NO levels, we observed an increase in basal O-geNOp signals in chronically H_2O_2-exposed cells, with a significant difference in basal NO levels compared to control cells. However, there was no significant difference in basal NO levels between cells adapted to 100 µM H_2O_2 and those adapted to 300 µM H_2O_2 (**Figure 3.6B**).

ATP-derived NO responses were similar across conditions, except that the geNOp response in 300 µM H_2O_2-adapted cells was significantly lower compared to 100 µM H_2O_2-adapted cells but similar to control cells (**Figure 3.6C**). In contrast to basal NO conditions, chronic H_2O_2 exposure did not substantially affect ATP-derived NO responses.

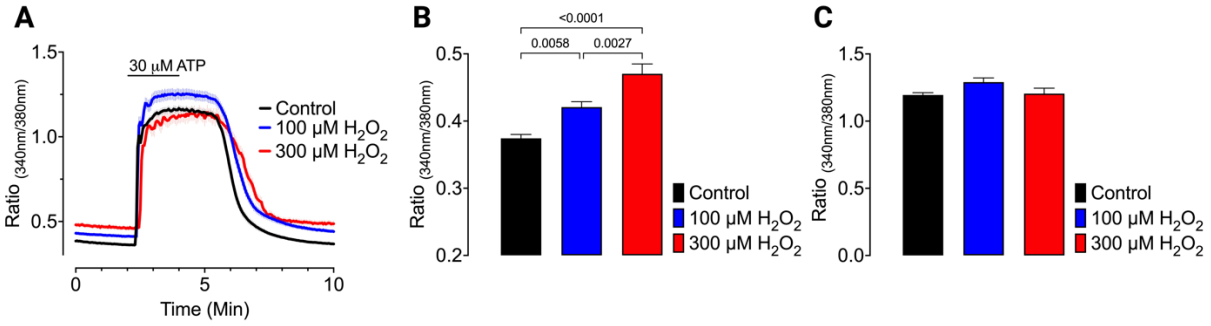

Figure 3.7: Effect of chronic exposure of extracellular H_2O_2 on Ca^{2+} signaling

EA.hy926 cells expressing O-geNOp-NES and H.7-NES were cultured under different conditions for 5 days with no H_2O_2 (Control), with 100 µM H_2O_2 and 300 µM H_2O_2. After chronic exposure to H_2O_2 cells were imaged using FURA2-AM **(A)** Curves represent FURA2 signals of cells adapted to control (black curve), 100 µM H_2O_2 (blue curve) and 300 µM H_2O_2 (red curve) conditions in response to 30 µM ATP. **(B)** Bar graphic represents average signals of FURA obtained from cells adapted to control (black bar), 100 µM H_2O_2 (blue bar) and 300 µM H2O2 (red bar) conditions under resting state (basal) before ATP challenge. **(C)** Bar graphic represents average signals of FURA obtained from cells adapted to control (black bar), 100 µM H_2O_2 (blue bar) and 300 µM H_2O_2 (red bar) conditions in response to 30 µM ATP. Data presented as mean±SEM. One-way ANOVA and Tukey's multiple comparison test are performed. p-values were indicated in bar graphs (n=3)

The observation of higher basal NO levels prompted us to examine Ca^{2+} dynamics in cells chronically exposed to extracellular H_2O_2. We used live-cell Ca^{2+} imaging with cells loaded with FURA2-AM. In live-cell imaging, cells were treated with ATP to initiate Ca^{2+} signaling. ATP induced a robust intracellular Ca^{2+} increase in all cells, and the removal of ATP returned Ca^{2+} levels to their initial state (**Figure 3.7A**). Basal intracellular Ca^{2+} levels showed that chronic exposure to H_2O_2 significantly increases basal Ca^{2+} levels, with higher H_2O_2 concentrations leading to increased intracellular Ca^{2+} levels (**Figure 3.7B**). Additionally, ATP-derived Ca^{2+} increases were comparable across conditions when comparing the maximum FURA signals (**Figure 3.7C**).

In conclusion, this part of the study investigated the acute and chronic effects of extracellular H_2O_2 on NO signaling using a double stable cell line capable of measuring both H_2O_2 and NO. We observed that a short pulse of H_2O_2 did not change NO levels, highlighting the transient nature of acute H_2O_2 exposure (**Figure 3.5**). However, chronic exposure to H_2O_2 revealed significant changes in NO dynamics in terms of resting NO

levels. Cells adapted to chronic oxidative conditions exhibited elevated basal NO levels, irrespective of the H_2O_2 concentration (100 μM or 300 μM). This suggests that chronic oxidative stress has an effect on basal NO levels (**Figure 3.6**).

Furthermore, ATP-induced NO responses remained largely unaffected by chronic H_2O_2 exposure, indicating that the capacity for NO production in response to ATP stimulation is preserved even under prolonged oxidative conditions. Additionally, our examination of Ca^{2+} dynamics revealed that chronic H_2O_2 exposure significantly increases basal intracellular Ca^{2+} levels, with higher H_2O_2 concentrations resulting in greater Ca^{2+} accumulation (**Figure 3.7**). However, ATP-induced Ca^{2+} responses were comparable across all conditions, demonstrating that the ability to mobilize Ca^{2+} in response to ATP remains intact despite chronic H_2O_2 exposure. These observations can help us to understand why basal NO levels are higher in stress adapted cells. Extracellular H_2O_2 can oxidize lipids on membranes of the cells. Lipid peroxidation causes disruption of membrane integrity in plasma membrane or organelles' membranes [75]. In contrast to our observations other studies have shown that NO levels are decreased [44]. However, in these studies cells were exposed to H_2O_2 for 24 hours. In our case, we adapted cells to oxidative conditions has more NO levels in resting state. Moreover, studies that propose decreased NO lack of techniques that can measure NO levels directly. To explain this difference, we assume that cells respond chronic oxidative stress with increasing NO levels to prevent oxidative stress to produce more superoxide [94]. Although we assume oxidative stress affect permeability of membrane, to understand serious detrimental effect of chronic oxidative stress we need to further this study to adapt cells more than a week.

Effect of long-term adaptation in NO signaling of cells exposed to differentially produced H_2O_2

The observation of chronically exposed extracellular H_2O_2 effects on NO signaling prompted us to investigate the effect of intracellular and localized production of H_2O_2 on NO signaling. Previous studies have shown that localized production of H_2O_2 can influence eNOS phosphorylation in a time-dependent manner [95]. Building on this, we aimed to adapt cells for localized intracellular H_2O_2 production and subsequently measure NO levels using geNOp. To achieve this, we utilized differentially localized mDAAO. For these experiments, endothelial cells needed to stably express both mDAAO and geNOp. As before, we used lentiviral systems to create cell lines expressing differentially localized mDAAO with geNOp. However, the mDAAO constructs contain mCherry2, which is unsuitable for O-geNOp imaging due to the spectral properties of mCherry2 and mKOκ. Therefore, we employed the green version of geNOp, called g-geNOp, to overcome spectral problems.

After establishing endothelial cells expressing both mDAAO and geNOp, we investigated the appropriate dose of D-Ala that would not be lethal to the cells after 24 hours. To determine this, we performed an MTT assay using various concentrations of D-Ala. Cells expressing cytosolic (mCherry-mDAAO-NES), nuclear (mCherry-mDAAO-NLS), and mitochondrial (Mito-mCherry-mDAAO) mDAAO were used to find a suitable concentration of D-Ala. The results indicated that 1 mM of D-Ala did not affect the viability of any cell types (**Figure 3.8**). Consequently, for the adaptation process, we used 1 mM D-Ala for each endothelial cell type to adapt to chronically produced local H_2O_2. The cells were cultured in a medium containing 1 mM D-Ala to induce chronic oxidative stress adaptation. Every two days culture medium is replaced with fresh medium containing 1mM of D-Ala.

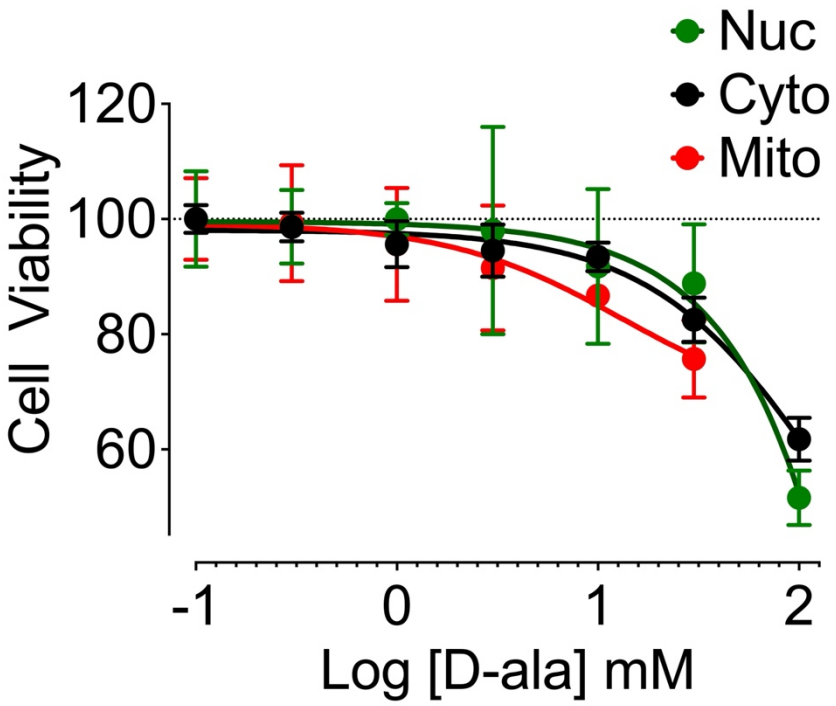

Figure 3.8: Viability of EA.hy926 cells expressing differentially targeted mDAAO in response to various concentrations of D-Ala.

EA.hy926 cells expressing mCherry-mDAAO-NES (black curve with dots), mCherry-mDAAO-NLS (green curve with dots) and mito-mCherry-mDAAO (red curve with dots) treated with different concentrations of D-Ala for 24 hours and MTT assay is performed. Y-axis represents percentage of cell viability and X-axis represents log concentration of D-Ala. Data presented as mean±SD. (n=3)

To investigate NO levels, we began with cells adapted to chronic cytosolic production of H_2O_2 via cytosolic mDAAO. For this purpose, cells expressing cytosolic mDAAO and geNOp, adapted to oxidative stress, were used for live-cell imaging. The cells were treated with ATP to induce an increase in NO, followed by the addition of L-NAME to determine the resting levels of NO. As a control, cells expressing both constructs were maintained in culture medium without D-Ala. Both control and adapted cells were stimulated with ATP, and NO responses were measured using G-geNOp. ATP induced a robust NO response in both control and adapted cells (**Figure 3.9A**). The subsequent addition of L-NAME led to a decrease in NO levels after ATP stimulation.

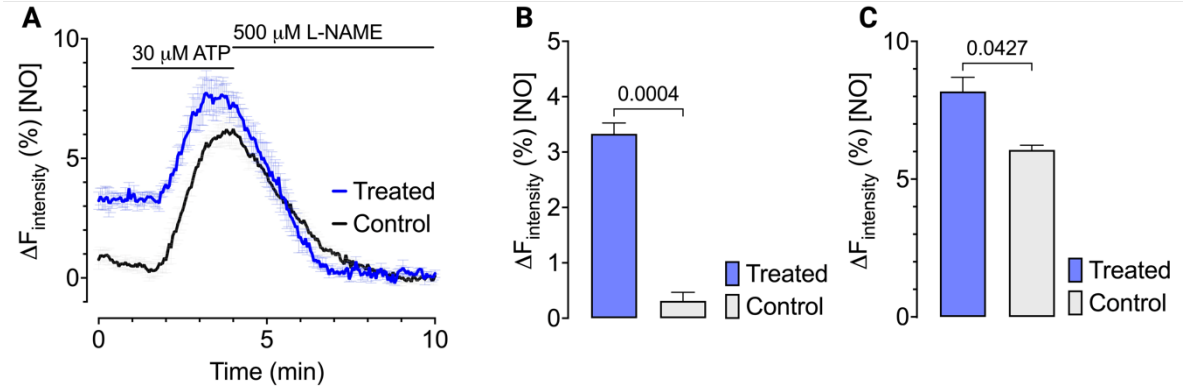

Figure 3.9: Effect of chronic production of cytosolic H_2O_2 using mCherry-mDAAO-NES in NO signals.

EA.hy926 cells expressing mCherry-mDAAO-NES and G-geNOp were cultured at least for 5 days in the presence (Treated) or absence (Control) of 1 mM D-Ala. After adaptation cells were used to perform live-cell imaging experiments using G-geNOp. **(A)** Average signals of G-geNOp obtained from cells either treated with 1 mM D-Ala (blue curve) or no treatment (black curve) in response to 30 μM ATP and 500 μM L-NAME consecutively. **(B)** Bar graph represents average of basal G-geNOp signals of cells either treated with 1 mM D-Ala (blue box) or no treatment (black box). **(C)** Bar graph represents average of maximum G-geNOp signals of cells either treated with 1 mM D-Ala (blue box) or no treatment (black box) in response to 30 μM ATP. Data presented as mean±SEM. Student's t-test is performed. p-values were indicated in bar graphs (n=3)

The resting NO levels (basal NO levels) were significantly higher in adapted cells compared to control cells (**Figure 3.9B**). When comparing ATP-derived NO responses, adapted cells produced more ATP-derived NO. The difference in NO production between control and adapted cells in response to ATP was slightly but significantly higher in adapted cells (**Figure 3.9C**). Thus, continuous production of cytosolic H_2O_2 not only increased the ATP-derived NO response but also elevated resting NO levels in endothelial cells. This suggests that chronic exposure to cytosolic H_2O_2 induces more responsive NO signaling.

Following the investigation of cytosolic H_2O_2 production, we proceeded to examine the next cell line, which expresses mDAAO in the nucleus. By localizing H_2O_2 production to the nucleus, we aim to explore how nuclear oxidative stress influences NO dynamics.

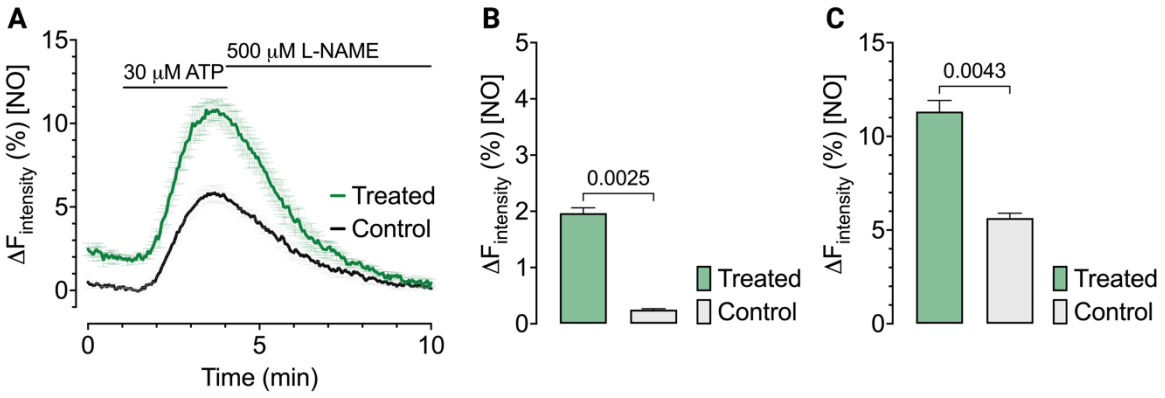

Figure 3.10: Effect of chronic production of nuclear H_2O_2 using mCherry-mDAAO-NLS in NO signals.

EA.hy926 cells expressing mCherry-mDAAO-NLS and G-geNOp were cultured at least for 5 days in the presence (Treated) or absence (Control) of 1 mM D-Ala. After adaptation cells were used to perform live-cell imaging experiments using G-geNOp. **(A)** Average signals of G-geNOp obtained from cells either treated with 1 mM D-Ala (green curve) or no treatment (black curve) in response to 30 μM ATP and 500 μM L-NAME consecutively. **(B)** Bar graph represents average of basal G-geNOp signals of cells either treated with 1 mM D-Ala (green box) or no treatment (black box). **(C)** Bar graph represents average of maximum G-geNOp signals of cells either treated with 1 mM D-Ala (green box) or no treatment (black box) in response to 30 μM ATP. Data presented as mean±SEM. One-way ANOVA and Tukey's multiple comparison test are performed. p-values were indicated in bar graphs (n=3)

EA.hy926 cells expressing nuclear mDAAO and geNOp were adapted to chronic local oxidative stress for five days. After this adaptation period, the cells were used for live-cell imaging. As with the cytosolic version, the cells were treated with ATP, followed by the addition of L-NAME to decrease ATP-derived NO production. ATP stimulation yielded a strong NO response in adapted cells and a moderate NO response in control cells (**Figure 3.10A**). Following the addition of L-NAME, NO levels decreased.

Basal NO levels, measured before ATP stimulation, were affected by nuclear oxidative stress adaptation. Adapted cells had higher resting NO levels compared to control cells (**Figure 3.10B**). The ATP-derived NO responses observed during live-cell imaging differed between the groups. Therefore, we compared the maximum NO response after ATP stimulation between control and treated cells. Statistical analysis demonstrated that treated cells exhibited a significantly higher NO response to ATP compared to control cells (**Figure 3.10C**).

In conclusion, chronic adaptation to nuclear local oxidative stress significantly elevates basal NO levels and enhances ATP-derived NO responses in endothelial cells. Building on these insights, we next investigated the effects of mitochondrial oxidative stress adaptation on NO signaling.

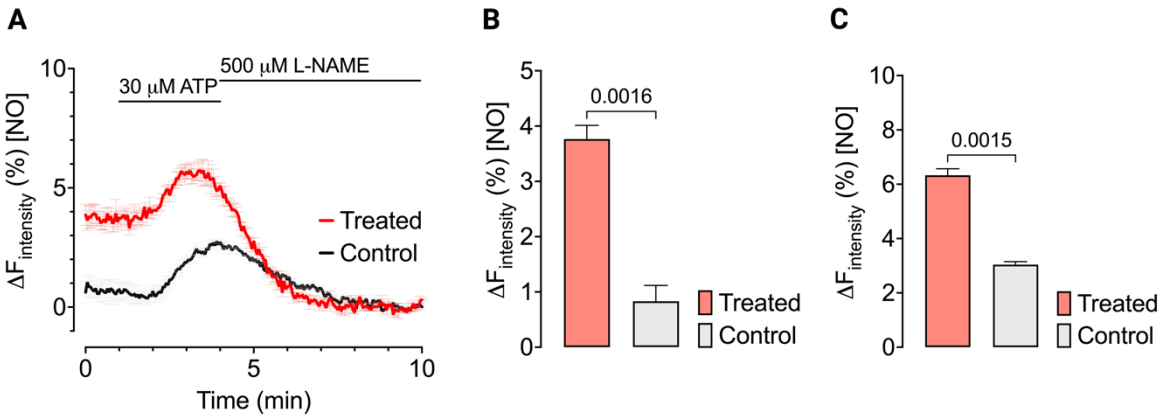

Figure 3.11: Effect of chronic production of mitochondrial H_2O_2 using Mito-mCherry-mDAAO in NO signals.

EA.hy926 cells expressing Mito-mCherry-mDAAO and G-geNOp were cultured at least for 5 days in the presence (Treated) or absence (Control) of 1 mM D-Ala. After adaptation cells were used to perform live-cell imaging experiments using G-geNOp. **(A)** Average signals of G-geNOp obtained from cells either treated with 1 mM D-Ala (red curve) or no treatment (black curve) in response to 30 µM ATP and 500 µM L-NAME consecutively. **(B)** Bar graph represents average of basal G-geNOp signals of cells either treated with 1 mM D-Ala (red box) or no treatment (black box). **(C)** Bar graph represents average of maximum G-geNOp signals of cells either treated with 1 mM D-Ala (red box) or no treatment (black box) in response to 30 µM ATP. Data presented as mean±SEM. One-way ANOVA and Tukey's multiple comparison test are performed. p-values were indicated in bar graphs (n=3)

EA.hy926 cells expressing Mito-mCherry-mDAAO and G-geNOp were adapted to local oxidative stress conditions using 1 mM D-Ala. After this adaptation period, the cells were used for live-cell imaging experiments. The cells were stimulated with ATP to induce NO production. According to the curves, ATP provoked a NO response in both treated and control cells (**Figure 3.11A**). Following ATP stimulation, L-NAME was applied to decrease NO levels. As expected, L-NAME caused a gradual decrease in NO levels.

When comparing the resting state NO levels, before the application of ATP, adapted cells showed higher NO levels compared to control cells (**Figure 3.11B**). Mitochondrial

production of H_2O_2 led to an increase in NO under resting conditions, similar to the effects observed with nuclear and cytosolic H_2O_2 production. This suggests that chronic oxidative stress, regardless of its subcellular origin, consistently elevates basal NO levels.

Moreover, we compared ATP-derived NO levels between the treated and control cells. Treated cells exhibited a higher responsiveness to ATP, as indicated by the maxima of the geNOp signal following ATP stimulation (**Figure 3.11C**). Statistically, the difference between control and adapted cells was significant. This enhanced responsiveness suggests that chronic mitochondrial H_2O_2 production not only increases basal NO levels but also amplifies the cellular NO response to external stimuli such as ATP.

In these experiments we have established that local production of H_2O_2 in various cellular compartments leads to significant changes in NO dynamics especially in nuclear oxidative stress affected the responsiveness of cells towards ATP. Given that NO and calcium signaling are related due to eNOS activation requires calcium. For that reason, understanding how chronic oxidative stress influences calcium dynamics is important. Therefore, we next investigated how the adaptation to local H_2O_2 production affects intracellular calcium levels and responses, providing a comprehensive view of the interplay between oxidative stress, NO signaling, and calcium homeostasis.

After investigating the NO dynamics in cells adapted to different local oxidative stress, we move forward to investigate calcium dynamics of each cell type using FURA imaging. As previously, cells expressing differentially located mDAAO and G-geNOp were adapted to oxidative stress conditions for five days. Then we used these cells for live-cell imaging of calcium.

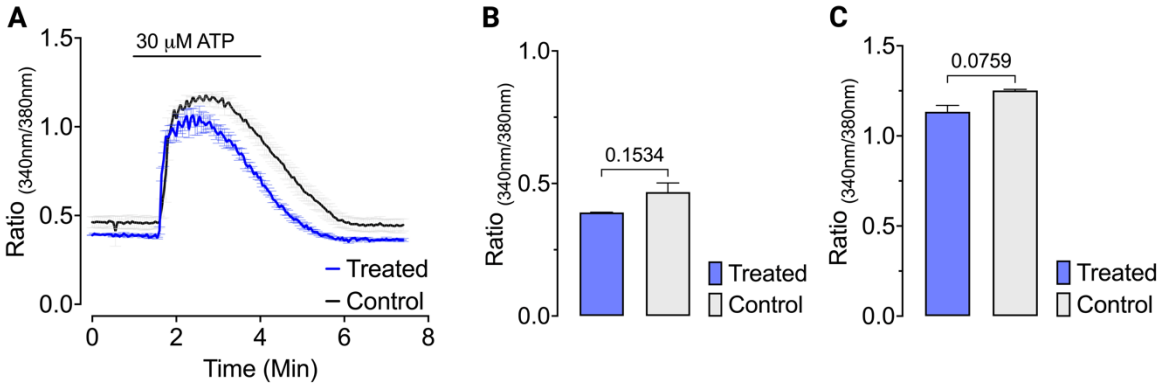

Figure 3.12: Effect of chronic production of cytosolic H_2O_2 using mCherry-mDAAO-NES in Ca^{2+} signals.

EA.hy926 cells expressing mCherry-mDAAO-NES and G-geNOp were cultured at least for 5 days in the presence (Treated) or absence (Control) of 1 mM D-Ala. After adaptation cells were used to perform live-cell imaging experiments using FURA2-AM**(A)** Average signals of FURA obtained from cells either treated with 1 mM D-Ala (blue curve) or no treatment (black curve) in response to 30 μM ATP **(B)** Bar graph represents average of basal FURA signals of cells either treated with 1 mM D-Ala (blue box) or no treatment (black box). **(C)** Bar graph represents average of maximum FURA signals of cells either treated with 1 mM D-Ala (blue box) or no treatment (black box) in response to 30 μM ATP. Data presented as mean±SEM. One-way ANOVA and Tukey's multiple comparison test are performed. p-values were indicated in bar graphs (n=3)

Initially, we used EA.hy926 cells expressing mCherry-mDAAO-NES and G-geNOp, which were adapted to chronically produced cytosolic H_2O_2. Live-cell imaging was employed to investigate Ca^{2+} dynamics. For this experiment, ATP was used to induce an increase in intracellular Ca^{2+} levels, as it had been previously used to evoke NO production. In both adapted and control cells, ATP provoked an immediate increase in intracellular Ca^{2+} levels, and the withdrawal of ATP resulted in a decrease in Ca^{2+} levels (**Figure 3.13A**).

Before ATP stimulation, we compared the initial Ca^{2+} state of the cells. According to the FURA signals, there was no significant difference in basal Ca^{2+} levels between control and adapted cells (**Figure 3.13B**). This was surprising, given that initial NO levels were significantly different.

Moreover, ATP-derived Ca^{2+} increase was also not significantly different according to maximum responses of treated cells and control cells (**Figure 3.13C**). ATP-derived NO responses were significantly different but Ca^{2+} responses were not.

After investigating Ca^{2+} signaling in cells chronically adapted to cytosolic H_2O_2, we turned our attention to the Ca^{2+} dynamics of cells chronically adapted to nuclear H_2O_2. In these adapted cells, NO dynamics were significantly different compared to control cells. Furthermore, the ATP-derived NO response was notably different and more pronounced compared to cells producing H_2O_2 in the cytosol or mitochondria.

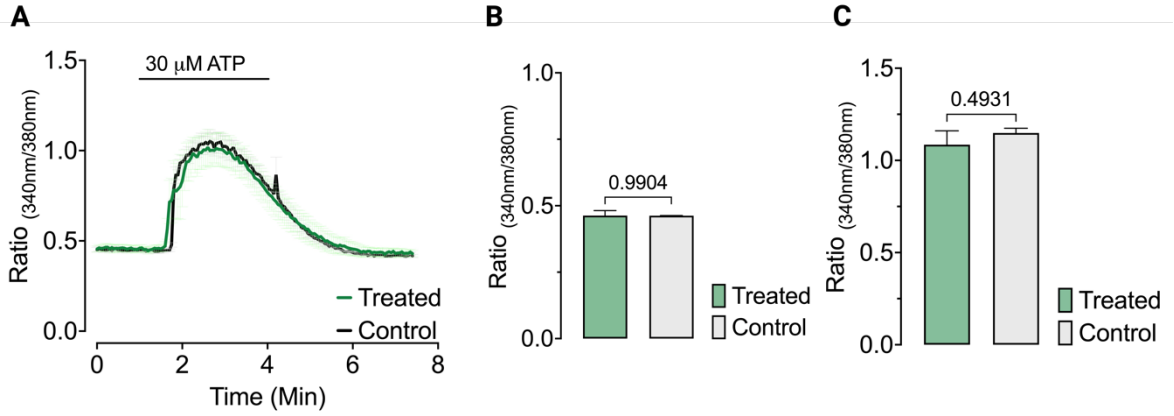

Figure 3.13: Effect of chronic production of nuclear H_2O_2 using mCherry-mDAAO-NLS in Ca^{2+} signals.

EA.hy926 cells expressing mCherry-mDAAO-NLS and G-geNOp were cultured at least for 5 days in the presence (Treated) or absence (Control) of 1 mM D-Ala. After adaptation cells were used to perform live-cell imaging experiments using FURA2-AM**(A)** Average signals of FURA obtained from cells either treated with 1 mM D-Ala (green curve) or no treatment (black curve) in response to 30 µM ATP **(B)** Bar graph represents average of basal FURA signals of cells either treated with 1 mM D-Ala (green box) or no treatment (black box). **(C)** Bar graph represents average of maximum FURA signals of cells either treated with 1 mM D-Ala (green box) or no treatment (black box) in response to 30 µM ATP. Data presented as mean±SEM. One-way ANOVA and Tukey's multiple comparison test are performed. p-values were indicated in bar graphs (n=3)

After adapting cells expressing mCherry-mDAAO-NLS and G-geNOp using 1 mM D-Ala, we investigated Ca^{2+} dynamics using live-cell imaging. ATP was used to stimulate an increase in intracellular Ca^{2+} levels, and both treated and control cells responded to ATP with a rise in intracellular Ca^{2+} (**Figure 3.13A**).

We then compared the initial Ca^{2+} state of the cells before ATP stimulation. Unlike their NO levels under resting conditions, there was no significant difference in initial Ca^{2+} levels between control and adapted cells (**Figure 3.13B**). Furthermore, the ATP-derived Ca^{2+} increase was also similar between control and treated cells. Although ATP caused a

robust Ca^{2+} increase in both cell types, the amplitude of the Ca^{2+} signals was not significantly different (**Figure 3.13C**).

After the examination of the effects of chronic cytosolic and nuclear H_2O_2 production on Ca^{2+} and NO dynamics, we next focused on the role of mitochondrial oxidative stress in Ca^{2+} dynamics. By studying cells adapted to chronic mitochondrial H_2O_2 production, we aimed to understand how mitochondrial oxidative stress influences intracellular Ca^{2+} and after we investigated NO dynamics.

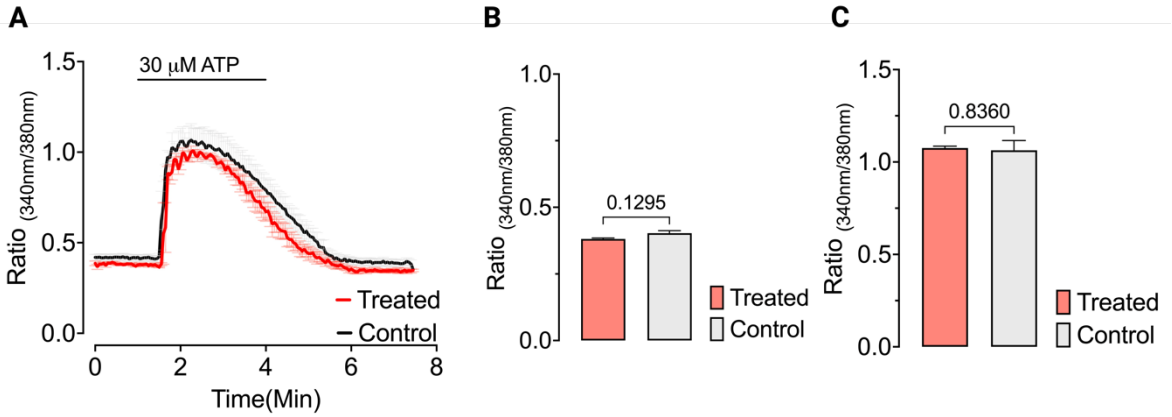

Figure 3.14: Effect of chronic production of mitochondrial H_2O_2 using Mito-mCherry-mDAAO in Ca^{2+} signals.

EA.hy926 cells expressing Mito-mCherry-mDAAO and G-geNOp were cultured at least for 5 days in the presence (Treated) or absence (Control) of 1 mM D-Ala. After adaptation cells were used to perform live-cell imaging experiments using FURA2-AM**(A)** Average signals of FURA obtained from cells either treated with 1 mM D-Ala (red curve) or no treatment (black curve) in response to 30 µM ATP **(B)** Bar graph represents average of basal FURA signals of cells either treated with 1 mM D-Ala (red box) or no treatment (black box). **(C)** Bar graph represents average of maximum FURA signals of cells either treated with 1 mM D-Ala (red box) or no treatment (black box) in response to 30 µM ATP. Data presented as mean±SEM. One-way ANOVA and Tukey's multiple comparison test are performed. p-values were indicated in bar graphs (n=3)

EA.hy926 cells expressing Mito-mCherry-mDAAO and G-geNOp were cultured with 1 mM D-Ala for five days. After adapting to chronic mitochondrial H_2O_2 production, the cells were used to image Ca^{2+} dynamics using FURA. To provoke a Ca^{2+} response in both adapted and control cells, ATP stimulation was performed, and signals from both cell types were traced (**Figure 3.14A**). In both adapted and control cells, ATP stimulation caused a substantial increase in Ca^{2+} levels, which decreased after ATP withdrawal.

Comparing the basal Ca^{2+} levels prior to ATP stimulation, the initial Ca^{2+} levels were comparable and showed no significant difference, unlike the NO signals obtained during G-geNOp imaging (**Figure 3.14B**). Additionally, the amplitude of Ca^{2+} signals after ATP stimulation was compared. While ATP-derived Ca^{2+} signals were observed in both cell types, the maximum levels were not significantly different (**Figure 3.14C**).

In this study, we explored the effects of chronic oxidative stress due to localized production of H_2O_2 in different cellular compartments, on NO and Ca^{2+} dynamics in EA.hy926 endothelial cells using stably expressing chemogenetic tool mDAAO and NO biosensor G-geNOp.

Chronic cytosolic, nuclear, mitochondrial H_2O_2 production led to significant increases in both basal NO levels and ATP-derived NO responses (**Figure 3.9**, **Figure 3.10** and **Figure 3.11** respectively). This suggests that chronic oxidative stress in these compartments enhances the cells' capacity for NO production, likely due to increased eNOS activity or expression. On previous study highlighted that localized production of H_2O_2 contribute one of eNOS activating phosphorylation at residue S1177 [95]. In this study, cytosolic, caveolar and nuclear production of H_2O_2 increased eNOS phosphorylation. Although it was previously demonstrated by Eroglu et al. phosphorylation does not necessarily cause production of NO [38]. For this case, we can assume that increased phosphorylation can enhance the production or responsiveness of NO to stimulator.

Interestingly, while chronic localized production of H_2O_2 adaptation elevated NO levels, the same effect in Ca^{2+} signaling was not observed. In previous part, exogenous application of H_2O_2 had an effect on both basal NO levels and basal Ca^{2+} levels (**Figure 3.7**). We discussed this observation and made assumptions on membrane permeability. In this case, we did not observe significant changes in both basal and amplitude of ATP-derived Ca^{2+} increase in cells experienced localized H_2O_2 chronically (**Figure3.12**, **Figure 3.13** and **Figure 3.14**). However, we observed significant changes in ATP-derived

NO production. The difference between NO dynamics and Ca^{2+} most likely due to the effect of localized H_2O_2 primarily influence eNOS phosphorylation.

Our study demonstrates that chronic localized oxidative stress can differentially modulate NO and Ca^{2+} signaling dynamics in endothelial cells. These findings provide valuable insights into the compartmentalized nature of oxidative stress signaling and its broader implications for endothelial cell function and pathology. Difference between localized or extracellular application of H_2O_2 would lead differential outcomes in terms of NO dynamics and Ca^{2+} dynamics. This part of the study highlights the importance of application of oxidative stress in endothelial signaling.

Optimizations in live-cell imaging for HyPer7 and O-geNOp

After discovering that H_2O_2 influence varies under different oxidative stress conditions, we aimed to optimize our imaging methods. Multiparametric imaging requires fine-tuning of specific parameters to enhance the signals obtained from biosensors. Previously, we generated a double stable cell line expressing both HyPer and O-geNOp to study the effects of short pulse H_2O_2 on NO signaling (**Figure 3.5**). To understand the dynamics of both molecules, we needed an imaging protocol with the highest signal-to-noise ratio. Studies have shown the effect of H_2O_2 on eNOS within hours [38], [95], so it was essential to demonstrate the direct interaction of H_2O_2 and NO. For this purpose, we generated an EA.hy926 cell line expressing both biosensors. To optimize multiparametric imaging, we adjusted several parameters that could affect the biosensors' dynamics, such as camera binning, different imaging devices, and temperature.

Camera binning is a commonly used technique in digital imaging. It groups adjacent pixels on an image sensor, which reduces image resolution but enhances

sensitivity by improving the signal-to-noise ratio (SNR). This method allows for the detection of weaker signals and shortens acquisition times, making it ideal for real-time imaging [96]. However, enhancement in SNR costs reduced spatial resolution and increased noise.

We have two biosensors expressed in a single cell: HyPer7 and O-geNOp. Spectrally, HyPer7 is excited at two different wavelengths, 430 nm and 475 nm, and emission is collected at 525 nm for our experiments. HyPer7 has ratiometric imaging capability due to this dual excitation. When excited at 430 nm and with emission collected at 525 nm, it is referred to as the HyPer-Low channel. In this setup, signal intensity decreases in the presence of H_2O_2. In another optical path, HyPer7 is excited at 475 nm, with emission collected at 525 nm, referred to as the HyPer-High channel. The HyPer ratio is obtained by dividing the fluorescence of HyPer-High by the fluorescence of HyPer-Low.

To observe the effect of camera binning, we imaged HyPer-expressing cells under varying binning setups (**Figure 3.15A**). As expected, increasing the binning factor resulted in a decrease in resolution. We then investigated the HyPer signals under different binning setups. The addition of H_2O_2 evoked robust HyPer signals in all binning setups, but the amplitude of the signal varied (**Figure 3.15B**). To compare the amplitudes, we normalized the HyPer signals obtained and found that 4x4 binning produced the highest signal in response to H_2O_2. In the 1x1 (no binning) setup, the signal amplitude was the lowest and tended to decrease even with continuous H_2O_2 perfusion. Examining the close-up curves for H_2O_2 response of HyPer under different camera binning setups, we observed that the signal was acquired faster with 4x4 binning (**Figure 3.15C**). Additionally, the fold changes of HyPer signals in response to the same concentration of H_2O_2 were significantly different: the 1x1 binning setup had the lowest fold change, while the 4x4 binning had the highest fold change (**Figure 3.15D**). Finally, we compared the rate of change in HyPer signals upon the addition of H_2O_2. The fastest response was obtained using the 4x4 camera binning setup, whereas the 1x1 binning had the lowest response rate (**Figure 3.15E**).

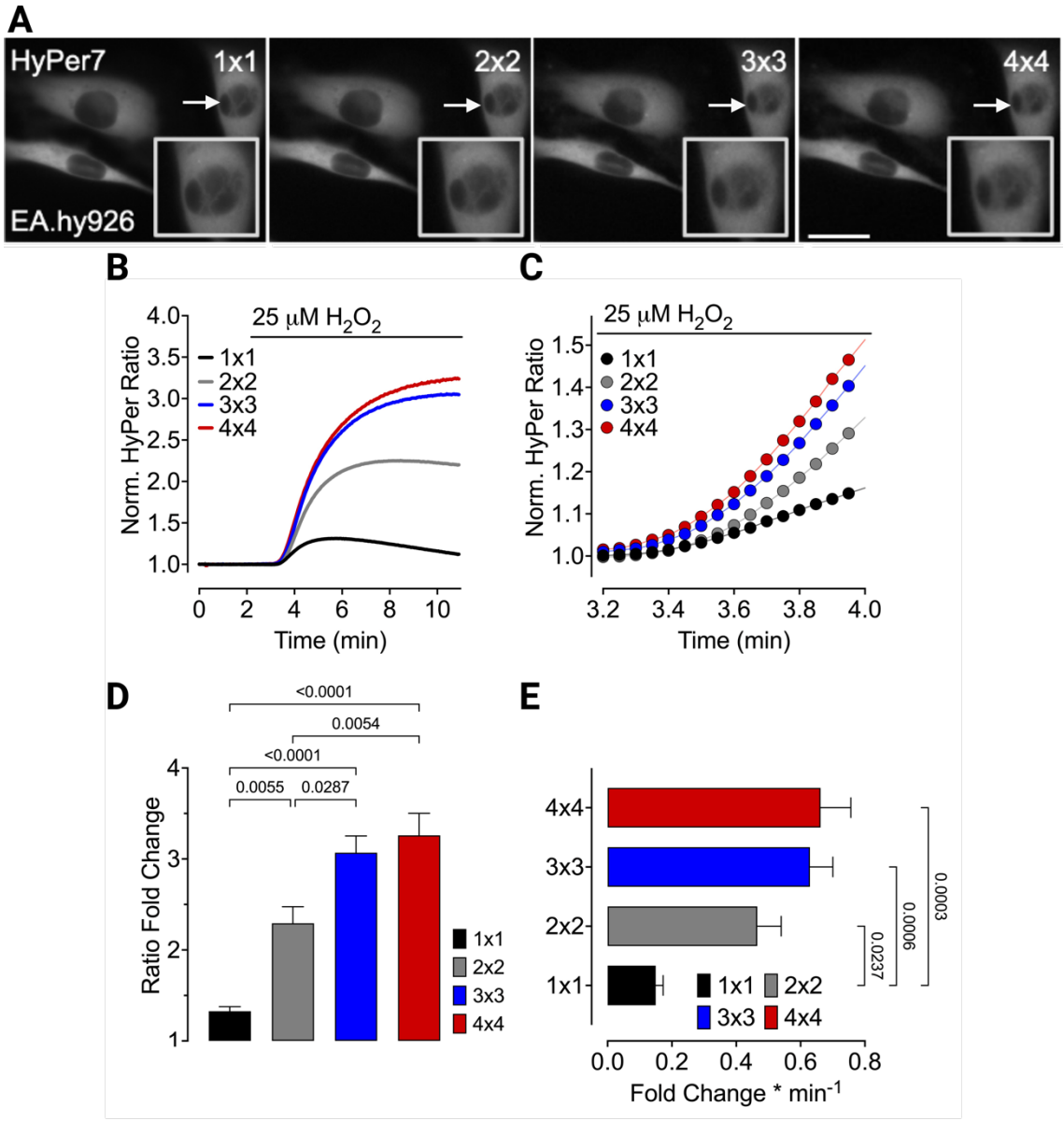

Figure 3.15: Binning factor influences HyPer imaging

(A) Representative fluorescence images of EA.hy926 cells expressing H.7-NES under different binning setup 1x1, 2x2, 3x3 and 4x4. Arrows indicate resolution decrease in same images. Insets shows close-up images of area where resolution decrease observed. **(B)** Curves represent HyPer signals of cells expressing H.7-NES in response to 25 µM H_2O_2 using different camera binning setups: 1x1 (black curve), 2x2 (grey curve), 3x3(blue curve) and 4x4 (red curve) (n=3) **(C)** Close-up curves shows the dynamics of HyPer signals in part A. **(D)** Bar graphic represents average fold change of H.7-NES signals in response to 25 µM H_2O_2 under different binning conditions: 1x1 (black bar), 2x2 (grey bar), 3x3(blue bar), 4x4 (red bar). **(E)** Bar graphic represents average rate of fold change in HyPer signals in response to 25 µM H_2O_2 under different binning conditions: 1x1 (black bar), 2x2 (grey bar), 3x3(blue bar), 4x4 (red bar). Data presented as mean±SEM. One-way ANOVA and Tukey's multiple comparison test are performed. p-values were indicated in bar graphs (n=3)

To understand the difference between binning factors, we analyzed the raw HyPer ratio under two different binning conditions: 1x1 and 4x4. Raw HyPer ratios were monitored, and in the 1x1 binning setup, we observed that the ratio is increased even in the absence of H_2O_2. Additionally, the addition of H_2O_2 caused an increase in the HyPer ratio, but the trend indicated bleaching in the raw signals. However, in the 4x4 binning setup, HyPer responded to H_2O_2 in a robust manner, and the ratio remained steady in the absence of H_2O_2 (**Figure 3.16A**). Furthermore, signals that are constituents of HyPer ratio were traced with the HyPer ratio during H_2O_2 provision. In the 1x1 binning setup, HyPer Low signals were severely bleached, and HyPer High signals were moderately bleached. The HyPer ratio, obtained by dividing these two signals, showed a false increase due to bleaching in both signals (**Figure 3.16B**). In contrast, signals in the 4x4 binning setup were not affected by bleaching and showed an accurate HyPer ratio in response to H_2O_2 (**Figure 3.16C**).

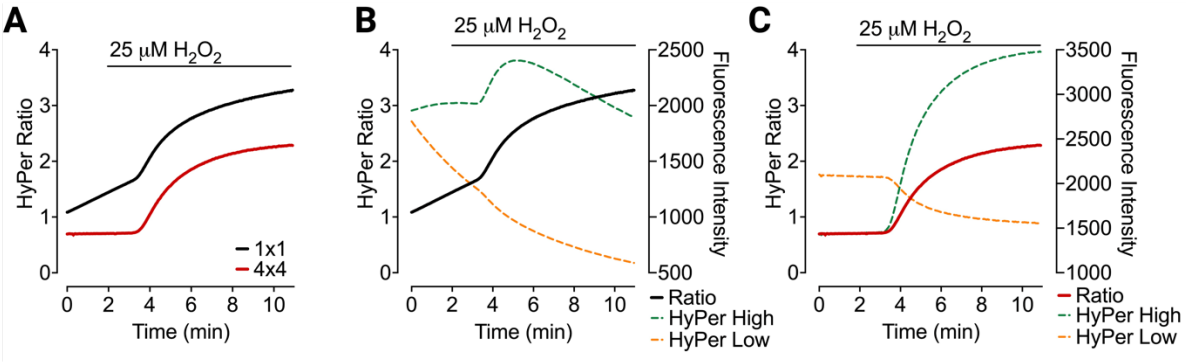

Figure 3.16: Raw HyPer signals under different binning conditions.

(A) The average curves show HyPer ratios following the addition of 25 μM H_2O_2. The black line represents measurements with 1x1 camera binning, while the red line represents measurements with 4x4 binning. **(B)** The average curves depict HyPer signals using 1x1 camera binning when cells were treated with 25 μM H_2O_2. The solid black line indicates the HyPer ratio signals, the dashed green line indicates HyPer High (Ex/Em: 475/525) signals, and the dashed orange line indicates HyPer Low (Ex/Em: 430/525) signals. **(C)** The average curves illustrate HyPer7 signals using 4x4 camera binning when cells were treated with 25 μM H2O2. The solid red line shows the HyPer ratio signals, the dashed green line shows HyPer High (Ex/Em: 475/525) signals, and the dashed orange line shows HyPer Low (Ex/Em: 430/525) signals.

To understand the effect of the binning factor, we need to examine the formulas for signal and noise. Signal is represented by I, noise by σ, and the binning factor by M. In SNR (signal-to-noise ratio) calculations, the signal increases by a factor of M, while noise increases by the √M. Normally, we would expect a 4-fold increase in SNR with 4x4 binning, but we observed an approximately 8-fold increase. This prompted us to investigate the components of noise further.

$$Signal\ (I) = M(Photon\ Flux\ x\ Quantum\ Efficiency\ of\ Camera\ x\ Time)$$

$$Noise\ (\sigma) = \sqrt{M(Dark\ noise)\ x\ M(I)\ \ x\ Read\ Noise}$$

Dark noise in our experiments is defined as the background fluorescence present without any fluorescent source, such as cells or non-fluorescent cells[97]. We maintained constant read noise across all experiments, which was determined by the excitation light intensity used to activate the HyPer biosensor. To achieve consistent total fluorescence within the field of view, we optimized conditions by keeping the exposure time constant and adjusting the excitation light intensity based on the binning factor. Increasing binning factor caused decrease in excitation light intensity This method resulted in similar background fluorescence levels across all experiments (**Figure 3.17**). For HyPer7 measurements, the background fluorescence in each channel and the ratio remained consistent at various camera binning settings. Despite experiencing photobleaching at lower camera binning settings in the HyPer Low channel, the background signals were stable over time.

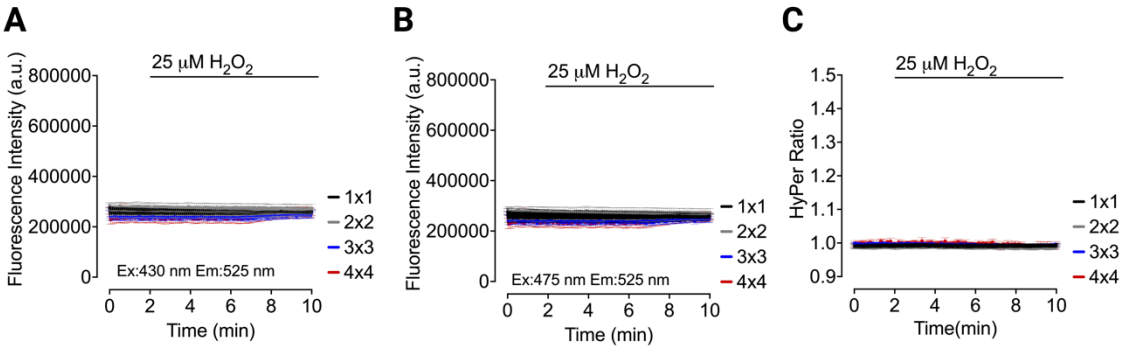

Figure 3.17: Effect of camera binning on background noise.

HyPer Low **(A)**, HyPer High **(B)** and HyPer ratio **(C)** signals were measured with different binning setups upon addition of 25 μM H_2O_2. Different background regions (ROI) were selected, and signals were traced over time.

After examining the binning setup for HyPer signals, we proceeded to investigate O-geNOp signals under different camera binning setups. O-geNOp expressing cells were visualized under a fluorescence microscope using various camera binning setups, and a decrease in resolution was observed (**Figure 3.18A**). We then examined the NO signals in different binning setups using the NO donor NOC-7, but before administering NOC-7, we provided L-NAME to prevent interference from endogenously produced NO due to eNOS function. The geNOp signals in response to NOC-7 indicated that the binning factor did not affect O-geNOp kinetics (**Figure 3.18B**). Additionally, the close-up curves of O-geNOp were similar across all binning setups (**Figure 3.18C**). The amplitudes of the O-geNOp signals were compared statistically across all binning setups. In each setup, the provision of NOC-7 yielded similar responses, with no significant differences observed (**Figure 3.18D**). Additionally, we compared the rate of change in signals across the different binning setups and found no significant differences here either (**Figure 3.18E**). These results indicate that camera binning does not significantly impact the amplitude or kinetics of O-geNOp signals, suggesting that the biosensor's performance remains consistent regardless of the binning setup used.

This was surprising to us because we observed significant changes in HyPer imaging but not in O-geNOp imaging. To understand this discrepancy, we examined the quantum efficiency of the camera, which refers to its ability to capture photons emitted from biosensors, considering the different fluorescent proteins used by the biosensors. HyPer emits around 525 nm, while O-geNOp emits around 605 nm. At these wavelengths, the quantum efficiency of the Axiocam 503 mono camera was similar, approximately 70%. Therefore, the difference in imaging results is not due to the camera's quantum efficiency at different fluorescence emissions.

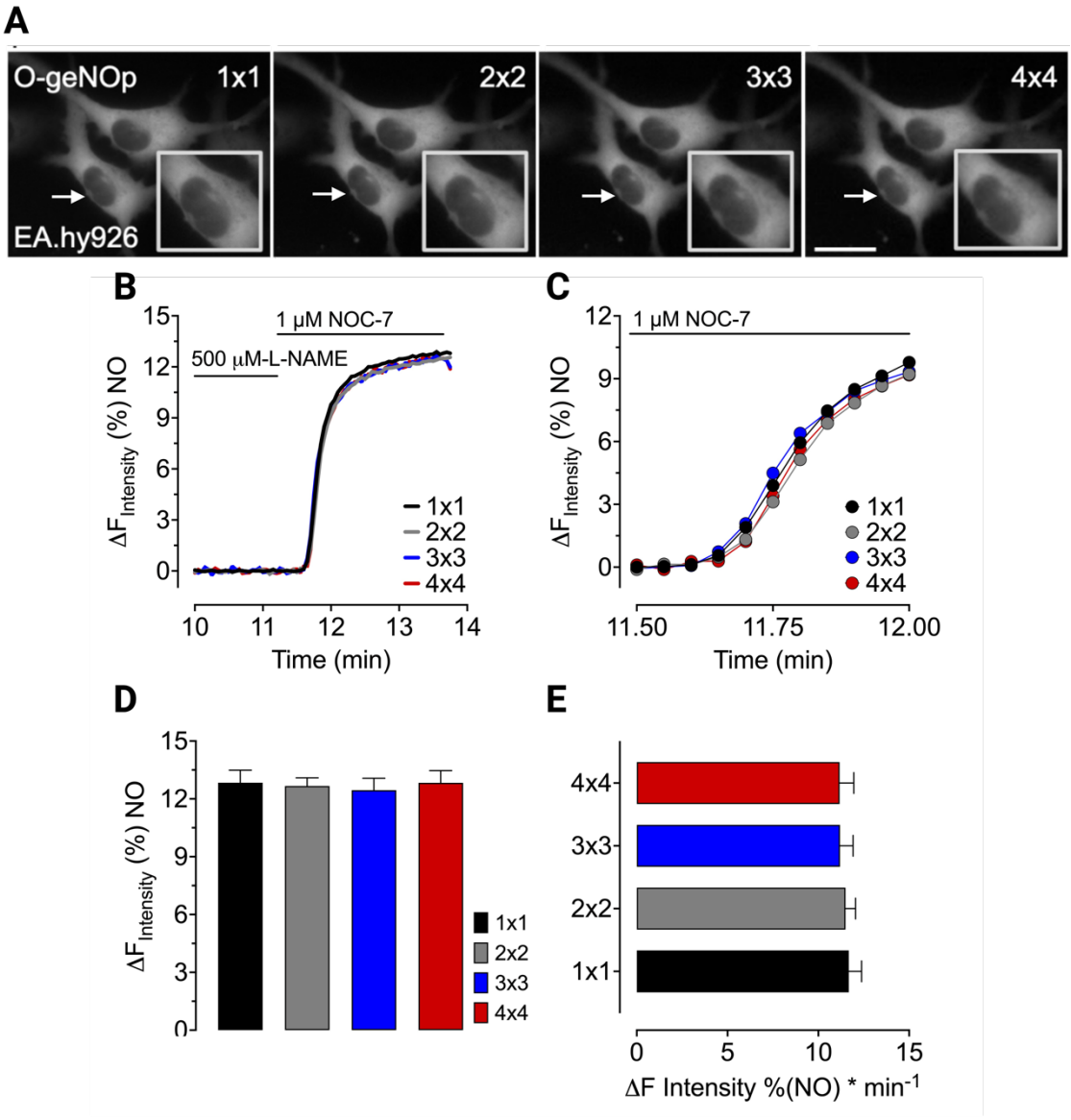

Figure 3.18: Binning factor does affect O-geNOp signals

(A) Representative fluorescence images of EA.hy926 cells expressing O-geNOp-NES under different binning setup 1x1, 2x2, 3x3 and 4x4. Arrows indicate resolution decrease in same images. Insets shows close-up images of area where resolution decrease observed. **(B)** Curves represent O-geNOp signals of cells pre-treated with 500 µM L-NAME and expressing O-geNOp-NES in response to 1 µM NOC-7 using different camera binning setups: 1x1 (black curve), 2x2 (grey curve), 3x3(blue curve) and 4x4 (red curve) (n=3) **(C)** Close-up curves shows the dynamics of o-geNOp signals in part A. **(D)** Bar graphic represents average maximum responses of O-geNOp signals in addition to 1 µM NOC-7 under different binning conditions: 1x1 (black bar), 2x2 (grey bar), 3x3(blue bar), 4x4 (red bar). **(E)** Bar graphic represents average rate of change in O-geNOp signals in response to 1 µM NOC-7 under different binning conditions: 1x1 (black bar), 2x2 (grey bar), 3x3(blue bar), 4x4 (red bar). Data presented as mean±SEM. One-way ANOVA and Tukey's multiple comparison test are performed. p-values were indicated in bar graphs (n=3)

In HyPer imaging, we observed that the HyPer Low channel was severely affected by the binning factor due to higher excitation light intensity under low binning conditions. To excite HyPer, we use shorter wavelengths compared to O-geNOp, specifically 430 nm excitation light for the HyPer Low setup, which has higher energy. We suspect that 430 nm light can cause photobleaching in HyPer imaging. To investigate this, we conducted experiments using the green version of geNOp, which has a similar emission wavelength as HyPer.

We imaged G-geNOp using two different optical setups. The first setup was a regular GFP setup with a 475 nm excitation wavelength and emission collected at 525 nm. The second setup was the HyPer7 optical setup, which uses two excitation wavelengths, 430 nm and 475 nm, with emission collected at 525 nm. We started with the first setup, using G-geNOp expressing endothelial cells, and provided NOC-7 after treatment with L-NAME under two different camera binning setups: 1x1 and 4x4.

In the regular GFP setup, we compared the responses of G-geNOp to NOC-7 using varying binning setups. Signals obtained using the 1x1 binning setup were slightly slower, but not significantly so (**Figure 3.19A, left panel**). We also compared the amplitude of the signals between the 1x1 and 4x4 setups and found no significant difference in amplitude (**Figure 3.19A, right panel**).

Next, we used the second optical setup, imaging G-geNOp using the HyPer7 optical setup. We observed that 1x1 binning significantly affected the NOC-7 responses of G-geNOp, while signals obtained with 4x4 binning were robust (**Figure 3.19B, left panel)**. Additionally, we compared the amplitude of the signals and found that 1x1 binning significantly decreased the maximum response of G-geNOp to the same concentration of the NO donor compared to 4x4 binning.

Thus, the presence of higher energy wavelength during the excitation of biosensors affects the performance of a biosensor because higher energy wavelength causes photostress [98]. Binning factor comes with an importance due to decrease in binning

factor requires increase excitation light intensity due to resolution increase. This issue is important for multiparametric imaging where two different biosensors is used.

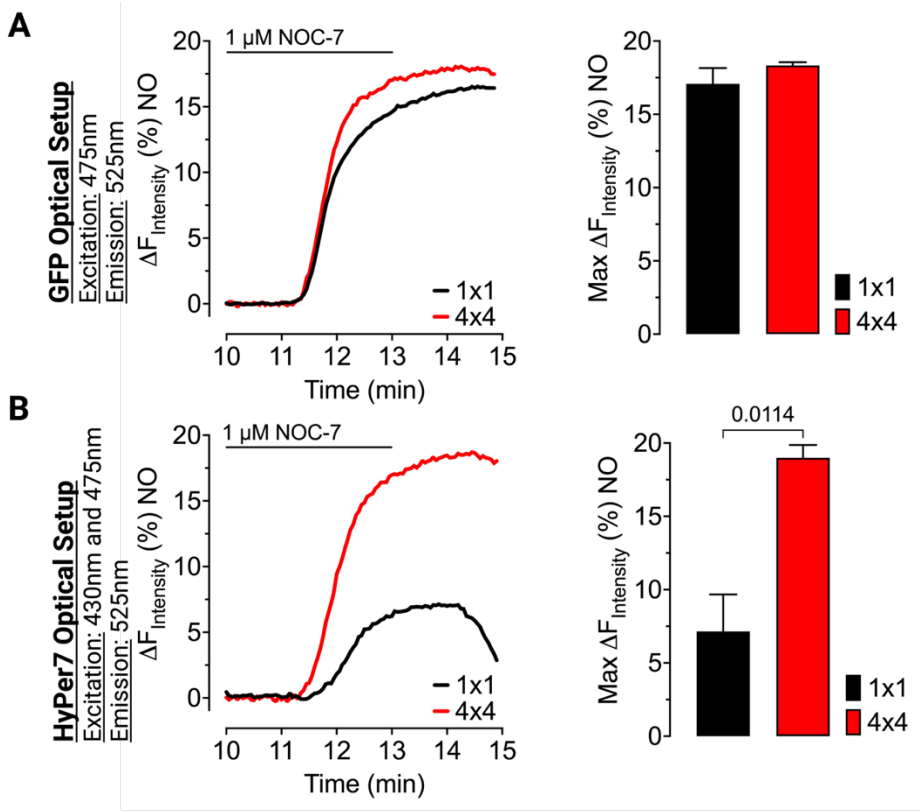

Figure 3.19: Effects of camera binning and visualization method on G-geNOp signals

(A) Average curves represent real-time G-geNOp signals in response 1 µM NOC-7 using different camera binning settings including 4x4 (red curve) and 1x1 (grey curve). All experiments have been visualized with standard GFP imaging settings using Ex: 475 nm and Em: 525 nm. Bars show maximum amplitudes of G-geNOp signals in EA.hy926 cells in response to 1 µM NOC-7 (n=3). **(B)** Average curves represent real-time G-geNOp signals in response 1 µM NOC-7 using different camera binning settings including 4x4 (red curve) and 1x1 (grey curve). All experiments have been visualized with HyPer optical setup Ex:430nm and 475 nm and Em: 525 nm. Bars show maximum amplitudes of G-geNOp signals in EA.hy926 cells in response to 1 µM NOC-7 (n=3). Data presented as mean±SEM. Student's t-test is performed. p-values were indicated in bar graphs (n=3)

After optimizing the binning factor for each biosensor, we proceeded to investigate the differences between imaging devices. Until now, we have used a widefield epifluorescence microscope for live-cell imaging. However, spinning disk confocal microscopes offer high contrast and fast live-cell imaging. Therefore, we examined the performance of HyPer7 and O-geNOp using both widefield epifluorescence and spinning

disk confocal microscopes.To investigate HyPer responses using different imaging devices, EA.hy926 cells expressing HyPer were subjected to live-cell imaging. Representative images were obtained using either a widefield microscope (WF) or a spinning disk confocal microscope (SD), demonstrating that SD provides higher contrast compared to WF (**Figure 3.20A**). Additionally, the SD is equipped with a specialized camera dedicated to live-cell imaging. Cells were treated with H_2O_2, and the responses were compared. Both WF and SD imaging resulted in robust HyPer responses with similar trends (**Figure 3.20B, left panel**). Comparing the maximum responses revealed no significant difference in HyPer signals between the two imaging devices (**Figure 3.20B, right panel**). This indicates that HyPer imaging is not affected by higher contrast imaging.

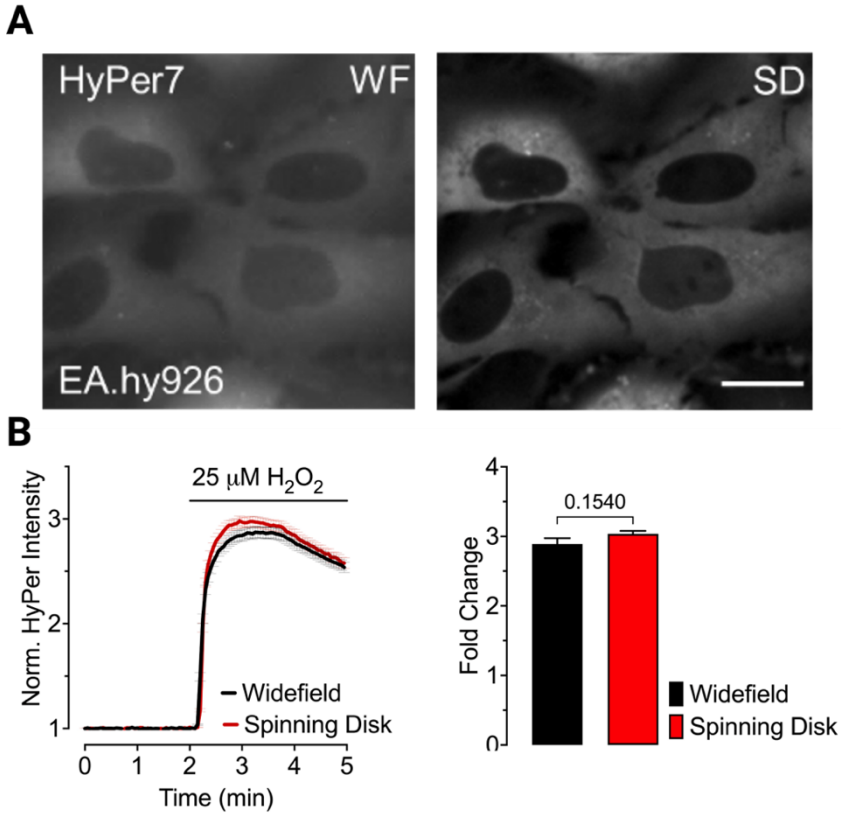

Figure 3.20: Visualizing HyPer signals in different imaging rigs.

(A) Representative fluorescence images of EA.hy926 cells expressing H.7-NES using widefield fluorescence microscope (left panel) and spinning disk confocal microscope (right panel). Scale bar represents 20 µm **(B)** Graphic in left panel represents average HyPer signals in response to 25 µM of H_2O_2 utilizing different imaging devices widefield (black line) and spinning disk (red line) microscopes. Bar graph in right panel indicates fold change in HyPer signals of cells in response 25 µM of H_2O_2 . HyPer signal obtained via widefield (black bar) or spinning disk (red bar) microscopes. Data presented as mean±SEM. Student's t-test is performed. p-values were indicated in bar graphs (n=3).

Next, we investigated O-geNOp using different imaging devices. EA.hy926 cells expressing O-geNOp were imaged using either a WF or SD. The SD images demonstrated higher contrast compared to the WF images (**Figure 3.21A**). These cells were then used for live-cell imaging with WF and SD by providing NOC-7 after treatment with L-NAME. O-geNOp signals obtained in response to NOC-7 were similar across both imaging devices (**Figure 3.21B, left panel**). Additionally, when comparing the maximum responses of O-geNOp, there was no significant difference between signals obtained via WF or SD (**Figure 3.21B, right panel**). Thus, O-geNOp dynamics were also not affected by the imaging device.

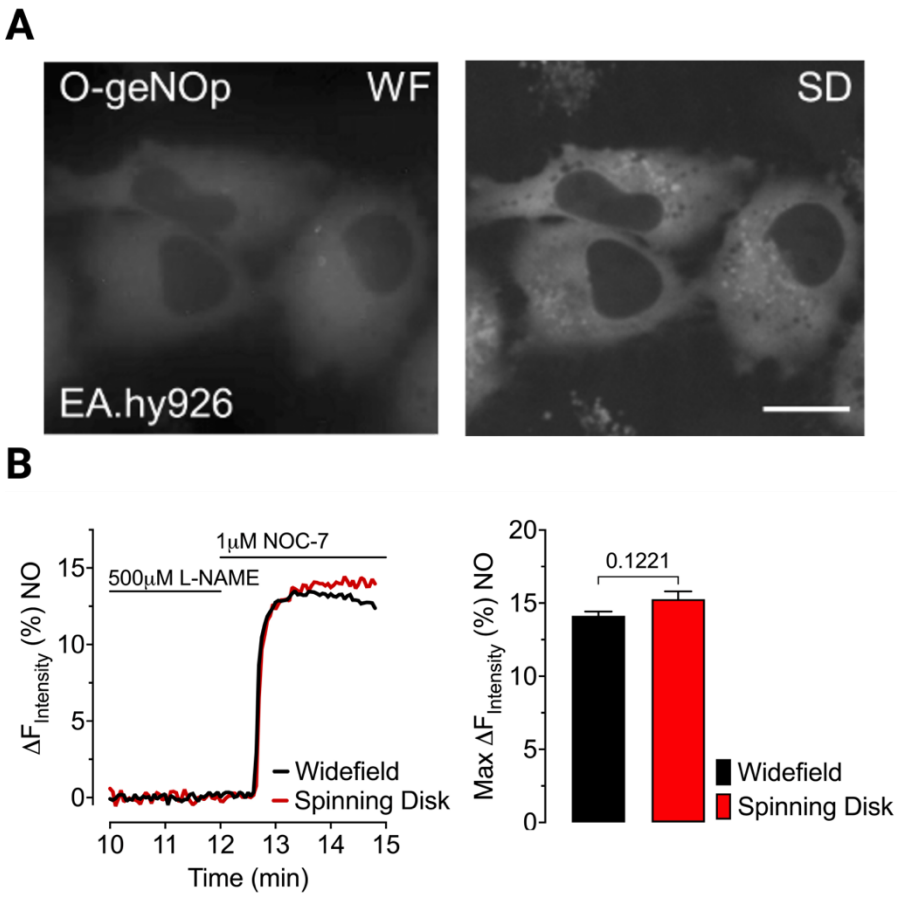

Figure 3.21: Visualizing geNOp signals in different imaging rigs.

(A) Representative fluorescence images of EA.hy926 cells expressing O-geNOp-NES using widefield fluorescence microscope (left panel) and spinning disk confocal microscope (right panel). Scale bar represents 20 μm **(B)** Graphic in left panel represents average O-geNOp signals in response to 1 μM of NOC-7 and pre-treated with 500 μM L-NAME utilizing different imaging devices widefield (black line) and spinning disk (red line) microscopes. Bar graph in right panel indicates fold change in geNOp signals of cells in response1 μM of NOC-7. geNOp signal obtained via widefield (black bar) or spinning disk (red bar) microscopes. Data presented as mean±SEM. Student's t-test is performed. p-values were indicated in bar graphs (n=3).

Ambient temperature is physiologically important because mammalian-derived cells typically experience conditions at 37°C, unlike room temperature (RT). Additionally, biosensors contain fluorescent proteins derived from cold-blooded animals[99]. Therefore, we hypothesized that temperature could affect the kinetics of these biosensors. To test this, we compared the performance of each biosensor at different temperatures, specifically RT and 37°C.

EA.hy926 cells expressing HyPer were imaged under different ambient temperatures. During live-cell imaging, H_2O_2 was provided, and HyPer responses were traced. According to the HyPer signals, temperature change did not affect the responses in the presence of H_2O_2 (**Figure 3.22A, left panel**). Comparing the maximum responses, there was no significant difference (**Figure 3.22A, right panel**). Next, we compared O-geNOp signals using cells expressing O-geNOp. After L-NAME treatment, cells were provided with NOC-7, and signals were recorded. Similar to the HyPer results, we observed comparable signals at both ambient temperatures (**Figure 3.22B, left panel**). Additionally, the maximum responses at different ambient temperatures were not significantly different (**Figure 3.22B, right panel**).

Our study demonstrated that ambient temperature variations between room temperature (RT) and physiological temperature (37°C) do not significantly affect the performance of the HyPer7 and O-geNOp biosensors. Both biosensors showed similar responses to H_2O_2 and NO donors, respectively, regardless of the ambient temperature. This shows that the fluorescent proteins in these biosensors are stable and reliable under different temperature conditions, making them suitable for various experimental setups. These findings provide confidence that HyPer7 and O-geNOp can be effectively used in live-cell imaging studies without concern for temperature-induced variability in their signal kinetics.

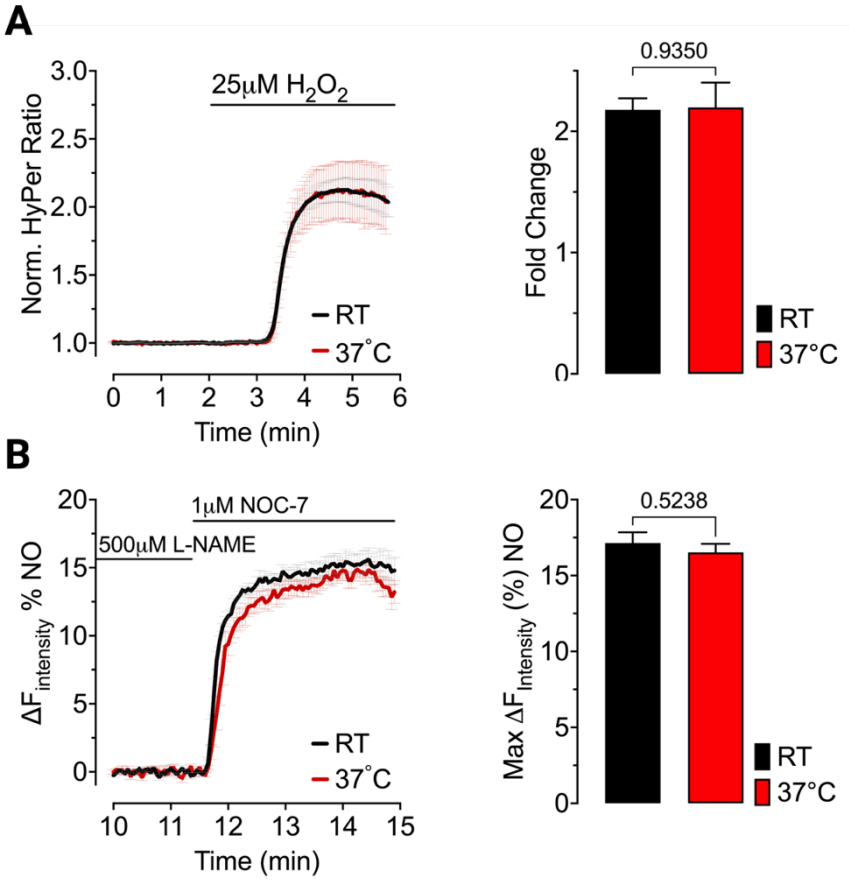

Figure 3.22:Effect of ambient temperature on HyPer and geNOp signals

(A) Graphic shows responses of EA.hy926 cells expressing H.7-NES imaged under RT (black line) or 37 °C (red line) in response to 25 μM H_2O_2. Right panel shows the maximum responses of HyPer while ambient temperature is RT (black bar) or 37 °C (red bar). **(B)** Graphic shows responses geNOp signals of EA.hy926 cells expressing O-geNOp-NES imaged under RT (black line) or 37 °C (red line) pre-treated with 500 μM L-NAME then provided with 1 μM NOC-7 as indicated. Right panel shows the maximum responses of geNOp while ambient temperature is RT (black bar) or 37 °C (red bar). Data presented as mean±SEM. Student's t-test is performed. p-values were indicated in bar graphs (n=3).

After determining the optimal imaging parameters, we used these settings for multiparametric imaging. We chose to use 4x4 binning for live-cell imaging. For ease of use, we decided to image cells using a widefield fluorescence microscope under room temperature conditions. Access to the spinning disk confocal microscope is limited and maintaining ambient temperature of 37°C requires special equipment. Therefore, for live-cell imaging, we set the parameters to 4x4 binning, room temperature conditions, and the use of a widefield fluorescence microscope.

To visualize both molecules, cells expressing both biosensors were imaged under optimized conditions. Both H_2O_2 and NO were administered exogenously. In the first set of experiments, H_2O_2 was provided first, followed by NO (**Figure 3.23A**). In the presence of H_2O_2, there was no change in NO signals, and the provision of NO did not affect H_2O_2 levels. We then performed the same experiment in reverse order, providing NO first and then H_2O_2 (**Figure 3.23B**). Under optimized parameters, we successfully visualized both molecules simultaneously.

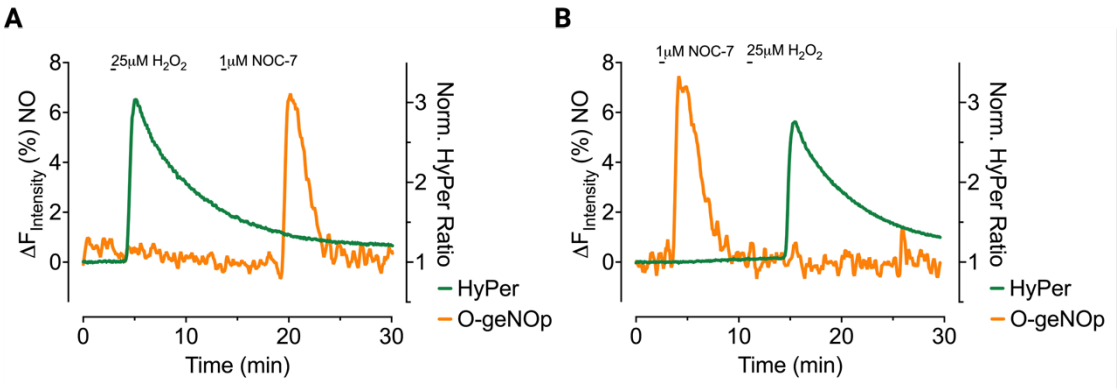

Figure 3.23: Simultaneous imaging of exogenous NO and H_2O_2 in different order under optimized conditions.

(A) Average curve represents simultaneous measurements of cells expressing both H.7-NES and O-geNOp-NES. Curves represent signals of HyPer (green line, right Y-axis) and O-geNOp (orange line, left-axis) after providing 25µM H_2O_2 and 1µM NOC-7, respectively **(B)** Same experimental setup in part A but NO and H2O2 provided in opposite order.

After successfully imaging exogenous H_2O_2 and NO simultaneously, we conducted experiments where both molecules were endogenously produced. We used two different binning setups to emphasize the effect of binning on measuring low concentrations of NO and H_2O_2. Histamine was used to produce endogenous NO, while auranofin, an inhibitor of thioredoxin reductase, was used to accumulate H_2O_2 intracellularly. Initially, we set the camera binning to 1x1. Histamine stimulation did not produce a robust NO signal, but auranofin treatment led to an increase in the HyPer signal (**Figure 3.24A**). Additionally, auranofin did not yield any NO signals. When we set the camera binning to 4x4, we observed robust NO production following histamine treatment. Auranofin also resulted in strong H_2O_2 production compared to 1x1 binning (**Figure 3.24B**). Comparing the responses of O-geNOp in the presence of histamine or auranofin showed that histamine stimulation was not visible with 1x1 binning and significantly lower when comparing O-

geNOp signals between 1x1 and 4x4 binning. Auranofin did not produce robust NO signals under either condition (**Figure 3.24C**).

Maximum responses of HyPer were compared, and auranofin-derived H2O2 production was significantly more pronounced with 4x4 binning. Histamine did not yield any HyPer response (**Figure 3.24D**). The binning factor affected both HyPer and O-geNOp signals during simultaneous imaging when both molecules were endogenously produced because concentration of endogenous production was lower compared to exogenous application. Therefore, lower binning is not suitable for endogenous signaling during simultaneous imaging.

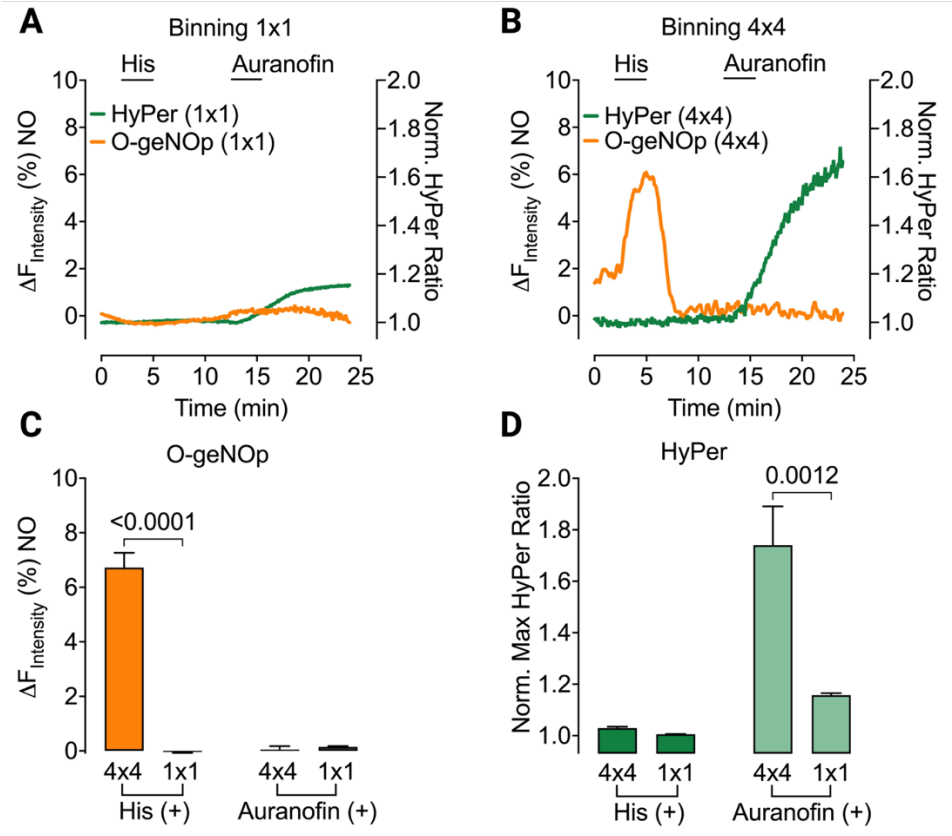

Figure 3.24: Simultaneous imaging of endogenously produced H_2O_2 and NO under different binning conditions.

(A) EA.hy926 cells expressing both H.7-NES and O-geNOp-NES imaged using 1x1 binning setup. Traces represent signals of HyPer (green line, right Y-axis) and geNOp (orange line, left Y-axis) in response to 30 µM histamine and 3 µM auranofin. **(B)** Same experimental setup with part A but 4x4 binning setup is used. **(C)** Maximum responses of geNOp in different binning setups in the presence of histamine or auranofin **(D)** Maximum responses of HyPer in different binning setups in the presence of histamine or auranofin. Data presented as mean±SEM. Student's t-test is performed. p-values were indicated in bar graphs (n=3).

In this part of the study, we focused on optimizing live-cell imaging for the simultaneous detection of H_2O_2 and NO using the biosensors HyPer7 and O-geNOp. Our experiments demonstrated that the camera binning factor plays a crucial role in enhancing signal detection in HyPer but not in O-geNOp, if a biosensor excited using high energy photons such as HyPer Low channel of Hyper7 biosensor (**Figure 3.15** and **Figure 3.16**). Low binning increases resolution but it requires more excitation light intensity. Studies shown that fluorescent proteins when illuminated with a high energy light can cause photobleaching and phototoxicity [100], [101].Using a 4x4 binning setup significantly improved the signal-to-noise ratio, making it more effective for capturing endogenous signals compared to the 1x1 binning setup. This improvement was evident in the robust detection of NO following histamine stimulation and H_2O_2 accumulation via auranofin treatment (**Figure 3.24**).

Additionally, we evaluated the impact of different imaging devices on biosensor performance. Both widefield epifluorescence and spinning disk confocal microscopy provided consistent results for HyPer7 and O-geNOp signals, indicating that high contrast imaging does not significantly affect responses of these biosensors (**Figure 3.21** and **Figure 3.22**). Furthermore, our assessment of ambient temperature effects revealed that both HyPer7 and O-geNOp maintained stable performance at room temperature and physiological temperature (37°C), underscoring their reliability under varying experimental conditions (**Figure 3.23**). Although we did not observe any intervention related to temperature but before doing multiparametric imaging scientist should consider physiological temperatures to monitor signaling events using various biosensors.

These optimizations are critical for accurate multiparametric imaging, as they ensure that both biosensors function optimally without interference from imaging parameters. Although we successfully measured both molecules simultaneously, we couldn't find any evidence that acute increase in H_2O_2 affects the production of NO or vice versa. For that reason, we need to focus more on physiology after we optimized the imaging parameters.

Effect of pericellular O_2 in relationship of H_2O_2 and NO

Oxygen is a critical factor, primarily used as an electron acceptor in physiological processes. It plays a pivotal role in many functions, such as in the electron transport chain (ETC), where O_2 is reduced to H_2O. However, during electron transport, superoxide is also formed. The utilization of O_2 is central to the topic of reactive oxygen species (ROS) because superoxide is the most studied form of ROS. O_2 affects the production of H_2O_2 through the dismutation of superoxide and is directly involved in H_2O_2 production via enzymes like NADPH oxidases [102]. Additionally, O_2 influences NO formation, impacting production steps and the formation of peroxynitrite through reactions with superoxide [103].

Atmospheric O_2 is about 20.9 kPa, but our body experiences O_2 levels ranging between 12 and 0.5 kPa, depending on the organ [104]. Endothelial cells experience O_2 levels around 5 kPa. In vitro studies are often conducted under room air conditions, which have higher O_2 concentrations (18 kPa) compared to physiological conditions. Studies indicate that high O_2 levels affect antioxidant mechanisms [105], [106], due to increased ROS formation. Moreover, recent findings highlight that physiologically relevant O_2 conditions increase the bioavailability of NO and increases the expression of eNOS [107], [108]

Due to its role in ROS formation and NO bioavailability, we need to consider the ambient O_2 conditions while we are investigating the relationship of H_2O_2 and NO. Our recent work highlighted the importance of O_2 levels in NO signaling and geNOp function. In that study we compared the room air condition (18 kPa O_2 or Hyperoxic) with physiologically relevant O_2 condition (5 kPa O2 or Normoxic). Normoxic conditions increased NO bioavailability and uptake of iron which positively affects geNOp function

[107]. However, there is no study highlights that redox tone of the cells using HyPer under normoxic conditions.

To investigate the relationship between H_2O_2 and NO under more physiological conditions, we need to understand the behavior of cells expressing HyPer and geNOp. While we have previously demonstrated the activity of geNOp, we have not yet done so for HyPer. Therefore, we began our investigation by using HyPer under physiological normoxia (5 kPa) and hyperoxia (18 kPa).

Initially, we aimed to determine the optimal adaptation period for cells to physiological normoxia. To this end, HyPer-expressing endothelial cells were incubated at 5 kPa O_2 levels for 24 hours, while another set of cells was adapted to 5 kPa O_2 by culturing them for at least 5 days. These cells were then used for experiments with a plate reader equipped with atmospheric control to maintain O_2 levels at 5 kPa. During the experiments, cells were challenged with auranofin to induce intracellular production of H_2O_2. According to HyPer signals, cells incubated for 24 hours were more responsive to auranofin compared to adapted cells (**Figure 3.25A**). Additionally, the kinetics of HyPer signals were different.

Comparing the basal levels of H_2O_2 using basal HyPer signals prior to auranofin challenge demonstrated that adaptation to physiological normoxia (5 kPa O_2) led to a substantial decrease in basal levels of H_2O_2 (**Figure 3.25B**). We also compared the maximum responses of HyPer upon auranofin challenge. HyPer signals indicated that adaptation to 5 kPa O_2 conditions significantly influenced the production of H_2O_2 (**Figure 3.25C**). Furthermore, examining the HyPer kinetics revealed that adaptation to physiological normoxia significantly slowed the production rate of H_2O_2 (**Figure 3.25D**).

To obtain physiologically relevant redox tone. Cells need to be adapted to physiological normoxia at least for 5 days.

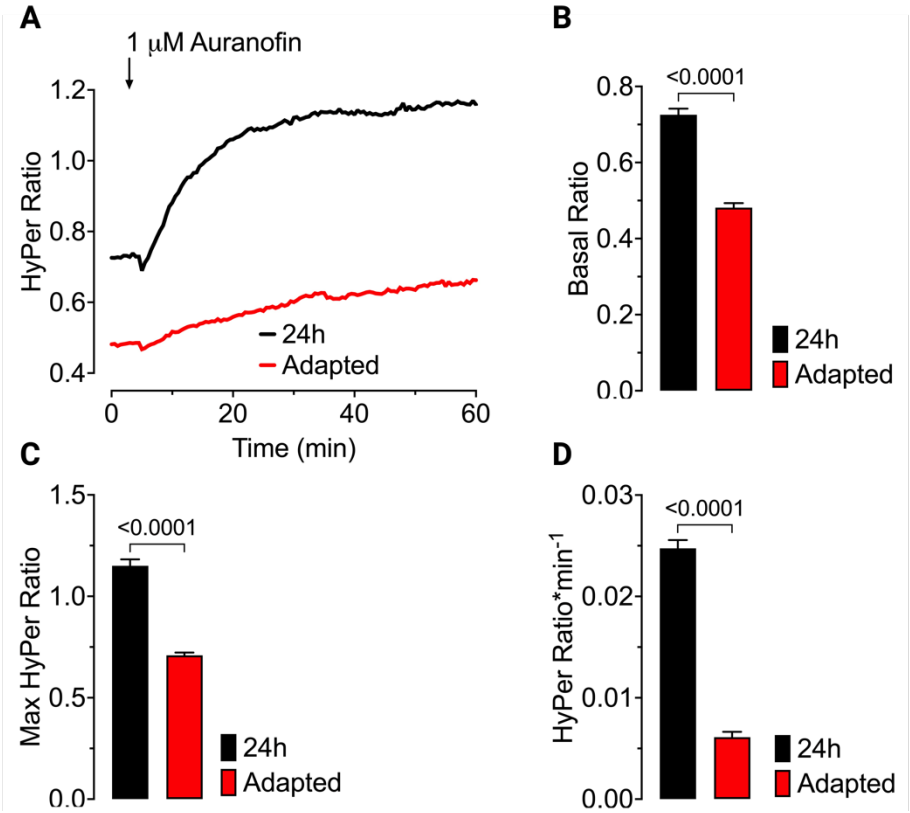

Figure 3.25: Adaptation of cells to 5 kPa affects HyPer dynamics

Double stable EA.hy926 cells were cultured under 5 kPa O_2 conditions either for 24 hours (24 h) or cultured at least 5 days (Adapted). **(A)** Cells challenged with 1 μM auranofin then HyPer responses were recorded under 5 kPa O_2. Adapted cells' responses were traced in red and 24 hour incubated cells' responses (24h) traced in black. **(B)** Basal HyPer ratios of each group calculated. Bar graph represents average HyPer basal ratios of 24 hours incubated cells (black bar), adapted cells (red bar) **(C)** Bar graph represents the maximum HyPer responses of cells either 24 hours incubated (black bar) or adapted cells (red bar) challenged with auranofin. **(D)** Bar graph represents rate of HyPer ratio change in response to auranofin challenge in cells either 24 hours incubated (black bar) or adapted cells (red bar). Data presented as mean±SEM. Student's t-test is performed. p-values were indicated in bar graphs (n=3).

After determining that cells require adaptation to 5 kPa O_2 to achieve physiological conditions, we cultured the cells for at least 5 days prior to experiments. Following adaptation, we began comparing HyPer dynamics in cells adapted to hyperoxia (18 kPa O_2) versus normoxia (5 kPa O_2). Cells were injected with H_2O_2 exogenously. HyPer signals demonstrated that the addition of H_2O_2 caused an instant increase in both conditions (**Figure 3.26A**). Surprisingly, the decrease in HyPer signals after H_2O_2 addition was faster in cells adapted to 5 kPa O_2. Additionally, we compared the basal H_2O_2 levels by examining the basal HyPer signals before the addition of H_2O_2. As

expected, adaptation to normoxia led to a significant decrease in basal H_2O_2 levels (**Figure 3.26B**). However, when comparing the amplitude of maximum HyPer signals, there was no significant difference (**Figure 3.26C**). Finally, we analyzed the decrease in HyPer signals, representing the scavenging rate of H_2O_2. Normoxia adaptation caused a significant increase in the scavenging rate of H_2O_2 compared to hyperoxia-adapted cells (**Figure 3.26D**).

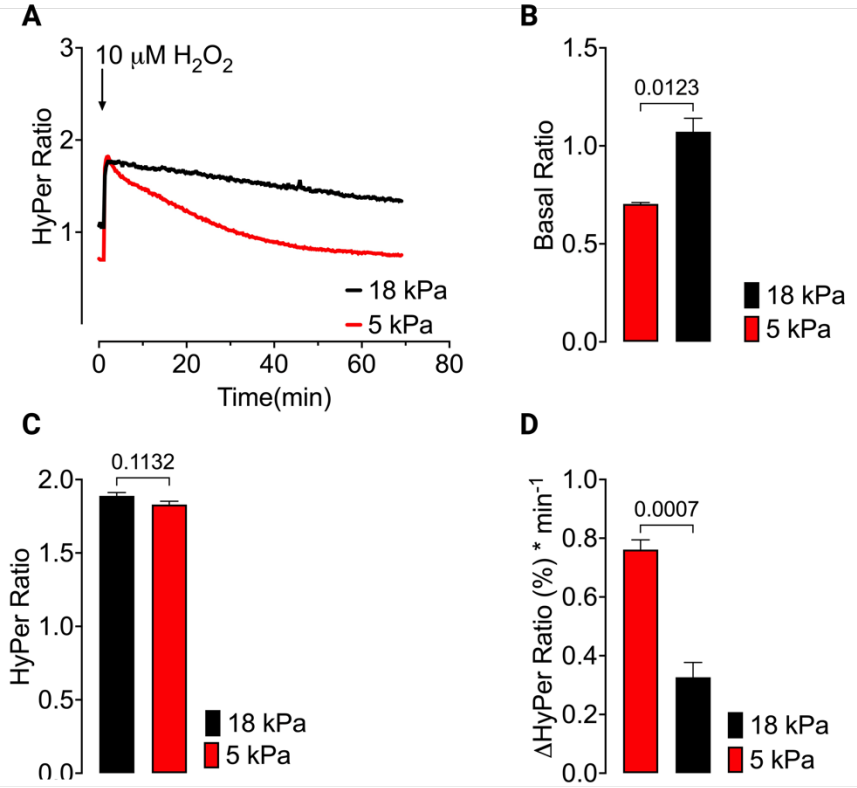

Figure 3.26: HyPer kinetics under varying O_2 conditions in response to exogenous H_2O_2.

Double stable EA.hy926 cells were maintained under 18 kPa or 5 kPa O_2 conditions at least 5 days. After adaptation cells were used for HyPer experiments. **(A)** Graphic represents HyPer responses of cells adapted to 18 kPa (black line) or 5 kPa O_2 (red line) in response to 10 µM H_2O_2 injection. **(B)** Bar graph represents basal HyPer ratio of cells adapted to 18 kPa (black bar) or 5 kPa O_2 (red bar). Ratios were measured before addition of H_2O_2. **(C)** Bar graph indicates maximum HyPer responses of the cells adapted to 18 kPa (black bar) or 5 kPa O_2 (red bar) in response to 10 µM H_2O_2. (D) Bar graphic demonstrates rate of change in HyPer ratio of the cells adapted to 18 kPa (black bar) or 5 kPa O_2 (red bar) after HyPer ratio is peaked in addition to 10 µM H_2O_2. Data presented as mean±SEM. Student's t-test is performed. p-values were indicated in bar graphs (n=3).

After observing the increased scavenging rate of H_2O_2 under 5 kPa O_2 levels, we examined the effect of antioxidant enzymes such as catalase (CAT) and superoxide dismutase (SOD). EA.hy926 cells expressing HyPer were adapted to physiological normoxia (5 kPa O_2) or hyperoxia (18 kPa O_2). These cells were then pre-treated with PEG-CAT or PEG-SOD prior to the experiments. As a control, some cells were not treated with any enzyme. During the experiments, 5 kPa O_2 adapted cells were challenged with auranofin. According to the HyPer curves, CAT treatment reduced HyPer signals, whereas SOD treatment did not have the same effect (**Figure 3.27A**). Cells adapted to 18 kPa O_2 were also challenged with auranofin. CAT treatment attenuated the auranofin-induced HyPer response even more effectively in the 18 kPa adapted cells compared to the 5 kPa adapted cells (**Figure 3.27B**).

When comparing the maximum responses of HyPer to auranofin challenge in the presence of CAT or SOD under varying O_2 conditions, CAT treatment attenuated the production of H_2O_2 in both physiological normoxia-adapted cells and hyperoxia-adapted cells, as indicated by the maximum HyPer responses. Control cells and SOD-treated cells showed significantly different maximum responses under varying O_2 conditions (**Figure 3.27C**). Additionally, we compared the production rate of H_2O_2 by analyzing the change in HyPer ratio after auranofin challenge. CAT treatment under varying O_2 conditions substantially decreased the rate of H_2O_2 production, whereas SOD treatment did not (**Figure 3.27D**).

These experiments demonstrated that auranofin directly induces the production of H_2O_2 rather than producing superoxide, which is then converted to H_2O_2. This conclusion is supported by the fact that only catalase treatment significantly attenuated both the amount and rate of H_2O_2 production under both O_2 conditions. Additionally, we observed that cells adapted to 5 kPa O_2 produced less H_2O_2 compared to those adapted to 18 kPa O_2, as expected. Notably, catalase treatment in 18 kPa O_2 conditions resulted in H_2O_2 production levels similar to those seen in cells adapted to 5 kPa O_2. This observation suggests that cells adapted to 5 kPa O_2 may possess higher antioxidant activity compared to those adapted to 18 kPa O_2.

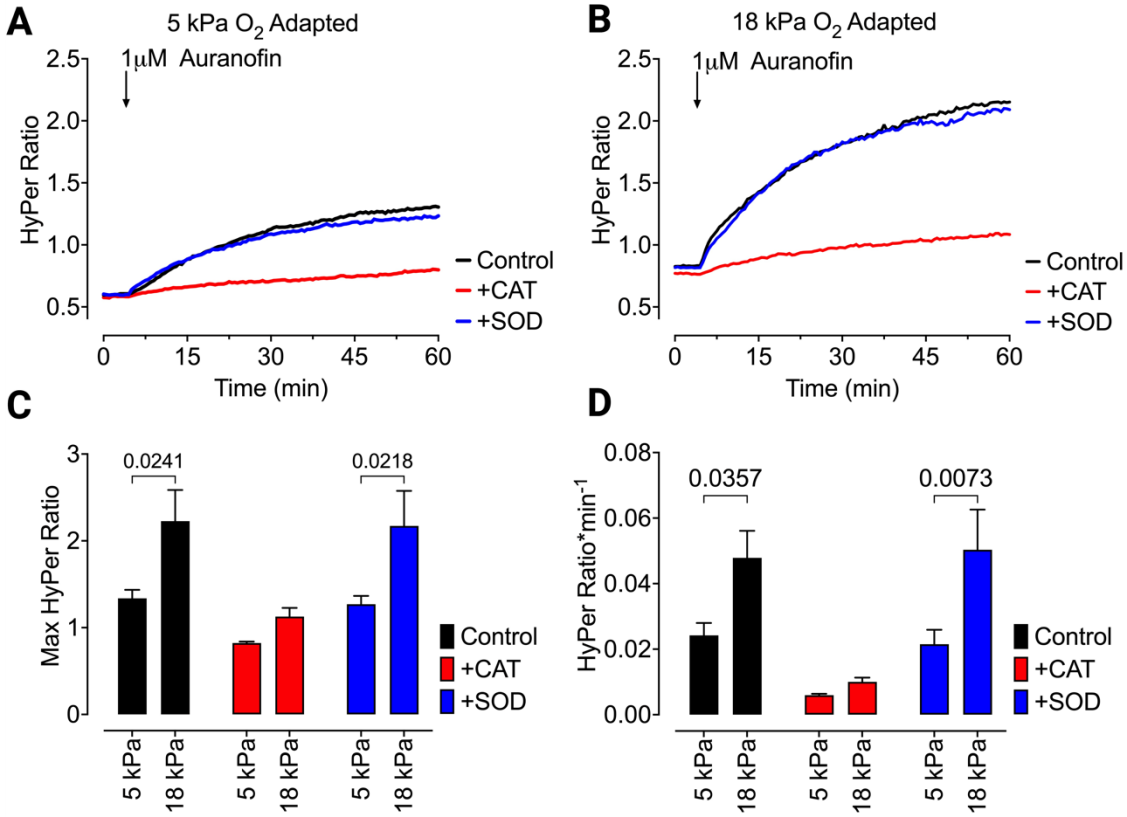

Figure 3.27: Effect of SOD and CAT HyPer dynamics under varying O_2 conditions.

EAhy.926 cells expressing H.7-NES cultured under 18 kPa or 5 kPa O_2 for 5 days. 2 hours prior to experiments cells were treated with 200 U/ml PEG-Catalase (+CAT) or 20 U/ml PEG-SOD (+SOD) or no treatement (Control). **(A)** Cells were cultured under 5 kPa challenged with 1 μM auranofin and graphic represents the HyPer responses of Control (black line), +CAT (red line) and +SOD (blue line) cells. **(B)** Same experimental setup in Part A but performed under 18 kPa O_2 condition. **(C)** Bar graph represents maximum HyPer ratio of cells cultured under 18 kPa or 5 kPa O_2 conditions in response to auranofin challenge. Bars represent maximum responses of cells treated with catalase (red bars), SOD (blue bars) or control (black bars). **(D)** Bar graph represents rate of change in HyPer ratio of cells cultured under 18 kPa or 5 kPa O_2 conditions and treated with catalase (red bars), SOD (blue bars). Black bars represent the rate of change in HyPer ratios of control cells Data presented as mean±SEM. Student's t-test is performed for each condition. p-values were indicated in bar graphs (n=3).

After elucidating H_2O_2 dynamics under physiological normoxia using HyPer, we aimed to understand the relationship between H_2O_2 and NO under 5 kPa O_2 conditions. The interplay between these two molecules might be influenced by the excessive presence of O_2 due to changes in NO bioavailability and differences in antioxidant machinery. To investigate this, EA.hy926 cells expressing HyPer and O-geNOp were adapted to both 5 kPa O_2 and 18 kPa O_2 levels. Adapted cells were treated with exogenous H_2O_2, and both

NO and H_2O_2 levels were monitored. In cells adapted to both 18 kPa O_2 and 5 kPa O_2, a short pulse of exogenous H_2O_2 elicited a robust response. However, no changes in NO signals were observed upon the addition of H_2O_2 (**Figure 3.28A and Figure 3.28B**).

We compared the basal levels of H_2O_2 under varying O_2 conditions and found that cells adapted to 5 kPa O_2 had significantly lower H_2O_2 levels under resting conditions (**Figure 3.28C, left panel**). The response to a short pulse of exogenous H_2O_2 was similar when comparing the maximum responses of HyPer under different O_2 conditions (**Figure 3.28C, middle panel**). Following H_2O_2 provision, we assessed geNOp responses to determine if H_2O_2 provision led to an increase in NO levels. However, no significant differences were observed (**Figure 3.28C, right panel**).

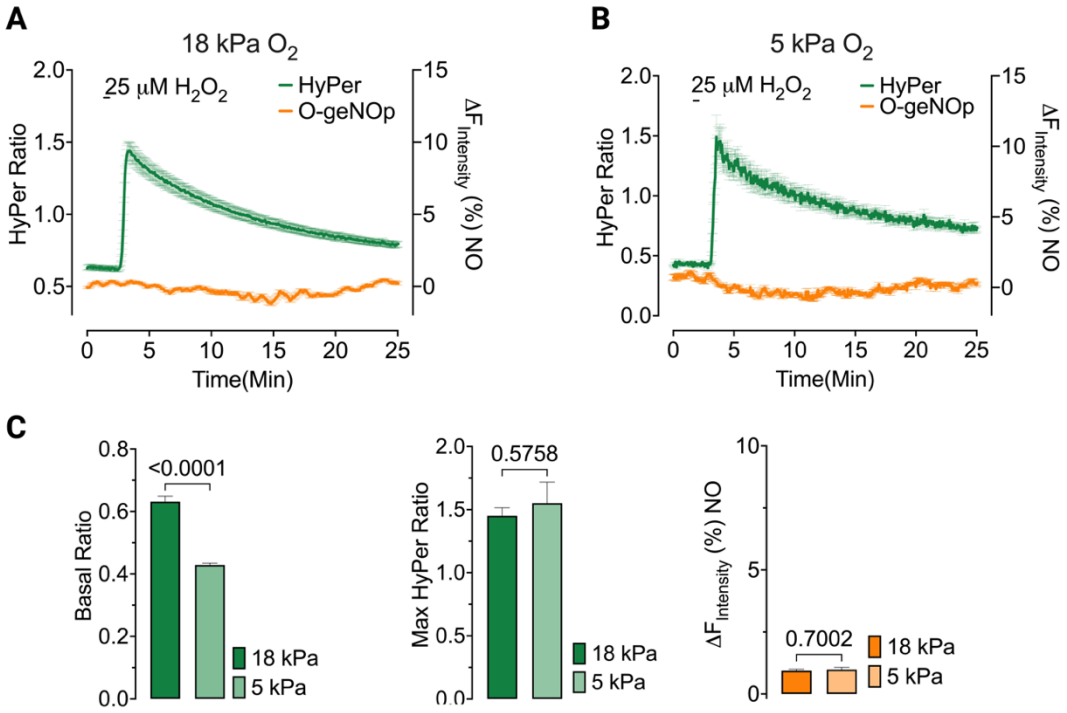

Figure 3.28: Exogenous H_2O_2 did not yield robust NO response under varying O_2 conditions.

EA.hy926 cells expressing H.7-NES and O-geNOp-NES were cultured under 18 kPa or 5 kPa O_2 at least for 5 days. Cells were challenged with 25 μM H_2O_2 and responses were recorded. **(A)** Graphic represents simultaneous imaging cells cultured under 18 kPa O2 provided with 25 μM H_2O_2 as indicated. Traces demonstrate average HyPer (green line, left Y-axis), and O-geNOp (orange line, right Y-axis) signals in response to H_2O_2. **(B)** Same experiments were performed with cells cultured under 5 kPa O_2. **(C)** Bar graphs demonstrate basal HyPer ratios (left panel), maximum HyPer responses in response to H_2O_2 (middle panel) and average O-geNOp signals in response to H_2O_2 (right panel). Bars have bold color indicate signals obtained from cells adapted to 18 kPa and light-colored bars represent 5 kPa adapted cells. Data presented as mean±SEM. Student's t-test is performed for each condition. p-values were indicated in bar graphs (n=3).

Then we investigated the H_2O_2 and NO relationship under varying O_2 conditions by producing intracellular H_2O_2 using auranofin instead of exogenously applied H_2O_2. For that purpose, cells expressing both biosensors adapted to 5 kPa O_2 and 18 kPa O_2.

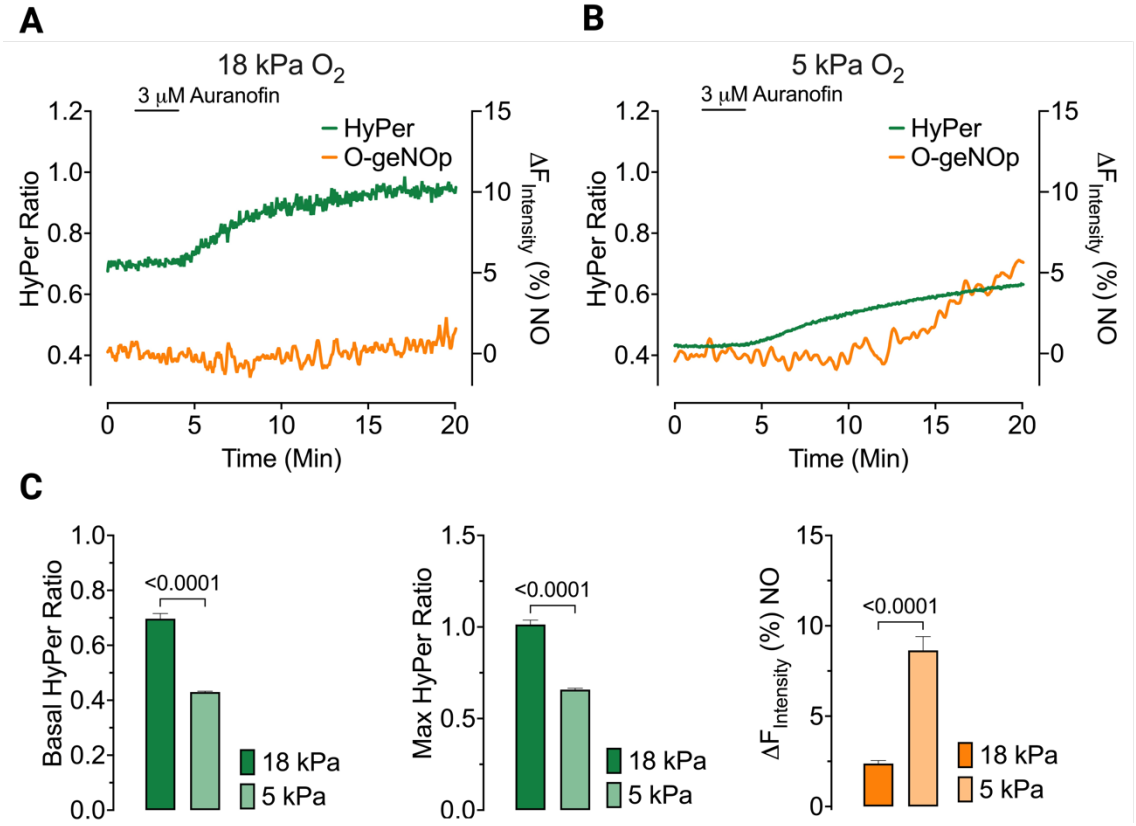

Figure 3.29: Endogenous production of H_2O_2 yielded robust NO response under 5 kPa O_2 conditions.

EA.hy926 cells expressing H.7-NES and O-geNOp-NES were cultured under 18 kPa or 5 kPa O_2 at least for 5 days. Cells were challenged with 3 µM auranofin and responses were recorded. **(A)** Graphic represents simultaneous imaging cells cultured under 18 kPa O_2 provided with 3 µM auranofin as indicated. Traces demonstrate average HyPer (green line, left Y-axis), and O-geNOp (orange line, right Y-axis) signals in response to auranofin challenge. **(B)** Same experiments were performed with cells cultured under 5 kPa O_2. **(C)** Bar graphs demonstrate basal HyPer ratios (left panel), maximum HyPer responses in response to auranofin (middle panel) and average O-geNOp signals in response to auranofin (right panel). Bars have bold color indicate signals obtained from cells adapted to 18 kPa and light-colored bars represent 5 kPa adapted cells. Data presented as mean±SEM. Student's t-test is performed for each condition. p-values were indicated in bar graphs (n=3).

Cells were used in live-cell imaging and challenged with auranofin. Under both O_2 conditions, auranofin induced robust production of H_2O_2. Surprisingly, we observed an increase in O-geNOp signals in response to auranofin in cells adapted to 5 kPa O_2

(**Figure 3.29A and Figure 3.29B**). Additionally, we compared the basal H_2O_2 levels of differentially adapted cells and found that cells adapted to 5 kPa O_2 had significantly lower H_2O_2 levels under resting conditions (**Figure 3.29C, left panel**). Maximum responses of HyPer upon auranofin challenge were also significantly lower in 5 kPa O_2 adapted cells, as previously demonstrated (**Figure 3.29C, middle panel**). Moreover, maximum O-geNOp signals were compared after auranofin challenge, revealing that 5 kPa O_2 adapted cells showed a robust NO increase compared to 18 kPa O_2 adapted cells. This was the first demonstration of a direct relationship between H_2O_2 and NO.

After observing NO signals upon auranofin challenge, we sought to investigate the source of this signal. We initially decided to use L-NAME, an inhibitor of eNOS function. For this purpose, cells adapted to 18 kPa or 5 kPa O_2 levels were used in live-cell imaging. Cells were challenged with auranofin, followed by the addition of L-NAME. As expected, auranofin induced robust H_2O_2 production in both 18 kPa and 5 kPa O_2 adapted cells. No NO signals were observed during live-cell imaging (**Figure 3.30A and Figure 3.30B**).

Consistent with our previous findings, basal H_2O_2 levels were significantly different between the two conditions, with 5 kPa O_2 adapted cells showing lower basal H_2O_2 levels (**Figure 3.30C, left panel**). Additionally, auranofin-induced H_2O_2 production was significantly higher in 18 kPa O_2 adapted cells (**Figure 3.30C, middle panel**). When we compared O-geNOp signals after auranofin challenge in the presence of L-NAME, we found that there were no robust NO signals under either condition, and there was no significant difference between cells adapted to 18 kPa and 5 kPa O_2. Previously, we observed significant NO signals under 5 kPa O_2 conditions, but these signals were diminished by L-NAME, confirming the involvement of eNOS in NO production.

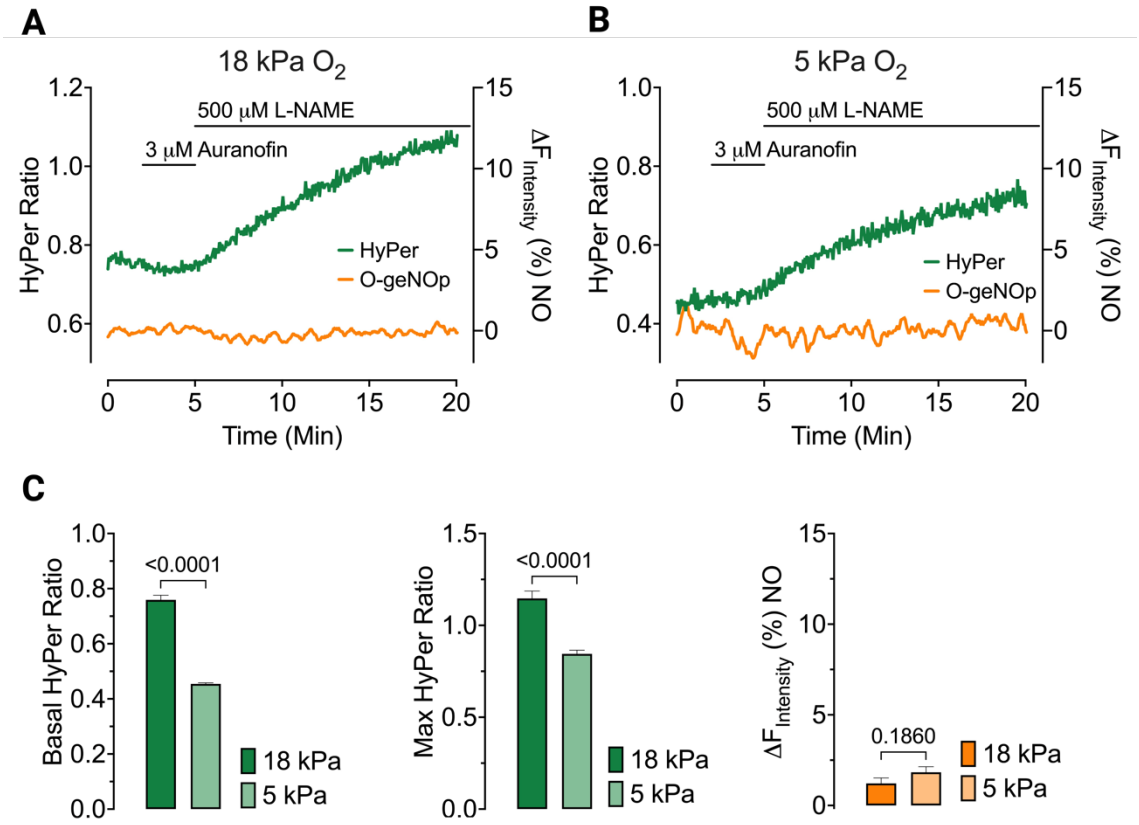

Figure 3.30: L-NAME diminished NO signals in response to endogenous production of H_2O_2 in 5 kPa O_2.

EA.hy926 cells expressing H.7-NES and O-geNOp-NES were cultured under 18 kPa or 5 kPa O_2 at least for 5 days. Cells were challenged with 3 µM auranofin and subsequently 500 µM L-NAME is provided to cells. **(A)** Graphic represents simultaneous imaging cells cultured under 18 kPa O_2 provided with 3 µM auranofin and 500 µM L-NAME as indicated. Traces demonstrate average HyPer (green line, left Y-axis), and O-geNOp (orange line, right Y-axis) signals in response to auranofin challenge. **(B)** Same experiments were performed with cells cultured under 5 kPa O_2. **(C)** Bar graphs demonstrate basal HyPer ratios (left panel), maximum HyPer responses in response to auranofin (middle panel) and average O-geNOp signals in response to auranofin and L-NAME (right panel). Bars have bold color indicate signals obtained from cells adapted to 18 kPa and light-colored bars represent 5 kPa adapted cells. Data presented as mean±SEM. Student's t-test is performed for each condition. p-values were indicated in bar graphs (n=3).

We observed that 5 kPa O_2 adaptation led to an investigation of the direct relationship between H_2O_2 and NO. Next, we sought to investigate the effect of low levels of H_2O_2 adaptation on NO dynamics using cells adapted to 5 kPa O_2 and 18 kPa O_2. To this end, we treated cells expressing O-geNOp with 25 µM H_2O_2 under different ambient O_2 conditions. The purpose of this experiment was to demonstrate how differential antioxidant capacity affects NO signals.

We prepared an experimental setup using O-geNOp-expressing cells. Cells were adapted to 25 μM H_2O_2 for 5 days under either 18 kPa O_2 or 5 kPa O_2 conditions. The cells were then used for live-cell imaging. To evoke NO production, we used ATP followed by the addition of L-NAME. Cells adapted to 18 kPa O_2 responded to ATP and produced NO, but H_2O_2-treated cells were more responsive to ATP (**Figure 3.31A, left panel**). The ATP responses of treated and control cells were significantly different, with low levels of H_2O_2 treatment leading to an increase in maximum NO responses (**Figure 3.31A, right panel**).

Next, we used treated and control cells adapted to 5 kPa O_2. ATP stimulation created robust NO responses in both sets of cells, but the NO response was significantly higher in treated cells (**Figure 3.31B, left panel**). Surprisingly, the decrease in NO levels took longer in 5 kPa O_2-adapted cells compared to 18 kPa O_2-adapted cells upon the addition of L-NAME. Additionally, when comparing the maximum geNOp responses to ATP stimulation, there was no significant difference between the responses of treated cells and control cells (**Figure 3.31B, right panel**).

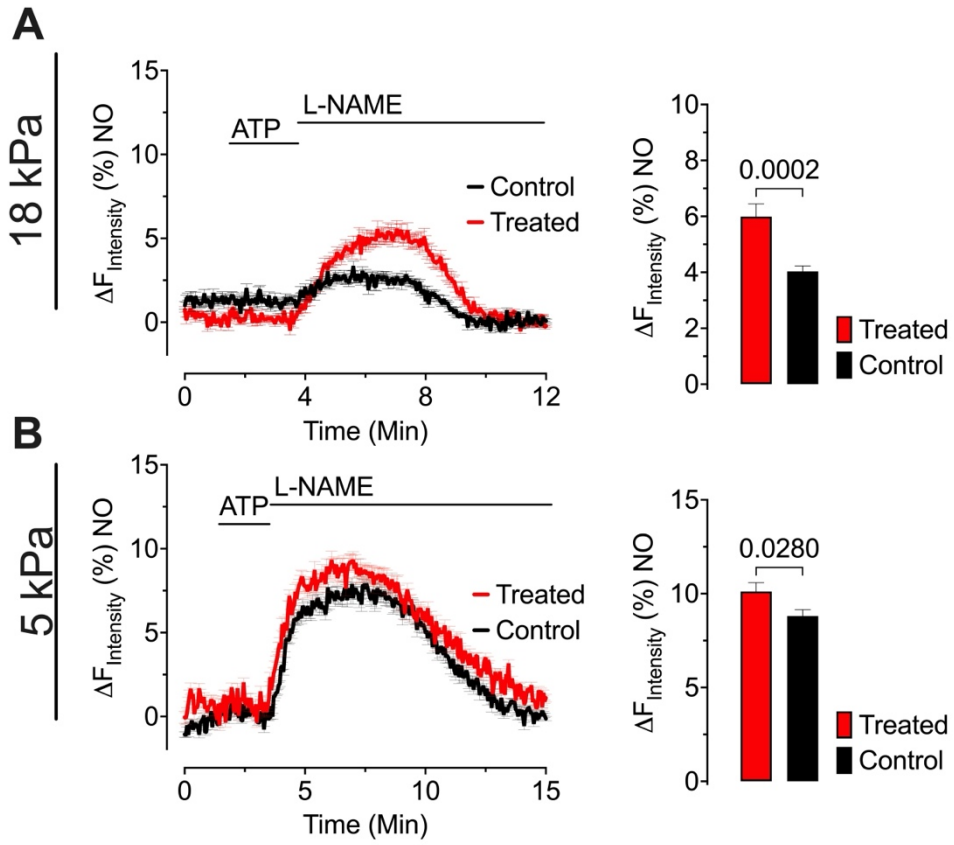

Figure 3.31:Effect of low levels of H_2O_2 treatment in NO signaling under varying O_2 conditions.

EA.hy926 cells expressing O-geNOp were cultured with 25 µM H_2O_2 (Treated) or without (Control) for five days under 18 kPa O_2 or 5 kPa O_2 conditions. **(A)** EA.hy926 cells cultured under 18 kPa O_2 were used for live-cell imaging. O-geNOp signals were traced using cells either treated with H_2O_2 (Treated, red line) or not (Control, black line) upon stimulation with 30 µM ATP and subsequent addition 500 µM L-NAME. Bar graph on the left panel represents the maximum responses of treated cells (red bar) or control cells (black bar) adapted to 18 kPa O_2. **(B)** Same experimental setup in part A for cells cultured under 5 kPa O_2 conditions. Data presented as mean±SEM. Student's t-test is performed for each condition. p-values were indicated in bar graphs (n=3).

In this study, we aimed to explain the relationship between H_2O_2 and NO under varying pericellular O_2 conditions, focusing on the physiological normoxia (5 kPa O_2) and hyperoxia (18 kPa O_2). Our experiments employed EA.hy926 endothelial cells expressing the biosensors HyPer and O-geNOp, which allowed us to monitor H_2O_2 and NO dynamics in real-time.

Initially, we established that cells require adaptation to 5 kPa O_2 to mimic physiological conditions accurately (**Figure 3.25**). The adaptation process involved culturing the cells at 5 kPa O_2 for at least five days, which led to significant changes in H_2O_2 dynamics compared to cells adapted to hyperoxia (18 kPa O_2). The reduced basal levels of H_2O_2 in normoxia-adapted cells indicate a lower oxidative stress environment.

Our findings showed that upon exogenous H_2O_2 administration, HyPer signals increased instantly in both normoxia- and hyperoxia-adapted cells. However, the subsequent decrease in HyPer signals, indicative of H_2O_2 scavenging, was faster in normoxia-adapted cells (**Figure 3.26**). This suggests that cells adapted to 5 kPa O_2 possess more active antioxidant mechanisms although, adaptation to 5 kPa O_2 causes a decrease in expression of certain antioxidant genes such as HO-1 and NQO1 [106].The increased scavenging rate of H_2O_2 in normoxia-adapted cells underscores the importance of maintaining physiological O_2 levels for optimal cellular function and redox homeostasis. Moreover, we demonstrated that catalase is effective in attenuating auranofin-related H_2O_2 production, whereas SOD is not (**Figure 3.27**). Additionally, maintaining the cells under 5 kPa O_2 creates an effect similar to catalase treatment. In these experiments, we provided catalase extracellularly. To prevent an instant increase or higher production rate of H_2O_2, more catalase is required by the cells. From this perspective, we can consider that adaptation to 5 kPa O_2 enhances the availability of antioxidant enzymes such as catalase.

When investigating the interplay between H_2O_2 and NO, we observed that exogenous H_2O_2 did not alter NO signals in either normoxia- or hyperoxia-adapted cells (**Figure 3.28**). This result was consistent across different experimental setups, indicating that acute H_2O_2 exposure does not directly affect NO bioavailability under the conditions tested. However, when cells were challenged with auranofin, a thioredoxin reductase inhibitor, we observed robust H_2O_2 production in both O_2 conditions. Interestingly, normoxia-adapted cells showed a significant increase in NO production upon auranofin challenge, which was not observed in hyperoxia-adapted cells (**Figure 3.29**). This suggests a unique interplay between H_2O_2 and NO under physiological O_2 levels, possibly mediated by enhanced eNOS activity or altered redox-sensitive signaling pathways. To

further investigate the source of NO production in response to auranofin, we employed L-NAME, an eNOS inhibitor. The addition of L-NAME abolished the NO signals observed in normoxia-adapted cells upon auranofin challenge, confirming the involvement of eNOS in this process (**Figure 3.30**). The lack of NO response in hyperoxia-adapted cells suggests that excessive O_2 levels may impair eNOS function or NO bioavailability, possibly due to increased oxidative stress and subsequent NO scavenging by reactive oxygen species.

Moreover, we explored the effect of low-level H_2O_2 adaptation on NO dynamics. Cells were treated with 25 μM H_2O_2 for five days under both normoxia and hyperoxia conditions. The results indicated that H_2O_2-treated cells were more responsive to ATP-induced NO production compared to control cells under hyperoxia, but ATP responses were similar under normoxia conditions (**Figure 3.31**). This enhanced responsiveness highlights the potential role of low-level H_2O_2 as a preconditioning agent, potentially upregulating eNOS expression or activity and improving NO bioavailability under hyperoxic conditions. However, ATP responses of cells adapted normoxia were higher compared to hyperoxia adapted cells indicating enhanced NO dynamics under normoxic conditions. The prolonged decrease in NO levels upon L-NAME addition in normoxia-adapted cells further supports the notion of heightened eNOS activity under physiological O_2 conditions.

Overall, this part of the study provides critical insights into the differential effects of physiological normoxia and hyperoxia on H_2O_2 and NO dynamics in endothelial cells. The enhanced antioxidant capacity and eNOS activity observed in normoxia-adapted cells underscore the importance of maintaining appropriate O_2 levels for endothelial function and redox balance. These findings have significant implications for understanding the role of oxidative stress in vascular physiology and pathology, particularly in conditions characterized by altered O_2 levels, such as ischemia-reperfusion injury, chronic inflammation, and cardiovascular diseases.

Concluding reflections and future studies

In this part of the study, we investigated the complicated relationship H_2O_2 and NO in endothelial cells, emphasizing the use of genetically encoded biosensors, HyPer7 and O-geNOp, to understand these dynamics. The chapter's comprehensive approach covers various aspects, from the historical context and development of geNOps to the optimization of live-cell imaging techniques and the impact of ambient oxygen conditions on redox biology. The findings showcased in this chapter not only enhance our understanding of H_2O_2 and NO interplay but also provide valuable insights into the broader implications of oxidative stress and redox signaling in vascular physiology and pathology.

The chapter begins by tracing the history and development of geNOps, highlighting their significance in overcoming the limitations of traditional NO detection methods. The introduction of genetically encoded biosensors marked a significant advancement in redox biology, enabling real-time, intracellular measurement of NO. The ability of geNOps to provide reversible signals, unlike many conventional methods, makes them invaluable tools for studying dynamic processes within live cells. The successful development and application of these biosensors in our laboratory underscore their robustness and reliability in various experimental settings.

In this chapter we also explored the acute and chronic effects of extracellular H_2O_2 on NO signaling using a double stable cell line expressing both HyPer7 and O-geNOp. The study demonstrated that short pulses of H_2O_2 did not alter NO levels, emphasizing the transient nature of acute H_2O_2 exposure. However, chronic exposure to H_2O_2 resulted in significant changes in NO dynamics, particularly in basal NO levels. Cells exposed to chronic oxidative conditions exhibited elevated basal NO levels, irrespective of the H_2O_2

concentration (100 µM or 300 µM). These findings suggest that prolonged oxidative stress influences basal NO levels.

Additionally, the chapter highlights the importance of investigating Ca^{2+} dynamics in cells chronically exposed to H_2O_2. The experiments revealed that chronic H_2O_2 exposure significantly increases basal intracellular Ca^{2+} levels, with higher H_2O_2 concentrations leading to greater resting Ca^{2+} accumulation. However, ATP-induced Ca^{2+} responses remained comparable across all conditions, indicating that the ability to mobilize Ca^{2+} in response to ATP is preserved despite chronic H_2O_2 exposure.

The chapter further investigates the impact of localized intracellular H_2O_2 production on NO dynamics using mDAAO targeted to different cellular compartments (cytosol, nucleus, and mitochondria). The study found that chronic production of H_2O_2 in these compartments leads to significant increases in both basal NO levels and ATP-derived NO responses. This suggests that localized oxidative stress enhances the cells' responsiveness for NO production especially in the case of chronic nuclear oxidative stress, likely due to increased eNOS activity or expression. Interestingly, while chronic localized H_2O_2 production elevated NO levels, the same effect was not observed in Ca^{2+} signaling, indicating that the primary influence of localized H_2O_2 can be eNOS phosphorylation and NO production rather than Ca^{2+} dynamics.

A significant portion of this chapter focuses on the technical optimizations necessary for effective multiparametric imaging using HyPer7 and O-geNOp. The need to balance signal intensity, resolution, and acquisition speed is critical for capturing accurate and meaningful data. Our experiments demonstrated that the choice of camera binning setup significantly affects the signal-to-noise ratio (SNR). Specifically, the 4x4 binning setup provided superior SNR and faster signal acquisition compared to the 1x1 setup. This optimization is crucial for detecting endogenous signals, which are often present at lower concentrations than exogenously applied analytes.

Moreover, our investigation into the effects of different imaging devices, namely widefield epifluorescence and spinning disk confocal microscopy, revealed that both techniques produce consistent results for HyPer7 and O-geNOp signals. This finding indicates that high-contrast imaging does not adversely affect the performance of these biosensors, thus providing flexibility in the choice of imaging platform based on experimental requirements. Additionally, our assessment of ambient temperature effects confirmed that both HyPer7 and O-geNOp maintain stable performance at room temperature and physiological temperature (37°C). This stability is essential for ensuring the reliability of these biosensors across various experimental conditions.

The last section of Chapter 3 investigates the physiological relevance of ambient oxygen levels and their impact on H_2O_2 and NO dynamics. Our experiments comparing normoxia (5 kPa O_2) and hyperoxia (18 kPa O_2) highlighted significant differences in cellular redox balance and antioxidant capacity. Cells adapted to physiological normoxia exhibited lower basal levels of H_2O_2 and a higher scavenging rate, indicating enhanced antioxidant mechanisms. This finding is consistent with the fact that maintaining physiological O_2 levels is crucial for optimal cellular function and redox homeostasis.

In contrast, hyperoxia-adapted cells demonstrated higher basal H_2O_2 levels and a reduced scavenging rate, suggesting increased oxidative stress under these conditions. These observations underscore the importance of considering ambient O_2 levels in redox biology studies, as variations in O_2 concentration can significantly influence cellular responses and experimental outcomes. Moreover, the enhanced NO production observed in normoxia-adapted cells upon auranofin challenge further emphasizes the interplay between H_2O_2 and NO under physiological conditions. The use of L-NAME, an eNOS inhibitor, confirmed that the observed NO signals were indeed mediated by eNOS activity, highlighting the critical role of NO in vascular function and redox signaling. This finding was the first finding that demonstrate direct relationship between H_2O_2 and NO using genetically encoded biosensors.

The insights gained from this chapter have profound implications for our understanding of endothelial function and vascular health. The differential effects of normoxia and hyperoxia on H_2O_2 and NO dynamics suggest that oxidative stress and redox imbalance are closely linked to vascular pathologies. Conditions characterized by altered O_2 levels, such as ischemia-reperfusion injury, chronic inflammation, and cardiovascular diseases, may benefit from therapeutic strategies aimed at restoring redox balance and enhancing NO bioavailability. Moreover, implications on in vitro studies are important because we directly showed that redox balance and dynamics changes when ambient O_2 levels are physiologically suitable and provides information while studying H_2O_2 and NO dynamics.

Furthermore, the ability to simultaneously measure H_2O_2 and NO in live cells using optimized imaging techniques provides a powerful tool for investigating the complex interactions between these molecules in real-time. This capability is particularly relevant for studying the acute and chronic effects of oxidative stress, as well as the role of redox signaling in cellular adaptation and resilience. By elucidating the mechanisms underlying redox regulation, we can better understand the cellular responses to oxidative challenges and identify potential targets for therapeutic intervention.

While Chapter 3 provides a comprehensive overview of H_2O_2 and NO dynamics under varying conditions, several gaps for future research remain. One potential direction is the exploration of localized H_2O_2 production and NO or another redox pathology model that affect NO signaling under physiological normoxia. For instance, differential redox hotspots can provide additional insight on ROS and NO signaling. Additionally, the development of more advanced biosensors with enhanced sensitivity and specificity could facilitate the detection of these reactive species at even lower concentrations.

In conclusion, Chapter 3 of this thesis has elucidated the intricate relationship between H_2O_2 and NO in endothelial cells, highlighting the importance of ambient O2 conditions and optimized imaging techniques. Although our findings are limited in terms of redox signaling and NO dynamics but in this study, we showed direct interaction of these two

molecules for the first time. The findings presented herein contribute to our understanding of redox biology and underscore the critical role of NO in vascular health. These insights are important for future in vitro research aimed at resolving the complexities of redox regulation.

Materials and Methods

Chemicals

Dulbecco's modified Eagle's Medium (DMEM), 100 U/ml penicillin and 100 µg/ml streptomycin, Fetal Bovine Serum (FBS) and trypsin were purchased from Pan Biotech (Aidenbach, Germany). 100 µg/mL normocin was purchased from InvivoGen (San Diego, CA,USA). 2% HAT solution (Sodium Hypoxanthine (5 mM), Aminopterin (20 µM), and Thymidine (0.8 mM)) was purchased from ATCC (Manassas, VA, USA). Polyjet transfection reagent was purchased from SignaGen Laboratories (Maryland, USA). 10 µg/mL Polybrene infection reagent was purchased from Sigma-Aldrich (St.Louis, MO, USA). $CaCl_2$, KCl, NaCl, $MgCl_2$, KH_2PO_4, $NaHCO_3$, NaH_2PO_4, D-Glucose were purchased from NeoFroxx (Darmstadt, Germany). 1 mM HEPES, 0.1% MEM Vitamins, 0.2% essential amino acids were purchased from Pan Biotech (Aidenbach, Germany). D-alanine was purchased from Alfa Aesar (Landau, Germany). FURA2-AM was purchased from Invitrogen (Waltham, MA,USA). Auranofin, PEG-Catalase, PEG-SOD and Earl's Balanced Salt Solution (EBSS) were purchased from Sigma Aldrich (St. Louis, MO, USA).

Buffers and Solutions

Live-cell imaging performed under HEPES-based buffer solution. Final concentrations of chemicals in this buffer are: 138 mM NaCl, 5 mM KCl, 2 mM $CaCl_2$,

1 mM $MgCl_2$, 10 mM D-glucose, 10 mM HEPES. Prior to experiments cell were stored in storage buffer solution for 1 hour. Final concentrations of each chemical in cell storage buffer are 138 mM NaCl, 5 mM KCl, 2 mM CaCl2, 1 mM $MgCl_2$, 10 mM D-glucose, 10 mM HEPES, 2.6 mM $NaHCO_3$, 0.44 mM KH_2PO_4, 0.34 mM Na_2HPO_4, 10 mM D-glucose, 0.1% vitamins, 0.2% essential amino acids, and 1% penicillin/streptomycin. Chemicals are used in live-cell imaging experiments were dissolved in live-cell imaging buffer solution. After preparation of solutions pH is adjusted to 7.42. For experiments performed under physiological normoxia buffers were kept under 5 kPa O_2 at least for 3 hours to balance O_2 content

Molecular Cloning and Plasmids

Differentially targeted mDAAO constructs were amplified using primers (Table 2) to obtain PCR products to subclone mDAAO constructs to empty lentiviral transfer vector called pLenti-MP2 (Addgene #36097) from the XhoI and XbaI restriction sites. O-geNOp-NES subcloned into pLenti-MP2 using XbaI and SalI restriction sites.

Table 2:Primers used in subcloning of differentially located mDAAO constructs

Name	Sequence (5'-3')
XhoI-mCherry-FOR	ataCTCGAGGCCACCATGGTGAGCAAGGGCG
XbaI-mCherry-NES-REV	ataTCTAGATTACAGGGTCAGCCGCTCCAGGG
XhoI-Mito-mCherry-FOR	ataCTCGAGGCCACCATGTCTGTTCTGACTCCTCT
XbaI-Stop-mDAAO-REV	ataTCTAGATTAGCTCTCCCTAGCTGCGCCG
XhoI-mCherry-FOR	ataCTCGAGGCCACCATGGTGAGCAAGGGC
XbaI-NLS-REV	ataTCTAGATTATACCTTTCTCTTCTTTTTTGGATCTACCT

Cell Culture and Lentivirus Generation

Maintaining cells and production of lentivirus steps previously described in Chapter 2. Double stable cells were generated via transduction of respective lentiviruses at the same time.

Live-cell Imaging Experiments

Widefield epifluorescence microscopy experiments were conducted using a Zeiss Axio Observer Z1.7 (Carl Zeiss AG, Oberkochen, Germany) equipped with a Plan-Apochromat 20x/0.8 dry objective and a Plan-Apochromat 40x/1.4 oil immersion objective. The imaging system included a monochrome CCD camera Axiocam 503 and a custom-made gravity-based perfusion system. For HyPer7 imaging, alternating excitation was achieved with 423/44 nm and 469/38 nm LED lights via a motorized filter wheel containing FT455 (HyPer low) and FT495 (HyPer high) beamsplitters (BS). Emissions were collected using a single emission filter (BP 525/50) for ratio imaging. O-geNOp imaging was performed with 555/30 nm LED light excitation, using FT570 BS and a 605/70 nm emission filter. For mDAAO imaging O-geNOp's optical setup was used and for G-geNop imaging, HyPer High's optical setup was used. The same optical setup was used for both mono-imaging and dual imaging of the two biosensors. Data acquisition and control were managed using Zen Blue 3.1 Pro software (Carl Zeiss AG, Oberkochen, Germany). Chemical provision and withdrawal were facilitated by an in-house gravity-based perfusion system connected to a perfusion chamber (NGFI, Graz, Austria).

Spinning disk microscopy experiments were carried out on a Zeiss Axio Observer.Z1 equipped with a Yokogawa CSU-X1 (Tokyo, Japan) confocal scanner unit and Colibri 2 light sources. The setup included an LD A-plan 20x/0.3 dry objective and two cameras: QuantEM:512SC (Teledyne Photometrics, AZ, USA) for confocal mode and AxioHrm for widefield measurements. HyPer7 signals were captured by exciting cells with a 488

nm laser and collecting emission at 509 nm in confocal mode. In widefield mode, cells were excited using 470/20 nm LED light, with FT495 BS and a 525/25 nm emission filter. For O-geNOp measurements, cells were excited with a 558 nm laser and emission was collected at 589 nm in confocal mode. In widefield mode, cells were excited using 550/12 nm LED light, with FT570 BS and a 605/35 nm emission filter. A gravity-based perfusion system connected to the perfusion chamber was used for chemical provision and withdrawal.

Temperature-controlled experiments were conducted using a Zeiss AxioObserver equipped with an LSM880 Confocal Laser Scan system. The microscope featured a PeCon on-stage incubator (Erbach, Germany) for maintaining and controlling ambient temperature. For HyPer7 excitation, 405 nm and 488 nm lasers were used, and a 543 nm laser was used for O-geNOp excitation, with a multibeamsplitter (MBS). Emissions were collected using a 32-channel GaAsp detector. Cells were imaged with a Plan-Apochromat 20x/0.8 M27 objective.

For FURA imaging Zeiss Axiovert A.1 (Carl Zeiss AG, Oberkochen, Germany) equipped with a Plan-Apochromat 20x/0.8 dry objective and CoolLED (Andover, UK) p340e light source was used. The imaging system included a monochrome CCD camera Axiocam 503 and a custom-made gravity-based perfusion system. To image FURA signals obtained using 340nm and 380nm alternating excitation pass through FURA/GFP 790004 filter set (Chroma, Bellows Falt, VT, USA).

Prior to live-cell imaging experiments cells were maintained under cell storage buffer. For O_2 related experiments, PeCon on-stage incubator were used to keep O_2 stable, and buffers were purged with 5% O_2 95% N_2 gas mixture.

For FURA experiments cells were loaded with FURA2-AM. 20 µl of FURA2-AM mixed with 6 ml of DMEM and cells plated in 6-well plated were loaded with 1 ml of mixture for each well. After 15 minutes of incubation under RT, cells were washed with PBS three times and cell storage buffer was added for 30 minutes incubation.

For geNOps experiment prior to experiments iron-loading was performed as indicated in ref 107.

Long-Term Adaptation of EA.hy926 Cells in an Oxygen-Controlled Workstation

For experiments requiring controlled oxygen levels, EA.hy926 cells that were stably transfected were cultured in monolayers for at least five days under conditions of either 5 kPa (physiological normoxia) or 18 kPa (hyperoxia) O_2 in a Scitive dual workstation (Baker, USA). This adaptation period ensures that the cells achieve a physiological redox phenotype without the stabilization of HIF1-α [104], [108]. Continuously maintaining the cells within the workstation eliminates the need to handle them under atmospheric oxygen conditions in a laminar flow hood [106].

Oxygen-Controlled Plate Reader

EA.hy926 cells were seeded in clear-bottom 96-well plates and pre-adapted for five days to either 18 kPa or 5 kPa O_2 in the Scitive dual workstation. For real-time imaging of Hyper7 or O-geNOp, a time-resolved fluorescence plate reader (CLARIOStar, BMG Labtech) equipped with an atmospheric control unit was used. Pre-adapted cells were quickly transferred to the plate reader, which was gassed with 18 or 5 kPa O_2 to replicate the oxygen levels during pre-adaptation. The excitation wavelengths used were 420/20 nm (HyPer low) and 473/20 nm (HyPer high), with emissions collected at 521/25 nm. Acute treatments were administered to cells maintained under 18 or 5 kPa O_2 using a dual injection system within the plate reader, applying the specified times and concentrations.

Data Analysis

For the analysis of O-geNOp signals, background subtraction was carried out using Microsoft Excel. Basal fluorescence intensities were analyzed using a one-phase decay function in GraphPad Prism software, which normalized O-geNOp signals to 100%. The raw fluorescence intensity is referred to as F, while the normalized fluorescence intensity is denoted as F_0. The following formula was used to obtain normalized signal curves:

$$\Delta F = \left(1 - \left(\frac{F}{F_0}\right)\right) * 100$$

For the analysis of HyPer7 signals, background subtraction was also performed using Microsoft Excel. HyPer7 utilizes two excitation wavelengths and a single emission wavelength, referred to as HyPer low and HyPer high. The HyPer7 ratio was calculated by dividing the HyPer high signal by the HyPer low signal. Normalized HyPer ratios were obtained by normalizing these ratios to their basal levels.

For the analysis of FURA signals background subtraction was also performed using Microsoft Excel. FURA has two excitation wavelengths and a single emission wavelength, referred to as F340 and F380. Ratio is calculated by dividing F380 to F340.

Statistical Analysis

Statistical analysis previously described in Chapter 2.

CHAPTER 4: BIBLIOGRAPHY

[1] C. A. K. Lundgren *et al.*, “Scavenging of superoxide by a membrane-bound superoxide oxidase,” *Nat Chem Biol*, vol. 14, no. 8, pp. 788–793, Aug. 2018, doi: 10.1038/s41589-018-0072-x.

[2] A. Phaniendra, D. B. Jestadi, and L. Periyasamy, “Free Radicals: Properties, Sources, Targets, and Their Implication in Various Diseases,” *Indian J Clin Biochem*, vol. 30, no. 1, pp. 11–26, Jan. 2015, doi: 10.1007/s12291-014-0446-0.

[3] H. Sies, R. J. Mailloux, and U. Jakob, “Fundamentals of redox regulation in biology,” *Nat Rev Mol Cell Biol*, pp. 1–19, Apr. 2024, doi: 10.1038/s41580-024-00730-2.

[4] V. J. Thannickal and B. L. Fanburg, “Reactive oxygen species in cell signaling,” *American Journal of Physiology-Lung Cellular and Molecular Physiology*, vol. 279, no. 6, pp. L1005–L1028, Dec. 2000, doi: 10.1152/ajplung.2000.279.6.L1005.

[5] C. Lennicke and H. M. Cochemé, “Redox metabolism: ROS as specific molecular regulators of cell signaling and function,” *Molecular Cell*, vol. 81, no. 18, pp. 3691–3707, Sep. 2021, doi: 10.1016/j.molcel.2021.08.018.

[6] H. Sies and D. P. Jones, “Reactive oxygen species (ROS) as pleiotropic physiological signalling agents,” *Nat Rev Mol Cell Biol*, vol. 21, no. 7, Art. no. 7, Jul. 2020, doi: 10.1038/s41580-020-0230-3.

[7] H. Sies *et al.*, “Defining roles of specific reactive oxygen species (ROS) in cell biology and physiology,” *Nat Rev Mol Cell Biol*, vol. 23, no. 7, pp. 499–515, Jul. 2022, doi: 10.1038/s41580-022-00456-z.

[8] L. J. H. C. Jacobs and J. Riemer, “Maintenance of small molecule redox homeostasis in mitochondria,” *FEBS Letters*, vol. 597, no. 2, pp. 205–223, 2023, doi: 10.1002/1873-3468.14485.

[9] H. Sies, C. Berndt, and D. P. Jones, “Oxidative Stress,” *Annual Review of Biochemistry*, vol. 86, no. Volume 86, 2017, pp. 715–748, Jun. 2017, doi: 10.1146/annurev-biochem-061516-045037.

[10] S. G. Rhee, “Redox signaling: hydrogen peroxide as intracellular messenger,” *Exp Mol Med*, vol. 31, no. 2, pp. 53–59, Jun. 1999, doi: 10.1038/emm.1999.9.

[11] N. M. Mishina *et al.*, “Which Antioxidant System Shapes Intracellular H2O2 Gradients?,” *Antioxidants & Redox Signaling*, vol. 31, no. 9, pp. 664–670, Sep. 2019, doi: 10.1089/ars.2018.7697.

[12] G. P. Bienert and F. Chaumont, “Aquaporin-facilitated transmembrane diffusion of hydrogen peroxide,” *Biochimica et Biophysica Acta (BBA) - General Subjects*, vol. 1840, no. 5, pp. 1596–1604, May 2014, doi: 10.1016/j.bbagen.2013.09.017.

[13] S. G. Rhee and I. S. Kil, “Multiple Functions and Regulation of Mammalian Peroxiredoxins,” *Annu. Rev. Biochem.*, vol. 86, no. 1, pp. 749–775, Jun. 2017, doi: 10.1146/annurev-biochem-060815-014431.
[14] R. Brigelius-Flohé and L. Flohé, “Regulatory Phenomena in the Glutathione Peroxidase Superfamily,” *Antioxidants & Redox Signaling*, vol. 33, no. 7, pp. 498–516, Sep. 2020, doi: 10.1089/ars.2019.7905.
[15] M. P. Murphy, “How mitochondria produce reactive oxygen species,” *Biochemical Journal*, vol. 417, no. 1, pp. 1–13, Dec. 2008, doi: 10.1042/BJ20081386.
[16] G. A. Knock, “NADPH oxidase in the vasculature: Expression, regulation and signalling pathways; role in normal cardiovascular physiology and its dysregulation in hypertension,” *Free Radical Biology and Medicine*, vol. 145, pp. 385–427, Dec. 2019, doi: 10.1016/j.freeradbiomed.2019.09.029.
[17] H. Sies, “Hydrogen peroxide as a central redox signaling molecule in physiological oxidative stress: Oxidative eustress,” *Redox Biology*, vol. 11, pp. 613–619, Apr. 2017, doi: 10.1016/j.redox.2016.12.035.
[18] G. Roos, N. Foloppe, and J. Messens, “Understanding the pKa of Redox Cysteines: The Key Role of Hydrogen Bonding,” *Antioxidants & Redox Signaling*, vol. 18, no. 1, pp. 94–127, Jan. 2013, doi: 10.1089/ars.2012.4521.
[19] C. Lismont *et al.*, “Peroxisome-Derived Hydrogen Peroxide Modulates the Sulfenylation Profiles of Key Redox Signaling Proteins in Flp-In T-REx 293 Cells,” *Front. Cell Dev. Biol.*, vol. 10, Apr. 2022, doi: 10.3389/fcell.2022.888873.
[20] D. Garrido Ruiz, A. Sandoval-Perez, A. V. Rangarajan, E. L. Gunderson, and M. P. Jacobson, “Cysteine Oxidation in Proteins: Structure, Biophysics, and Simulation,” *Biochemistry*, vol. 61, no. 20, pp. 2165–2176, Oct. 2022, doi: 10.1021/acs.biochem.2c00349.
[21] A. D. Londhe *et al.*, “Regulation of PTP1B activation through disruption of redox-complex formation,” *Nat Chem Biol*, vol. 16, no. 2, pp. 122–125, Feb. 2020, doi: 10.1038/s41589-019-0433-0.
[22] H. Sies, “Hydrogen peroxide as a central redox signaling molecule in physiological oxidative stress: Oxidative eustress,” *Redox Biology*, vol. 11, pp. 613–619, Apr. 2017, doi: 10.1016/j.redox.2016.12.035.
[23] A. N. Onyango, “Cellular Stresses and Stress Responses in the Pathogenesis of Insulin Resistance,” *Oxidative Medicine and Cellular Longevity*, vol. 2018, no. 1, p. 4321714, 2018, doi: 10.1155/2018/4321714.
[24] M. A. Incalza, R. D’Oria, A. Natalicchio, S. Perrini, L. Laviola, and F. Giorgino, “Oxidative stress and reactive oxygen species in endothelial dysfunction associated with cardiovascular and metabolic diseases,” *Vascular Pharmacology*, vol. 100, pp. 1–19, Jan. 2018, doi: 10.1016/j.vph.2017.05.005.
[25] C. Heiss, A. Rodriguez-Mateos, and M. Kelm, “Central Role of eNOS in the Maintenance of Endothelial Homeostasis,” *Antioxidants & Redox Signaling*, vol. 22, no. 14, pp. 1230–1242, May 2015, doi: 10.1089/ars.2014.6158.
[26] V. Garcia and W. C. Sessa, “Endothelial NOS: perspective and recent developments,” *British Journal of Pharmacology*, vol. 176, no. 2, pp. 189–196, 2019, doi: 10.1111/bph.14522.
[27] U. Förstermann and T. Münzel, “Endothelial Nitric Oxide Synthase in Vascular Disease,” *Circulation*, vol. 113, no. 13, pp. 1708–1714, Apr. 2006, doi: 10.1161/CIRCULATIONAHA.105.602532.
[28] C. S. Raman, H. Li, P. Martásek, V. Král, B. S. S. Masters, and T. L. Poulos, “Crystal Structure of Constitutive Endothelial Nitric Oxide Synthase: A Paradigm

for Pterin Function Involving a Novel Metal Center," *Cell*, vol. 95, no. 7, pp. 939–950, Dec. 1998, doi: 10.1016/S0092-8674(00)81718-3.

[29] M. J. Crabtree, C. L. Smith, G. Lam, M. S. Goligorsky, and S. S. Gross, "Ratio of 5,6,7,8-tetrahydrobiopterin to 7,8-dihydrobiopterin in endothelial cells determines glucose-elicited changes in NO vs. superoxide production by eNOS," *American Journal of Physiology-Heart and Circulatory Physiology*, vol. 294, no. 4, pp. H1530–H1540, Apr. 2008, doi: 10.1152/ajpheart.00823.2007.

[30] V. Gebhart, K. Reiß, A. Kollau, B. Mayer, and A. C. F. Gorren, "Site and mechanism of uncoupling of nitric-oxide synthase: Uncoupling by monomerization and other misconceptions," *Nitric Oxide*, vol. 89, pp. 14–21, Aug. 2019, doi: 10.1016/j.niox.2019.04.007.

[31] D. G. Hirst and T. Robson, "Nitric Oxide Physiology and Pathology," in *Nitric Oxide: Methods and Protocols*, H. O. McCarthy and J. A. Coulter, Eds., Totowa, NJ: Humana Press, 2011, pp. 1–13. doi: 10.1007/978-1-61737-964-2_1.

[32] C. N. Hall and J. Garthwaite, "What is the real physiological NO concentration *in vivo*?," *Nitric Oxide*, vol. 21, no. 2, pp. 92–103, Sep. 2009, doi: 10.1016/j.niox.2009.07.002.

[33] L. J. Ignarro, R. E. Byrns, G. M. Buga, and K. S. Wood, "Endothelium-derived relaxing factor from pulmonary artery and vein possesses pharmacologic and chemical properties identical to those of nitric oxide radical.," *Circulation Research*, vol. 61, no. 6, 1987, doi: 10.1161/01.res.61.6.866.

[34] R. Liu, Y. Kang, and L. Chen, "Activation mechanism of human soluble guanylate cyclase by stimulators and activators," *Nat Commun*, vol. 12, no. 1, p. 5492, Sep. 2021, doi: 10.1038/s41467-021-25617-0.

[35] Y. Iwakiri *et al.*, "Nitric oxide synthase generates nitric oxide locally to regulate compartmentalized protein S-nitrosylation and protein trafficking," *Proceedings of the National Academy of Sciences*, vol. 103, no. 52, pp. 19777–19782, Dec. 2006, doi: 10.1073/pnas.0605907103.

[36] G. K. Kolluru, J. H. Siamwala, and S. Chatterjee, "eNOS phosphorylation in health and disease," *Biochimie*, vol. 92, no. 9, pp. 1186–1198, Sep. 2010, doi: 10.1016/j.biochi.2010.03.020.

[37] X. Peng *et al.*, "Protective role of PI3-kinase/Akt/eNOS signaling in mechanical stress through inhibition of p38 mitogen-activated protein kinase in mouse lung," *Acta Pharmacol Sin*, vol. 31, no. 2, pp. 175–183, Feb. 2010, doi: 10.1038/aps.2009.190.

[38] E. Eroglu, S. S. S. Saravi, A. Sorrentino, B. Steinhorn, and T. Michel, "Discordance between eNOS phosphorylation and activation revealed by multispectral imaging and chemogenetic methods," *Proceedings of the National Academy of Sciences*, vol. 116, no. 40, pp. 20210–20217, Oct. 2019, doi: 10.1073/pnas.1910942116.

[39] N. Tran, T. Garcia, M. Aniqa, S. Ali, A. Ally, and S. Nauli, "Endothelial Nitric Oxide Synthase (eNOS) and the Cardiovascular System: in Physiology and in Disease States," *AJBSR*, vol. 15, no. 2, p. 155, Jan. 2022.

[40] J. S. Beckman and W. H. Koppenol, "Nitric oxide, superoxide, and peroxynitrite: the good, the bad, and ugly," *Am J Physiol*, vol. 271, no. 5 Pt 1, pp. C1424-1437, Nov. 1996, doi: 10.1152/ajpcell.1996.271.5.C1424.

[41] M. Hermann, A. Flammer, and T. F. Lüscher, "Nitric Oxide in Hypertension," *The Journal of Clinical Hypertension*, vol. 8, no. s12, pp. 17–29, 2006, doi: 10.1111/j.1524-6175.2006.06032.x.

[42] S. Kawashima and M. Yokoyama, "Dysfunction of Endothelial Nitric Oxide Synthase and Atherosclerosis," *Arteriosclerosis, Thrombosis, and Vascular*

Biology, vol. 24, no. 6, pp. 998–1005, Jun. 2004, doi: 10.1161/01.ATV.0000125114.88079.96.

[43] T. V. Fiorentino, A. Prioletta, P. Zuo, and F. Folli, "Hyperglycemia-induced Oxidative Stress and its Role in Diabetes Mellitus Related Cardiovascular Diseases," *Current Pharmaceutical Design*, Accessed: Jul. 14, 2024. [Online]. Available: https://www.eurekaselect.com/article/55343

[44] Z. Hu, J. Chen, Q. Wei, and Y. Xia, "Bidirectional Actions of Hydrogen Peroxide on Endothelial Nitric-oxide Synthase Phosphorylation and Function: CO-COMMITMENT AND INTERPLAY OF Akt AND AMPK *," *Journal of Biological Chemistry*, vol. 283, no. 37, pp. 25256–25263, Sep. 2008, doi: 10.1074/jbc.M802455200.

[45] C. M. C. Andrés, J. M. Pérez de la Lastra, C. Andrés Juan, F. J. Plou, and E. Pérez-Lebeña, "Superoxide Anion Chemistry—Its Role at the Core of the Innate Immunity," *International Journal of Molecular Sciences*, vol. 24, no. 3, Art. no. 3, Jan. 2023, doi: 10.3390/ijms24031841.

[46] A. Daiber *et al.*, "Vascular Redox Signaling, Redox Switches in Endothelial Nitric Oxide Synthase (eNOS Uncoupling), and Endothelial Dysfunction," in *Systems Biology of Free Radicals and Antioxidants*, I. Laher, Ed., Berlin, Heidelberg: Springer, 2014, pp. 1177–1211. doi: 10.1007/978-3-642-30018-9_48.

[47] C. Wittmann, P. Chockley, S. K. Singh, L. Pase, G. J. Lieschke, and C. Grabher, "Hydrogen Peroxide in Inflammation: Messenger, Guide, and Assassin," *Advances in Hematology*, vol. 2012, no. 1, p. 541471, 2012, doi: 10.1155/2012/541471.

[48] A. Ayala, M. F. Muñoz, and S. Argüelles, "Lipid Peroxidation: Production, Metabolism, and Signaling Mechanisms of Malondialdehyde and 4-Hydroxy-2-Nonenal," *Oxidative Medicine and Cellular Longevity*, vol. 2014, no. 1, p. 360438, 2014, doi: 10.1155/2014/360438.

[49] A. J. Kettle, A. C. Carr, and C. C. Winterbourn, "Assays using horseradish peroxidase and phenolic substrates require superoxide dismutase for accurate determination of hydrogen peroxide production by neutrophils," *Free Radical Biology and Medicine*, vol. 17, no. 2, pp. 161–164, Aug. 1994, doi: 10.1016/0891-5849(94)90111-2.

[50] X. Ye, S. S. Rubakhin, and J. V. Sweedler, "Detection of nitric oxide in single cells," *Analyst*, vol. 133, no. 4, pp. 423–433, Mar. 2008, doi: 10.1039/B716174C.

[51] T. Yoshimura, H. Yokoyama, S. Fujii, F. Takayama, K. Oikawa, and H. Kamada, "In vivo EPR detection and imaging of endogenous nitric oxide in lipopolysaccharide-treated mice," *Nat Biotechnol*, vol. 14, no. 8, pp. 992–994, Aug. 1996, doi: 10.1038/nbt0896-992.

[52] A. M. Leone, V. W. Furst, N. A. Foxwell, S. Cellek, and S. Moncada, "Visualisation of Nitric Oxide Generated by Activated Murine Macrophages," *Biochemical and Biophysical Research Communications*, vol. 221, no. 1, pp. 37–41, Apr. 1996, doi: 10.1006/bbrc.1996.0557.

[53] M. P. Murphy *et al.*, "Guidelines for measuring reactive oxygen species and oxidative damage in cells and in vivo," *Nat Metab*, vol. 4, no. 6, pp. 651–662, Jun. 2022, doi: 10.1038/s42255-022-00591-z.

[54] V. V. Pak *et al.*, "Ultrasensitive Genetically Encoded Indicator for Hydrogen Peroxide Identifies Roles for the Oxidant in Cell Migration and Mitochondrial Function," *Cell Metabolism*, vol. 31, no. 3, pp. 642-653.e6, Mar. 2020, doi: 10.1016/j.cmet.2020.02.003.

[55] B. Morgan *et al.*, “Real-time monitoring of basal H2O2 levels with peroxiredoxin-based probes,” *Nat Chem Biol*, vol. 12, no. 6, pp. 437–443, Jun. 2016, doi: 10.1038/nchembio.2067.
[56] E. Eroglu *et al.*, “Genetic biosensors for imaging nitric oxide in single cells,” *Free Radical Biology and Medicine*, vol. 128, pp. 50–58, Nov. 2018, doi: 10.1016/j.freeradbiomed.2018.01.027.
[57] E. Eroglu *et al.*, “Development of novel FP-based probes for live-cell imaging of nitric oxide dynamics,” *Nat Commun*, vol. 7, no. 1, Art. no. 1, Feb. 2016, doi: 10.1038/ncomms10623.
[58] V. V. Belousov *et al.*, “Genetically encoded fluorescent indicator for intracellular hydrogen peroxide,” *Nat Methods*, vol. 3, no. 4, Art. no. 4, Apr. 2006, doi: 10.1038/nmeth866.
[59] M. Zheng, F. Åslund, and G. Storz, “Activation of the OxyR Transcription Factor by Reversible Disulfide Bond Formation,” *Science*, vol. 279, no. 5357, pp. 1718–1722, Mar. 1998, doi: 10.1126/science.279.5357.1718.
[60] D. S. Bilan *et al.*, “HyPer-3: A Genetically Encoded H2O2 Probe with Improved Performance for Ratiometric and Fluorescence Lifetime Imaging,” *ACS Chem. Biol.*, vol. 8, no. 3, pp. 535–542, Mar. 2013, doi: 10.1021/cb300625g.
[61] Y. G. Ermakova *et al.*, “Red fluorescent genetically encoded indicator for intracellular hydrogen peroxide,” *Nat Commun*, vol. 5, no. 1, p. 5222, Oct. 2014, doi: 10.1038/ncomms6222.
[62] Y. Zhao *et al.*, “An Expanded Palette of Genetically Encoded Ca2+ Indicators,” *Science*, vol. 333, no. 6051, pp. 1888–1891, Sep. 2011, doi: 10.1126/science.1208592.
[63] L. de Cubas, V. V. Pak, V. V. Belousov, J. Ayté, and E. Hidalgo, “The Mitochondria-to-Cytosol H2O2 Gradient Is Caused by Peroxiredoxin-Dependent Cytosolic Scavenging,” *Antioxidants*, vol. 10, no. 5, Art. no. 5, May 2021, doi: 10.3390/antiox10050731.
[64] P. Kritsiligkou, K. Bosch, T. K. Shen, M. Meurer, M. Knop, and T. P. Dick, “Proteome-wide tagging with an H2O2 biosensor reveals highly localized and dynamic redox microenvironments,” *Proceedings of the National Academy of Sciences*, vol. 120, no. 48, p. e2314043120, Nov. 2023, doi: 10.1073/pnas.2314043120.
[65] M. R. Depaoli *et al.*, “Live cell imaging of signaling and metabolic activities,” *Pharmacology & Therapeutics*, vol. 202, pp. 98–119, Oct. 2019, doi: 10.1016/j.pharmthera.2019.06.003.
[66] M. E. Matlashov *et al.*, “Fluorescent ratiometric pH indicator SypHer2: Applications in neuroscience and regenerative biology,” *Biochimica et Biophysica Acta (BBA) - General Subjects*, vol. 1850, no. 11, pp. 2318–2328, Nov. 2015, doi: 10.1016/j.bbagen.2015.08.002.
[67] C. A. Werley, S. Boccardo, A. Rigamonti, E. M. Hansson, and A. E. Cohen, “Multiplexed Optical Sensors in Arrayed Islands of Cells for multimodal recordings of cellular physiology,” *Nat Commun*, vol. 11, no. 1, p. 3881, Aug. 2020, doi: 10.1038/s41467-020-17607-5.
[68] A. C. Nathwani, K. M. Gale, K. D. Pemberton, D. C. Crossman, E. G. D. Tuddenham, and J. H. McVey, “Efficient gene transfer into human umbilical vein endothelial cells allows functional analysis of the human tissue factor gene promoter,” *British Journal of Haematology*, vol. 88, no. 1, pp. 122–128, 1994, doi: 10.1111/j.1365-2141.1994.tb04987.x.

[69] P. M. de O. Balderas, “Mitochondria–plasma membrane interactions and communication,” *Journal of Biological Chemistry*, vol. 297, no. 4, Oct. 2021, doi: 10.1016/j.jbc.2021.101164.
[70] L. M. Kraft and L. L. Lackner, “Mitochondria-driven assembly of a cortical anchor for mitochondria and dynein,” *Journal of Cell Biology*, vol. 216, no. 10, pp. 3061–3071, Aug. 2017, doi: 10.1083/jcb.201702022.
[71] A. G. Cox, C. C. Winterbourn, and M. B. Hampton, “Mitochondrial peroxiredoxin involvement in antioxidant defence and redox signalling,” *Biochemical Journal*, vol. 425, no. 2, pp. 313–325, Dec. 2009, doi: 10.1042/BJ20091541.
[72] N. Shannon, R. Gravelle, and B. Cunniff, “Mitochondrial trafficking and redox/phosphorylation signaling supporting cell migration phenotypes,” *Front. Mol. Biosci.*, vol. 9, Jul. 2022, doi: 10.3389/fmolb.2022.925755.
[73] H. S. Chung, S.-B. Wang, V. Venkatraman, C. I. Murray, and J. E. Van Eyk, “Cysteine Oxidative Posttranslational Modifications,” *Circulation Research*, vol. 112, no. 2, pp. 382–392, Jan. 2013, doi: 10.1161/CIRCRESAHA.112.268680.
[74] H. J. Forman, “Use and abuse of exogenous H2O2 in studies of signal transduction,” *Free Radical Biology and Medicine*, vol. 42, no. 7, pp. 926–932, Apr. 2007, doi: 10.1016/j.freeradbiomed.2007.01.011.
[75] K. Uchida, “Lipid peroxidation and redox-sensitive signaling pathways,” *Curr Atheroscler Rep*, vol. 9, no. 3, pp. 216–221, May 2007, doi: 10.1007/s11883-007-0022-7.
[76] A. Sorrentino and T. Michel, “Redox à la carte: Novel chemogenetic models of heart failure,” *British Journal of Pharmacology*, vol. 177, no. 14, pp. 3162–3167, 2020, doi: 10.1111/bph.15093.
[77] B. Steinhorn, E. Eroglu, and T. Michel, “Chemogenetic Approaches to Probe Redox Pathways: Implications for Cardiovascular Pharmacology and Toxicology,” *Annual Review of Pharmacology and Toxicology*, vol. 62, no. Volume 62, 2022, pp. 551–571, Jan. 2022, doi: 10.1146/annurev-pharmtox-012221-082339.
[78] A. Laporte, A. Nordenbrock, S. Lenzen, and M. Elsner, “Light-induced intracellular hydrogen peroxide generation through genetically encoded photosensitizer KillerRed-SOD1,” *Free Radic Res*, vol. 52, no. 10, pp. 1170–1181, Oct. 2018, doi: 10.1080/10715762.2018.1540042.
[79] C. M. Wong, K. H. Wong, and X. D. Chen, “Glucose oxidase: natural occurrence, function, properties and industrial applications,” *Appl Microbiol Biotechnol*, vol. 78, no. 6, pp. 927–938, Apr. 2008, doi: 10.1007/s00253-008-1407-4.
[80] L. Pollegioni, B. Langkau, W. Tischer, S. Ghisla, and M. S. Pilone, “Kinetic mechanism of D-amino acid oxidases from Rhodotorula gracilis and Trigonopsis variabilis,” *J Biol Chem*, vol. 268, no. 19, pp. 13850–13857, Jul. 1993.
[81] Y. C. Erdogan *et al.*, “Complexities of the chemogenetic toolkit: Differential mDAAO activation by d-amino substrates and subcellular targeting,” *Free Radical Biology and Medicine*, vol. 177, pp. 132–142, Dec. 2021, doi: 10.1016/j.freeradbiomed.2021.10.023.
[82] E. Rosini, L. Pollegioni, S. Ghisla, R. Orru, and G. Molla, “Optimization of d-amino acid oxidase for low substrate concentrations – towards a cancer enzyme therapy,” *The FEBS Journal*, vol. 276, no. 17, pp. 4921–4932, 2009, doi: 10.1111/j.1742-4658.2009.07191.x.
[83] D. Tousoulis, A.-M. Kampoli, C. Tentolouris, N. Papageorgiou, and C. Stefanadis, “The role of nitric oxide on endothelial function,” *Curr Vasc Pharmacol*, vol. 10, no. 1, pp. 4–18, Jan. 2012, doi: 10.2174/157016112798829760.

[84] S. M. Krishnan, J. R. Kraehling, F. Eitner, A. Bénardeau, and P. Sandner, “The Impact of the Nitric Oxide (NO)/Soluble Guanylyl Cyclase (sGC) Signaling Cascade on Kidney Health and Disease: A Preclinical Perspective,” *Int J Mol Sci*, vol. 19, no. 6, p. 1712, Jun. 2018, doi: 10.3390/ijms19061712.
[85] R. Radi*, “Reactions of Nitric Oxide with Metalloproteins,” ACS Publications. Accessed: Jul. 14, 2024. [Online]. Available: https://pubs.acs.org/doi/pdf/10.1021/tx950176s
[86] J. W. Denninger and M. A. Marletta, “Guanylate cyclase and the ·NO/cGMP signaling pathway,” *Biochimica et Biophysica Acta (BBA) - Bioenergetics*, vol. 1411, no. 2, pp. 334–350, May 1999, doi: 10.1016/S0005-2728(99)00024-9.
[87] M. I. Hutchings, N. Mandhana, and S. Spiro, “The NorR Protein of Escherichia coli Activates Expression of the Flavorubredoxin Gene norV in Response to Reactive Nitrogen Species,” *J Bacteriol*, vol. 184, no. 16, pp. 4640–4643, Aug. 2002, doi: 10.1128/JB.184.16.4640-4643.2002.
[88] N. P. Tucker, B. D’Autréaux, F. K. Yousafzai, S. A. Fairhurst, S. Spiro, and R. Dixon, “Analysis of the Nitric Oxide-sensing Non-heme Iron Center in the NorR Regulatory Protein*,” *Journal of Biological Chemistry*, vol. 283, no. 2, pp. 908–918, Jan. 2008, doi: 10.1074/jbc.M705850200.
[89] M. Secilmis *et al.*, “A Co-Culture-Based Multiparametric Imaging Technique to Dissect Local H2O2 Signals with Targeted HyPer7,” *Biosensors (Basel)*, vol. 11, no. 9, p. 338, Sep. 2021, doi: 10.3390/bios11090338.
[90] S. Thomas, S. Kotamraju, J. Zielonka, D. R. Harder, and B. Kalyanaraman, “Hydrogen Peroxide Induces Nitric Oxide and Proteosome Activity in Endothelial Cells: A Bell-Shaped Signaling Response,” *Free Radic Biol Med*, vol. 42, no. 7, pp. 1049–1061, Apr. 2007, doi: 10.1016/j.freeradbiomed.2007.01.005.
[91] S. R. Thomas, K. Chen, and J. F. Keaney, “Hydrogen peroxide activates endothelial nitric-oxide synthase through coordinated phosphorylation and dephosphorylation via a phosphoinositide 3-kinase-dependent signaling pathway,” *J Biol Chem*, vol. 277, no. 8, pp. 6017–6024, Feb. 2002, doi: 10.1074/jbc.M109107200.
[92] H. Cai, “Hydrogen peroxide regulation of endothelial function: Origins, mechanisms, and consequences,” *Cardiovascular Research*, vol. 68, no. 1, pp. 26–36, Oct. 2005, doi: 10.1016/j.cardiores.2005.06.021.
[93] S. Kumar *et al.*, “Hydrogen Peroxide Decreases Endothelial Nitric Oxide Synthase Promoter Activity through the Inhibition of Sp1 Activity,” *DNA Cell Biol*, vol. 28, no. 3, pp. 119–129, Mar. 2009, doi: 10.1089/dna.2008.0775.
[94] L. Piacenza, A. Zeida, M. Trujillo, and R. Radi, “The superoxide radical switch in the biology of nitric oxide and peroxynitrite,” *Physiological Reviews*, vol. 102, no. 4, pp. 1881–1906, Oct. 2022, doi: 10.1152/physrev.00005.2022.
[95] S. S. Saeedi Saravi *et al.*, “Differential endothelial signaling responses elicited by chemogenetic H2O2 synthesis,” *Redox Biology*, vol. 36, p. 101605, Sep. 2020, doi: 10.1016/j.redox.2020.101605.
[96] P. M. Epperson and M. Bonner. Denton, “Binning spectral images in a charge-coupled device,” *Anal. Chem.*, vol. 61, no. 14, pp. 1513–1519, Jul. 1989, doi: 10.1021/ac00189a011.
[97] C. Scotté, F. Galland, and H. Rigneault, “Photon-noise: is a single-pixel camera better than point scanning? A signal-to-noise ratio analysis for Hadamard and Cosine positive modulation,” *J. Phys. Photonics*, vol. 5, no. 3, p. 035003, Jun. 2023, doi: 10.1088/2515-7647/acc70b.
[98] V. S. Ovechkina, S. M. Zakian, S. P. Medvedev, and K. R. Valetdinova, “Genetically Encoded Fluorescent Biosensors for Biomedical Applications,”

Biomedicines, vol. 9, no. 11, p. 1528, Oct. 2021, doi: 10.3390/biomedicines9111528.
[99] G.-J. Kremers, S. G. Gilbert, P. J. Cranfill, M. W. Davidson, and D. W. Piston, "Fluorescent proteins at a glance," *J Cell Sci*, vol. 124, no. 2, pp. 157–160, Jan. 2011, doi: 10.1242/jcs.072744.
[100] X. Ragàs, L. P. Cooper, J. H. White, S. Nonell, and C. Flors, "Quantification of Photosensitized Singlet Oxygen Production by a Fluorescent Protein," *ChemPhysChem*, vol. 12, no. 1, pp. 161–165, 2011, doi: 10.1002/cphc.201000919.
[101] A. P. Wojtovich and T. H. Foster, "Optogenetic control of ROS production," *Redox Biology*, vol. 2, pp. 368–376, Jan. 2014, doi: 10.1016/j.redox.2014.01.019.
[102] R. S. Frey, M. Ushio-Fukai, and A. B. Malik, "NADPH Oxidase-Dependent Signaling in Endothelial Cells: Role in Physiology and Pathophysiology," *Antioxid Redox Signal*, vol. 11, no. 4, pp. 791–810, Apr. 2009, doi: 10.1089/ars.2008.2220.
[103] G. L. Squadrito and W. A. Pryor, "The formation of peroxynitrite in vivo from nitric oxide and superoxide," *Chem Biol Interact*, vol. 96, no. 2, pp. 203–206, May 1995, doi: 10.1016/0009-2797(94)03591-u.
[104] T. P. Keeley and G. E. Mann, "Defining Physiological Normoxia for Improved Translation of Cell Physiology to Animal Models and Humans," *Physiological Reviews*, vol. 99, no. 1, pp. 161–234, Jan. 2019, doi: 10.1152/physrev.00041.2017.
[105] G. Warpsinski *et al.*, "Nrf2-regulated redox signaling in brain endothelial cells adapted to physiological oxygen levels: Consequences for sulforaphane mediated protection against hypoxia-reoxygenation," *Redox Biology*, vol. 37, p. 101708, Oct. 2020, doi: 10.1016/j.redox.2020.101708.
[106] S. J. Chapple *et al.*, "Bach1 differentially regulates distinct Nrf2-dependent genes in human venous and coronary artery endothelial cells adapted to physiological oxygen levels," *Free Radic Biol Med*, vol. 92, pp. 152–162, Mar. 2016, doi: 10.1016/j.freeradbiomed.2015.12.013.
[107] G. Sevimli *et al.*, "Nitric oxide biosensor uncovers diminished ferrous iron-dependency of cultured cells adapted to physiological oxygen levels," *Redox Biology*, vol. 53, p. 102319, Jul. 2022, doi: 10.1016/j.redox.2022.102319.
[108] T. P. Keeley, R. C. M. Siow, R. Jacob, and G. E. Mann, "A PP2A-mediated feedback mechanism controls Ca2+-dependent NO synthesis under physiological oxygen," *The FASEB Journal*, vol. 31, no. 12, pp. 5172–5183, 2017, doi: 10.1096/fj.201700211R.